High-pressure STM studies of oxidation catalysis

Bobaru, Ş.C.

Citation

High-Pressure STM
Studies of Oxidation Catalysis

S. C. Bobaru

High-Pressure STM
Studies of Oxidation Catalysis

PROEFSCHRIFT

TER VERKRIJGING VAN

DE GRAAD VAN DOCTOR AAN DE UNIVERSITEIT LEIDEN,

OP GEZAG VAN DE RECTOR MAGNIFICUS DR. D.D. BREIMER,

HOOGLERAAR IN DE FACULTEIT DER WISKUNDE EN

NATUURWETENSCHAPPEN EN DIE DER GENEESKUNDE,

VOLGENS BESLUIT VAN HET COLLEGE VOOR PROMOTIES

TE VERDEDIGEN OP WOENSDAG 25 OKTOBER 2006

KLOKKE 16:15 UUR

DOOR

ŞTEFANIA CARMEN BOBARU

GEBOREN TE DRĂGOEŞTI (ROEMENIË)

IN 1975

Promotiecommissie

Promotor: Prof .dr. Joost Frenken

Referent: Prof. dr. B. E. Nieuwenhuys

Overige leden: Prof. dr. J. A. Moulijn (DelftChemTech-Technische
                                        Universiteit Delft)

                Dr. J. C. van den Heuvel (Universiteit van Amsterdam)

                Prof. dr. M. T. M. Koper

                Prof. dr. P. H. Kes

                Prof. dr. J. Aarts

High-pressure STM studies of oxidation catalysis
Ştefania Carmen Bobaru

"Remember to play after every storm"
Matthew J. T. Stepanek

In the memory of my grandmothers:
Margareta and Constantina
To whom I owe being who I am

Contents

Chapter 1

Introduction

In this chapter the relevance of surface science studies to applied heterogeneous catalysis is discussed. The technique of Scanning Tunneling Microscopy (STM) and our experimental set-up for STM under high-pressure conditions are also described.

1.1 Heterogeneous catalysis

Berzelius has given the name "catalysis" in 1836 to a branch of chemistry that employs compounds, called catalysts, which accelerate chemical reactions without being consumed in the process. Catalysis has a great impact on our society. Without catalysts most chemical reactions used in today's chemical plants and for environmental protection would proceed so slowly that they could not even be detected, even when the reaction conditions (e.g. temperature and pressure) make the reactions thermodynamically favourable. In addition to their importance in the chemical and petrochemical industry, catalysts play a role in the preservation of our environment, by converting polluting waste gases into less harmful products [1]. A catalyst speeds up the reaction by lowering one or more activation barriers or by introducing an alternative reaction path with lower energy barriers. It is important to remember that the acceleration of reactions is not the only key factor in catalytic activity. Catalysts are designed not only to *accelerate* reactions; they also should be *selective*. In other words, a catalyst should speed up the right reaction, not simply every reaction. As a consequence, the activation barrier for the desired product should be decreased much more than the barriers for other, undesired products [2].

Catalysis can be classified into various types. One important type of catalysis is homogeneous catalysis where the catalyst and the reactants exist in the same phase. Two prime examples of homogeneous catalysis are the condensation of esters to polyesters and the hydroformulation of alkenes to aldehydes (solvents, detergents, alcohols). Biocatalysis forms another important branch of catalysis. In this discipline, enzymes are used as biochemical catalysts. One of the most common reactions in this field is photosynthesis. When the reactants and the catalyst are present in different phases, one speaks of heterogeneous catalysis. Heterogeneous catalysis plays a key role in the large-scale production of plastics, liquid fuels, fertilizers, pharmaceuticals and many other every-day chemicals. Another important application is pollution control, in particular in the automotive

industry [3-4]. Within heterogeneous catalysis the most common reactions are those in which the reactants and the products are in the gas phase while the catalyst is in the solid phase. Due to the fact that mass transport processes in the solid phase are slow compared to the reaction rates, the chemical reaction usually takes place at the gas-solid interphase, i.e. at the surface of the solid catalyst. The work presented in this thesis is related to heterogeneous catalysis.

1.2 The three-way catalyst

One of the best-known important applications of heterogeneous catalysis is the three-way catalyst, which is used to efficiently remove harmful components from the exhaust gas of car engines. This catalyst has high rates for the conversion of three different types of gases, namely NO_x, CO and hydrocarbons. These gases have harmful effects either for human health or for the environment. CO is poisonous. The oxides of nitrogen contribute to acid rain, low level ozone and smog formation, which exacerbate breathing problems [3-4]. The hydrocarbons are also involved in the formation of smog. The main reactions, which are important for controlling exhaust emissions, are given by the following stoichiometric equations:

$$CO + \tfrac{1}{2}O_2 \rightarrow CO_2 \tag{1}$$
$$Hydrocarbons + O_2 \rightarrow H_2O + CO_2 \tag{2}$$
$$NO + CO \rightarrow \tfrac{1}{2}N_2 + CO_2 \tag{3}$$
$$H_2 + \tfrac{1}{2}O_2 \rightarrow H_2O \tag{4}$$
$$NO + H_2 \rightarrow \tfrac{1}{2}N_2 + H_2O \tag{5}$$

On the basis of the above reactions the final products should be harmless: N_2, CO_2 and H_2O. These reaction products are thermodynamically favored at typical exhaust temperatures, e.g. 770 K. The three-way catalysts contain the noble metals platinum, rhodium and often palladium. Rhodium exhibits excellent activity for the selective reduction of NO to N_2, only a small amount of Rh being required in the composition of the three-way catalyst. Platinum is used for its contribution to the conversion of CO and hydrocarbons. Palladium plays a similar role. Therefore, commercial three-way catalysts for gasoline engines are often a bimetallic combination of two of these precious metals, e.g. Pt-Rh or Pd-Rh [3, 6-7].

1.3 Surface-science studies

The discipline that deals with the processes taking place on the surface of a solid is called "surface science". It is important to realize that the structure and electronic properties of the surface of a solid are very often different

from those of the rest of the solid, the bulk. Related to this also the binding energy for many atoms and molecules at surfaces is different from the equivalent energies in the bulk, and, hence, the chemical properties of the surface are special. In particular, the presence of dangling bonds, uncoordinated atoms, and special sites (at e.g. steps, kinks and point defects) makes the surface a very attractive place for strong chemical interactions. Studies of heterogeneous catalytic systems by means of surface-science tools aim to answer a variety of important, fundamental questions, such as:

(a) How do catalysts work at the atomic or molecular scale?
(b) What are the active sites of a solid catalyst?
(c) What are the intermediate compounds that form at the surface during a catalytic cycle?
(d) How does the morphology of the catalyst surface change during the reaction?

In order to characterize the relevant structural, electronic and chemical properties of a catalytic system a wide range of surface sensitive techniques has been developed over the last decades. Here, we mention just a few of them. The surface chemical composition can be probed by Auger electron spectroscopy (AES), ion scattering spectroscopy (ISS), and secondary ion mass (SIMS) spectroscopy. Techniques like low energy electron diffraction (LEED), surface X-ray diffraction (SXRD), low-, medium- and high- energy ion scattering (LEIS, MEIS and HEIS), thermal energy helium atom scattering (HAS), and photoelectron diffraction (XPD), constitute useful tools for determining the surface structure. Additional information about the geometry of the surface can be obtained by scanning and transmission electron microscopy (SEM and TEM), field-ion microscopy (FIM), scanning tunneling microscopy (STM) and atomic force microscopy (AFM). Surface vibrational properties can be investigated with infrared spectroscopy (IR), Raman spectroscopy, high-resolution electron energy loss spectroscopy (HREELS) and sum frequency generation (SFG) [8-11]. In addition knowledge about the surface composition and atomic geometry is provided by the 'ab initio' methods e.g.: the density functional theory (DFT), the Lattice-gas Hamiltonian, the recently introduced "Wang-Landau" algorithm or the Monte Carlo (MC) simulations. Such methods should quantitatively describe measurable properties without relying on experimental parameters, which implies that they have to start ab initio, e.g., from the self-consistent evaluation of the electronic structure. They provide detailed insight in the electronic rearrangements that lead to bonding and bond breaking. They also give estimations for the energies and energies barriers accompanying these processes [12-14]. The application of these techniques has resulted in important progress in understanding the fundamentals of surface chemistry and catalysis.

In spite of these achievements there are two significant drawbacks of these 'traditional' surface science studies that strongly affect their relevance

to the understanding of many practical catalytic systems. The first one arises from the so-called "pressure gap", which indicates that in industry catalytic processes are usually performed at relatively high pressures (1-100 atm), whereas typical surface-science studies are carried out under well-controlled vacuum conditions. The second discrepancy is that a heterogeneous industrial catalyst almost invariably has a complex structure, whereas only simple model systems (usually single crystals) are used in most surface-science laboratories. This problem is often referred to as the" materials gap". A growing effort has been made in the last decade to bridge these two gaps. Concerning the "materials gap", examining not only the simplest flat surfaces, but also the kinked or stepped surfaces, represents a small step in this context [15]. Another way to tackle the problem is to use metal alloys [16]. Also an increasing number of studies are devoted to more elaborate model systems that reproduce some of the complexity of a practical catalyst, in the form of an ensemble of metal catalyst particles deposited on flat supports of oxides or other, well-defined substrates [17].

In order to overcome the "pressure gap" several types of surface-science instruments have been re-designed in order to enable them to acquire data "in situ" under more realistic (or less unrealistic) conditions, such as higher pressures and higher temperatures [18-21]. As we have mentioned already, the difference between the pressures used in the traditional surface-science research (10^{-10} to 10^{-4} mbar) and the pressures used in typical industrial processes (1-100 bar) is more than 10 orders of magnitude. The pressure of the gas phase plays a weak role in the thermodynamics of the gas-surface interaction via the chemical potential. For example, the chemical potential of oxygen atoms depends as follows on the partial pressure of oxygen molecules in the gas phase and on temperature:

$$\mu_{\mathrm{O}}\left(T,p\right)=\mu_{\mathrm{O}}\left(T,p^{0}\right)+\tfrac{1}{2}k_{B}T\ln\left(p/p^{0}\right) \tag{1.1}$$

where p^{0} is the standard pressure [22], k_{B} is Boltzmann constant, while μ_{O} stands for the chemical potential. This means that if the oxygen pressure p changes for example by a factor 10^{10}, the chemical potential changes by $23k_{B}T$. Although the pressure has only a logarithmic (i.e. weak) effect, it adds up to a significant change in the chemical potential of e.g. 0.3 eV per atom at room temperature over these 10 orders of magnitude. This has the consequence that an oxygen-rich adsorption structure that is energetically unfavorable under ultrahigh vacuum (UHV) conditions might be stabilized by the presence of the high-pressure gas phase.

1.4 Scanning tunneling microscopy and catalysis studies

1.4.1 Introduction

Since its invention in 1981 by Binning, Rohrer, Gerber and Weibel [23], Scanning Tunneling Microscopy has had a tremendous impact on the development of surface science. First of all, it enabled the study of the atomic structure of conducting surfaces, with atomic resolution in real space. Secondly, it had a great influence on the study of homo- and heteroepitaxial thin film growth by investigating growth process at atomic scale [24]. In the last decade STM has also become a powerful technique for the characterization of physical and chemical processes involved in heterogeneous catalysis.

In short, the Scanning Tunneling Microscopy technique can be described as follows. If a sharp, conducting needle (tip) is brought within a few atomic distances from a conducting surface, quantum mechanics predicts that there is a probability for electrons to jump from the tip to the surface and vice versa: the tunneling effect. By applying a voltage V between the tip and the surface, a current I can be generated, which depends exponentially on the distance between the tip and the surface d:

$$I \propto V \exp(-2\kappa d), \tag{1.2}$$

where in simple approximation κ is given by $\sqrt{2m\Phi/\hbar^2}$. Φ is the average work function of the tip and the sample and $\hbar = h/2\pi$, where h is Planck's constant. The strong exponential dependence of the tunnel current on the distance between the tip and the sample leads to extremely high resolution in the STM measurements. The STM experiments in this thesis have been performed in so-called 'constant-current mode', which means that a feedback system has been active to continually adjust the height of the tip in order to keep the tunnel current constant. In order to obtain a topographic map of the surface the tip must be rastered or scanned back and forth across the surface. The resulting STM image can then be viewed as a height map of constant density of electronic states at a fixed energy difference with respect to the Fermi energy E_F. The instrument can also be used for spectroscopic purposes by temporarily freezing the position of the tip and recording a spectrum of the tunneling current as a function of the tip-substrate voltage. Such an *I-V* spectrum provides local information on the electronic structure of the surface [25-26].

In order to meet the requirements for the STM investigation of catalytic systems under realistic conditions, i.e. high pressure, high temperature and flowing gas mixtures, several new ideas have been implemented with respect to the 'classic' design of a scanning tunneling microscope. In the next section we introduce some of the details of our high-pressure scanning tunneling microscope, an innovative design which has allowed us to study catalytic systems under reaction conditions, at elevated temperatures and high pressures.

1.4.2 Our set-up

In this section we briefly introduce the apparatus that was used for the acquisition of the STM data presented in this thesis. A full description of the set-up can be found in previous publications of our group [27-28]. The most important components of our set-up are (1) the main UHV chamber, (2) the high-pressure, flow-reactor STM cell, which is integrated into the main chamber, (3) the sample holder, and finally (4) the gas handling system which allows dosing of highly purified gases mixed in adjustable ratios into the high-pressure cell. We refer to the high-pressure STM cell as the 'Reactor-STM'.

Main chamber

The main UVH chamber has a cylindrical shape and was made from a massive block of stainless steal. The UHV system is mounted in a frame supported on four vibration isolations legs. The base pressure of 1×10^{-10} mbar is achieved and maintained by the use of a combination of turbomolecular, ion getter and titanium sublimation pumps. In order to minimize the vibrations introduced by the pumping, a turbomolecular pump with magnetic bearings has been selected. The UHV chamber is divided in two parts, separated by a UHV manual gate valve. One part is used as the *preparation* chamber, where the sample is prepared and characterized by the means of traditional UHV techniques. For surface preparation there is an ion gun in combination with a high-purity Argon gas inlet for Ar^+ ion bombardment. The sample can be annealed to temperatures of approximately 1200 K with the filament mounted at the back of the sample by radiative heating and electron bombardment. For cleaning purposes a high-purity oxygen inlet is also attached to the chamber. In order to investigate the surface structure and composition before and after the high-pressure exposure this side of the chamber is equipped with a combined low-energy electron diffraction /Auger electron spectroscopy (LEED/AES) system. The Reactor–STM is situated in the other part of the main chamber, the *reactor* side. Except for the Reactor-STM, which is described below, the reactor side contains a quadrupole mass spectrometer (QMS). The QMS is used for residual gas analysis in the UHV system and for the analysis of the composition of the gas that leaves the reactor. As will be explained later, the reactor is closed via a replaceable Kalrez seal [29]. This part of the UHV chamber also contains a storage cassette for replacement of damaged Kalrez seals. By use of a wobble stick, located directly above the reactor cell, we can easily replace these seals without breaking the vacuum. The sample can be rotated and moved through the vacuum chamber by a linear transfer rod contained in a bellow. The movement of the transfer rod is driven by an external electromotor. The transfer rod contains electrical connections and

wiring for heating the sample and temperature measurements. Some of the heating elements for vacuum bake out are mounted on the individual vacuum components. Other heating elements have been integrated in the walls of the vacuum chamber. All pumps and gate valves of the main chamber are controlled by a home-built electronic control system.

Reactor-STM

Figure 1.1 shows a schematic representation of the reactor-STM. It mainly consists of a small (400 µl) cylindrical shaped reactor. The reactor walls are gold plated in order to avoid any interference of the walls in the investigated chemical reaction. From one side the reactor is closed by the polished surface of the sample. A thin plate of Kalrez acts like a seal between the polished surface of the sample and the reactor edges. The lower side of the reactor volume is closed by pressing an aluminum tube, which is closed at the bottom side, against a flexible Viton O-ring. This tube is connected to the piezo element of the STM and is used to carry the STM tip. The Viton ring is sufficiently flexible to allow the scanning motion. The piezo element is placed outside the reactor, while the tip (Pt/Ir alloy) is situated inside the reactor. Two gas lines: an inlet and an outlet are attached to the reactor. It should be stressed here that the reactor is not sealed perfectly. In particular, the flexible Kalrez seal constitutes a small leak into the UHV chamber. We put this continuous leak to good us, since it enables us to perform real-time analysis of the gas composition in the reactor during the high-pressure experiments, by use of the quadrupole mass spectrometer.
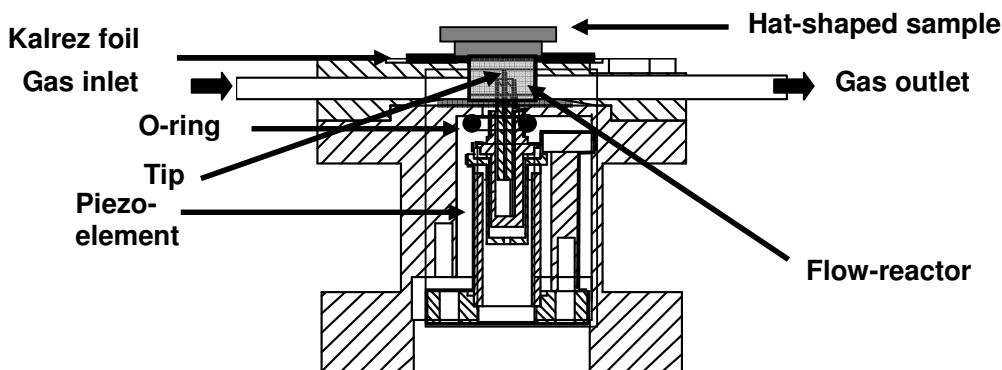

Figure 1.1: *Schematic cross section of the Reactor-STM combination*

Sample holder

The sample holder carries a hat-shaped sample, which is suspended in a tantalum ring. The design of the sample holder has been done in such a way

that it allows heating of the sample both in the flow-reactor and on the transfer rod in the UVH chamber. The heater that is mounted at the back of the sample, in two ceramic plates, consists of a tungsten filament from a commercial halogen light bulb. For focusing purposes during the electron bombardment a quartz tube surrounds the filament. A chromel-alumel thermocouple (pressed directly against the back of the sample), which is electrically isolated by a ceramic tube, provides measurements of the temperature. The sample holder has two wings that slide into clamps when it is placed above the reactor cell. These clamps are used to pull the sample holder down, so that the sample is firmly pressed against the Kalrez seal and closes off the reactor. Since even the compressed Kalrez is somewhat flexible, it forms a deformable element in the mechanical loop between the tip and the sample and thus makes the STM sensitive to vibrations, which limits the spatial resolution. In some of the experiments described in this thesis, we have used a metal support structure between the sample surface and the reactor to close the mechanical loop directly after a few hundred μm compression of the Kalrez seal. This greatly reduced the sensitivity to external vibrations and allowed us to obtain higher-resolution images, as is demonstrated e.g. in Chapter 5 and 6 of this thesis.

Gas handling system

The Reactor-STM inside the UHV chamber is attached to a gas manifold, which has the possibility of pre-mixing a maximum three high-purity gases with the use of mass-flow controllers and pressure regulators. This dedicated gas system consists entirely of stainless steal components. The pressure in the reactor (200 mbar up to 5 bar) is kept constant, independent of the flow settings, via a pressure regulator located in the exit gas line from the reactor. The mass flow controllers can sustain a constant flow between 0-20 ml per minute. In most of the measurements described in this thesis the flow rate have been $3ml_n$/min.

1.5 This thesis

The aim of this thesis is to gain insight into chemical reactions taking place under atmospheric pressures and elevated temperatures. We have made use of the Reactor-STM described above, which is a combination of a flow reactor and an STM. With this instrument we have examined the relation between the structure of metal model catalysts and their catalytic activity. A short introduction concerning CO bonding to transitional metals and the mechanisms proposed for CO oxidation on platinum group metals is given in Chapter 2. Chapter 3 concentrates on the CO oxidation reaction over low- and high-index palladium surfaces, Pd(100), Pd(1.1.17) and Pd(553). We find that by switching from a CO-rich flow to an O_2-rich flow we can

reversibly oxidize and reduce the palladium surface for each of these surface orientations. The reaction on the metal surface proceeds always by the Langmuir-Hinshelwood mechanism. By contrast, the reaction on the oxide occurs via a Mars van Krevelen type of mechanism. In the reaction kinetics, bistability is observed and oscillations in the reaction rate. We determine the experimental conditions for the oscillations and study the influence of catalyst structure, and in particular the effect of steps on the reaction rate. In Chapter 4 a mechanism is proposed for the reaction rate oscillations described in Chapter 3. Chapter 5 describes CO oxidation at atmospheric pressure on the Pt(111) surface, which proceeds similarly to that on Pd(100). In Chapter 6 we learn more about the reaction between CO and O_2 over the (100) surface of platinum. Pt(100) exhibits the so-called quasi-hex reconstruction. The effect of both gases CO and O_2 on the reconstructed structure is discussed. The differences in reactivity between Pt(111) and Pt(100) are also highlighted. Preliminary observations for two very important reactions are briefly presented in Appendix I (NO reduction by CO over Pt(100)) and Appendix II (ethylene epoxidation). The results in these appendices have didactical value and could constitute a basis for future experiments.

1.6 References

[1]   J. H. Sinfelt, *Surf. Sci.* **500** (2002) 923.
[2]   K. W. Kolansinski, *Foundations of catalysis and nanoscience*, John Willey and Sons, LDT 2001.
[3]   B. E. Nieuwenhuys, *Adv. Catal* .**44** (1994) 259.
[4]   H. P. Bonzel, *Surf. Sci.* **68** (1977) 236.
[5]   http://www.platinum.matthey.com/applications/autocatalyst.html
[6]   K. C. Taylor, Automobile catalytic converters, Springer, Berlin, 1984.
[7]   Society of Automotive Engineers, *Cold-start emission control and catalyst technologies*, SAE International, 1996.
[8]   F. Zaera, *Prog. Surf. Sci.* 69 (2001) 1.
[9]   J. W. Niemantsverdriet, Spectroscopy in Catalysis: An Introduction, Wiley-VCH, 2000.
[10]   G. A. Somorjai , Introduction to Surface Chemistry and Catalysis, Wiley-Interscience, 1984.
[11]   G. Attard and C. Barnes, *Surfaces,* Oxford University Press, 1998.
[12]   C. Stampfl, M. V. Ganduglia-Pirovano, K. Reuter, M. Scheffer, *Surf. Sci.* **500** (2002) 368.
[13]   S. Yip (Ed.), *Handbook of material Modelling, Fundamental Models, Methods,* Vol.1, Kluwer, 2005.
[14]   C. Stampfl, *Catalysis Today* **105** (2005) 17.
[15]   H. Y. Hirano, K. Tanaka, J. Siera , and B. E. Nieuwenhuys, *Surf. Sci.* **222** (1989) L804.
[16]   E. Backus, PhD. Thesis, Leiden University, The Netherlands, 2005.
[17]   A. M. de Jong et al., *J. Phys. Chem.* **97** (1993) 6477.
[18]   H. Bluhm, D. F. Ogletree, C. S. Fadley, Z. Hussain, and M. Salmeron, *J. Phys.:Condens. Matter* **14** (2002) L227.
[19]   T. W. Hansen, J. B. Wagner, P. L. Hansen, S. Dahl, H. Topsoe, and C. J. H. Jacobsen, *Science* **294** (2001) 508.
[20]   X. Su, P. S. Cremer, Y. R. Shen, and G. A. Somorjai, *Phys. Rev. Lett.* **77** (1996) 3858.
[21]   P. Bernard, K. Peters, J. Alvarez, and S. Ferrer, *Rev. Sci. Instrum.***70** (1999) 1478.
[22]   K. Reuter and M. Scheffler, *Phys. Rev. B* **65** (2002) 035406.
[23]   G. Binning, H. Rohrer, Ch. Gerber and E. Weibel, *Phys. Rev. Lett.* **49** (1982) 57.
[24]   M. Bischoff, PhD. Thesis, Nijmegen University, The Netherlands, 2002.
[25]   R. Wiesendanger (Ed.), *Scanning Probe Microscopy and Spectroscopy:Methods and Applications,* Cambridge University Press, 1994.
[26]   R. Wiesendanger (Ed.), *Scanning Probe Microscopy: Analytical Methods (Nanoscience and Technology),* Springer, 1998.
[27]   P. B. Rasmussen, B. L. M. Hendriksen, H. Zeijlemaker, H. G. Ficke and J.W.M. Frenken, *Rev. Sci. Instrum.* **69** (1998) 3879.
[28]   B. L. M. Hendriksen, PhD. Thesis, Leiden University, The Netherlands, 2003.
[29]   Kalrez perfluorelastomer, DuPont Dow elastomers L.L.C.; Eriks, Alkmaar, The Netherlands

Chapter 2

Introduction to the theory concerning CO oxidation over platinum group metals

In this chapter a review is given of the literature about CO oxidation on platinum group metals surfaces. First we discuss the CO interaction with these metals, and then we describe the mechanisms behind the CO oxidation on Pt-group metals and the oscillatory behaviour of this reaction.

2.1 CO interaction with platinum group metals

The interaction of CO with platinum group metals has been intensely studied in the last decades [1-3]. It is generally accepted today that carbon monoxide adsorbs as a molecule on such a metal with the carbon atom directed towards the surface and that it can coordinate in several geometries. The CO bonding to metal surfaces is described in the terms of the so-called Blyholder model, which invokes a donor-acceptor mechanism [4]. In this model the bonding occurs through a concerted electron transfer from the highest filled (5σ) molecular orbital of CO to unoccupied metal orbitals (essentially d orbitals), with back-donation occurring from occupied metal orbitals to the lowest unfilled (2π) orbital of CO (Fig. 2.1). The strength of the CO-metal bond might be expected to depend upon: 1) the nature of the adsorbent metal, 2) the crystallographic orientation of the surface, and 3) the geometric location of the adsorbed molecule on a given single crystal plane [5, 6]. Pavão and collaborators are given an excellent review regarding the early pioneering work of Blyholder and the improvements made in the following years by the means of quantum chemical calculations [7].

The three typical, symmetric adsorption positions for CO molecules that are usually considered on a metal terrace are 1) "on-top", the CO standing up on top of a metal atom, 2) "bridge-bonded", the CO being adsorbed above a position midway between two metal atoms and 3) "threefold-coordinated", the CO placed at above a position symmetrically between three atoms of the metal substrate. On the dense (111) and (100) surfaces of the FCC metals, CO prefers the on-top and bridge positions above the high coordination of the threefold adsorption geometry. On rhodium and platinum, CO adsorbs more strongly in the on-top position than in the bridge position, while on nickel and palladium the bridge position forms the stronger bond [8].
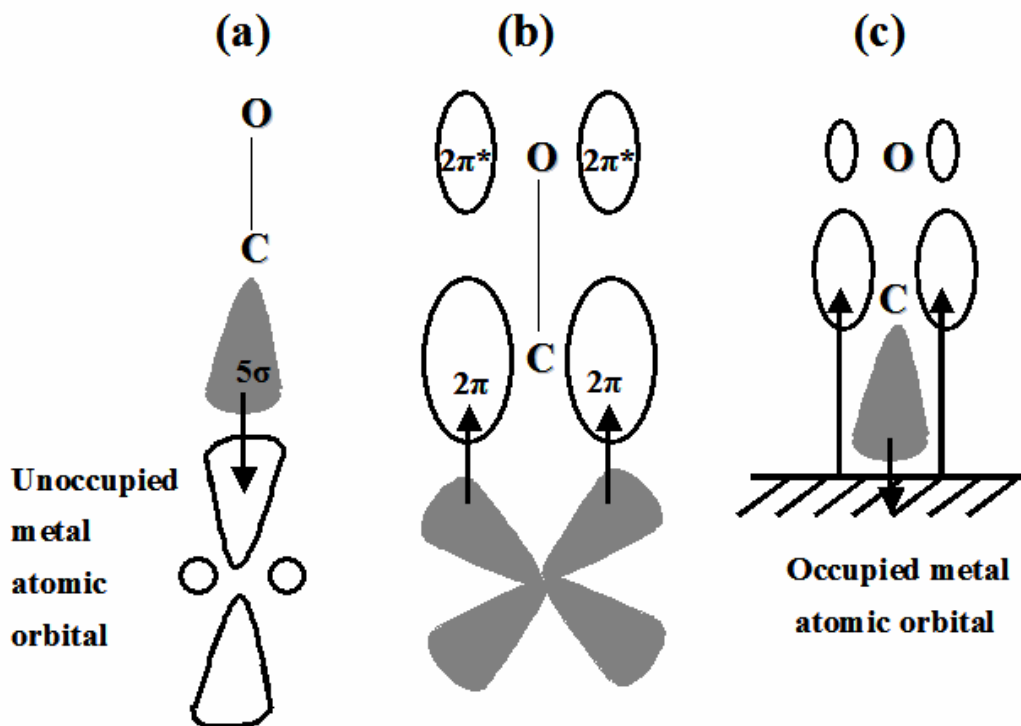
Figure 2.1: A schematic diagram of synergic bonding of CO to a metal. In CO the molecular orbitals are: $1\sigma^2 2\sigma^2 3\sigma^2 4\sigma^2 1\pi^4 5\sigma^2 2\pi^*$. The 4σ orbital is localized on the oxygen atom while the 5σ orbital is localized on the carbon atom and both of these orbitals are non-bonding. The empty $2\pi^*$ antibonding orbital is also available to take parting the interaction with the surface. This combination of σ and π orbitals of CO in the interaction with the surface is called synergic bonding. In the case of molecularly chemisorption of CO, a covalent bond is form by donation of electrons from the 5σ orbital to a vacant metal d orbital (a). At the same time, the full d orbitals are able to donate electron density into the vacant $2\pi^*$ orbitals (b). On adsorption the situation is analogous (c).(adapted after reference [9]).

2.2 CO oxidation over platinum group metals

CO oxidation on platinum group metals surfaces is one of the most widely studied subjects in surface chemistry as a model system of heterogeneously catalysed reactions:

$CO + \frac{1}{2}O_2 \rightarrow CO_2$
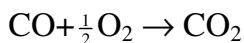
There are several mechanisms that one can imagine for such a reaction on a metal surface, and we will briefly discuss the three most "popular" ones.

Langmuir- Hinshelwood mechanism

Today it is widely accepted that the reaction mechanism for CO oxidation over platinum group metal catalysts follows the so-called Langmuir-Hinshelwood mechanism [10-12], explained in Fig.2.2 a. This mechanism consists of the following steps:

i) Adsorption of reactant molecules from the gas phase onto the surface.
ii) Dissociation of molecules on the surface.
iii) Reaction between adsorbed molecules.
iv) Desorption of the reaction product(s) to the gas phase.

The assumptions underlying the Langmuir-Hinshelwood mechanism are:

1. The solid surface is uniform and contains a number of equivalent sites each of which may be occupied by at most one adsorbate molecule. The surface itself is not modified by the presence of the molecules and molecules on neighbouring sites do not interact with each other.

2. At each temperature a dynamic equilibrium exists between the gas phase and the adsorbed layer. Adsorbate molecules from the gas phase are continually colliding with the surface. If they impact a vacant adsorption site, they can form a bond with the surface and stick. If they strike a filled site, they are reflected back into the gas phase.

3. Adsorption is random and the adsorbate layer is perfectly mixed. This means for example that no de-mixing (domain formation) occurs of adsorbate molecules in the adsorbate layer.

3. Usually one assumes that the reaction rate is sufficiently low with respect to the impingement rate of reactant molecules that the reaction itself does not modify the equilibrium between reactants and adsorbate layer.

Several refinements have been introduced to this basic form of the L-H mechanism, e.g. allowing the surface to respond (reconstruct and de-reconstruct) to the presence of the adsorbates and allowing the adsorbates to cluster into domains, the reaction then proceeding no longer uniformly over the surface but only at the borders between the domains of different reactants [13-16].

Eley-Rideal mechanism

Another reaction mechanism proposed for catalytic CO oxidation is the Eley-Rideal mechanism [17]. In this mechanism a surface reaction does not involve two adsorbed surface species. If a gas-phase molecule strikes a previously adsorbed molecule there is a possibility that the collision leads to reaction and that the product escapes directly into the gas phase as shown in Fig.2.2 b. Great efforts have been made to prove experimentally that this mechanism occurs [18-19]. Rettner provided the most convincing evidence for an E-R mechanism by investigating the following reactions: $H_{(g)}+D/Cu(111)$ and $D_{(g)}+H/Cu(111)$ [20].
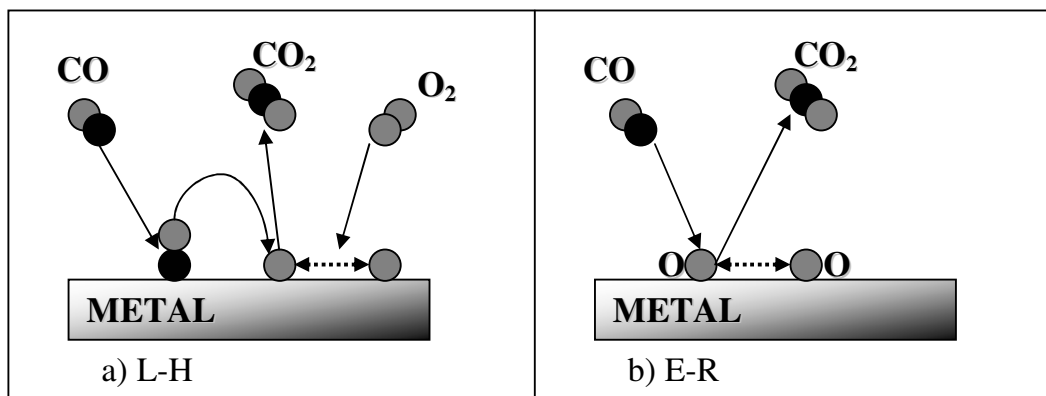
Figure 2.2: *Schematic representation of the Langmuir-Hinshelwood mechanism (a) and the Eley-Rideal mechanism (b) for the catalytic oxidation of CO. Dark balls correspond to the carbon atoms and grey balls correspond to the oxygen atoms.*

Mars van Krevelen mechanism

In a recent publication, Over and collaborators have proposed an alternative mechanism for CO oxidation over RuO_2 [21]. This mechanism is known as the Mars van Krevelen mechanism (MvK), named after the two scientists, who proposed it in 1954 [22]. Shortly after Over suggestion, Hendriksen and Frenken have provided direct evidence for the Mars van Krevelen mechanism being responsible for the oxidation of CO over the (110) orientation of platinum at atmospheric pressure [23]. In later publications the same authors showed that the MvK mechanism is also active in the CO oxidation over the (100) surface of palladium [24]. In short, the characteristic feature of the MvK mechanism is that some products of the reaction leave the solid catalysts' surface with one ore more constituents of the catalysts' lattice. In other words, the catalyst participates more actively in the reaction, playing the role of an intermediate product rather than merely a suitable substrate. The MvK mechanism consists of the following steps (Fig.2.3). First in an oxygen-rich environment, i.e. at a high partial pressure of O_2, and at elevated temperatures, the metal will oxidize. Depending on the detailed energetics of the metal and the oxide, either a thin film forms, as has been found for Pt(110) [25], or the oxidation slowly proceeds further into the metal, as seems to be the case for Pd(100) [26]. After the palladium oxide has been formed at the surface, CO molecules adsorbed on the oxide from the gas phase will react with oxygen atoms from the oxide to produce CO_2. The resulting oxygen vacancies are refilled rapidly by oxygen from the gas phase. In the STM observations by Hendriksen *et al.*, it was observed that during the MvK reaction roughness is formed as a 'by-product' of the reaction [23]. This is ascribed to the fact that each oxygen vacancy renders several palladium atoms temporarily under-coordinated, which introduces a small probability for them to diffuse out of

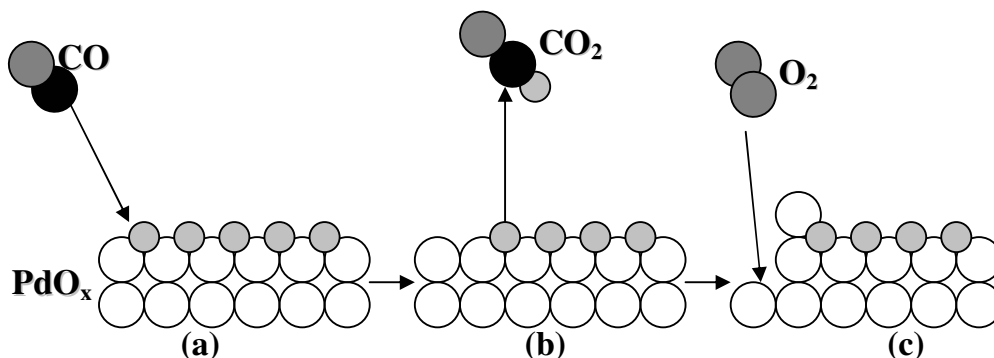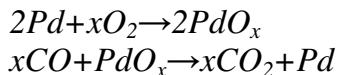their original position in the oxide, leaving behind pits in the surface and forming new protrusions on top.

$$2Pd + xO_2 \rightarrow 2PdO_x$$
$$xCO + PdO_x \rightarrow xCO_2 + Pd$$

Figure 2.3: *Schematic representations of the Mars Van Krevelen mechanism. The empty balls represent Pd atoms. Small grey balls represent the oxygen atoms from the palladium oxide, the dark balls correspond to the carbon atoms and the regular-sized grey balls correspond to the oxygen atoms from gas phase. (a) PdO_X and a CO molecule diffusing to the surface. (b) Reaction between the CO molecule and one oxygen atom from the palladium oxide, the formation of the CO_2 molecule and its diffusion in the gas phase. (c) The diffusion of the left uncoordinated Pd atom and the refill of the vacancy left by the oxygen atom, with oxygen from the gas phase.*

2.3 Oscillatory CO oxidation over platinum group metals

One of the most fascinating aspects of chemical reactions taking place under conditions far from equilibrium is the possibility to exhibit instabilities and oscillations. Two key features are used to describe such phenomena: "nonliniarity" and "feedback". If the first term is related to the mathematics behind these processes, the feedback arises when the products of later steps in the mechanism influence the rate of some of the earlier reactions steps (and, hence, the rate of their own production). This may take the form either of positive feedback (self-acceleration) or negative feedback (self-inhibition) [27]. Another phenomenon closely related to self-sustained oscillations is that of multiplicity of stationary states. In other words under constant external conditions the reaction has more than one stationary state compositions to choose from. A well-known example in heterogeneous catalysis is the oscillating oxidation of CO on platinum group metals (mainly Pt and Pd). As mentioned previously in this chapter, CO oxidation over Pd surfaces is thought to follow Langmuir-Hinshelwood kinetics, similar to the same reaction on other platinum group metals [2]. The kinetics

of a reaction that follows the Langmuir-Hinshelwood can be visualized quite well in a plot of the reaction rate r_{CO} vs. p_{CO}, which is sketched in figure 2.4. At low CO pressure adsorbed oxygen atoms predominantly cover the surface. In this range nearly every CO molecule that strikes the surface is adsorbed and rapidly consumed by reacting with neighbouring adsorbed oxygen atoms and the rate increases linearly with P_{CO} [8]. The rate is limited by CO adsorption in this range. With increasing P_{CO} the concentration of adsorbed CO molecules increases and begins to inhibit the adsorption of oxygen. The rate of CO_2 production passes through a maximum when the coverages of CO molecules and oxygen atoms, θ_{CO} and θ_O are equal and it decreases due to progressive inhibition of O_2 adsorption with further increase of CO pressure. The existence of high and low rate branches of the reaction can be associated with the asymmetric inhibition of the reaction by the two adsorbates. In this case CO forms a densely packed layer upon which O_2 cannot dissociatively adsorb. Conversely oxygen atoms form an open adlayer into which CO readily adsorbs. Therefore, the reaction is poisoned only by high coverages of CO and the reaction rate exhibits two branches. Is not the aim of this section to describe the mathematical modelling of the LH kinetics, but for a better understanding of fig.2.4 few notions must be introduced. Is generally accepted that the temporal evolution of a system can be described by a couple of differential equations:

$$\frac{dx_i}{dt} = F_i(x_i, \mu) \tag{2.1}$$

where F_i contains the kinetics of species *(i)* and μ is a vector representing the parameters of the system such as pressure, temperature, etc. The dynamical behaviour of the system is usually represented by a trajectory moving in an n-dimensional phase space where the concentrations of the n species $X_i......X_n$ denote the axes. For simplicity we will just refer at two-dimensional systems [28]. The solutions of the differential equations in this case are called stationary solutions, equilibrium points, steady state points, rest points or fixed points [29]. The term bifurcation denotes a qualitative change in the character of the solution as a parameter is varied such as, for example, a transition from a stable steady state to oscillatory behaviour. The simplest type of the bifurcation that can occur in a dynamical system is from monostability to bistability. This transition is known as the saddle-node bifurcation. In the monostable system all the trajectories converge to a single fixed point that represents the stable stationary state of the system. As the bifurcation parameter μ (pressure, temperature, etc.) is varied, a second stable node may be created so that two stable stationary states coexist, the system has become bistable. Together with the second stable node a third fixed point is created which is called a saddle point. If the stable node attracts the vector flow in all directions, a saddle point is characterized by

having an attractive as well as a repellent direction. If the appropriate feedback exists in a system with bistability of stationary states that link the two states, the system will start to oscillate. All this theory is illustrated in fig. 2.4 where the filled squares correspond to the two stable nodes, while the open squares correspond to the saddle points [27-29].
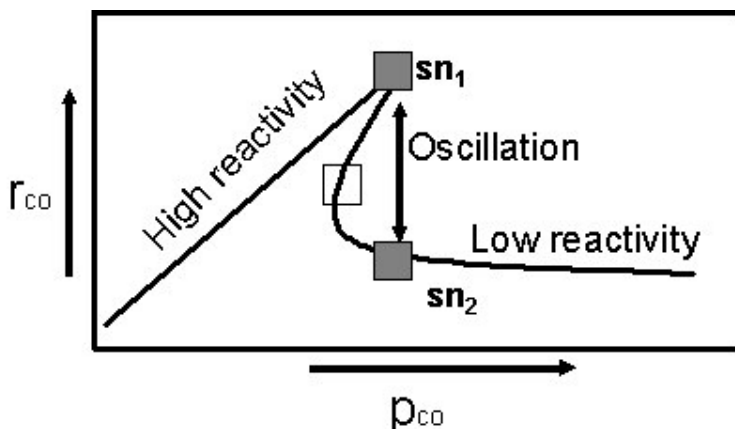
Figure 2.4: *The CO oxidation rate on a platinum group metal surface as a function of P_{CO}. Two branches of the reaction rate exist (adapted from ref. [28]).*

To summarize, under the steady flow of reactants the reaction rate exhibits three different reactive regimes. These are a *high reactivity* branch, a *low reactivity* branch and a *transition region* connecting the two branches. In the transition region, under specific reaction conditions, oscillations can occur when an additional feedback process is active.

2.4 Summary

In this Chapter we have tried to give a short review of the terms used in the literature to describe CO oxidation on platinum group metals. We have discussed the CO bonding to these metals, the existent mechanism in literature proposed in the literature for the catalytic CO oxidation on these metals and the oscillatory behaviour of such catalytic systems.

2.5 References

[1]   S. L. Bernasek and S. R. Leone, *Chem. Phys. Lett.* **84** (1981) 401.
[2]   G. W. Coulston and G. L. Haller, *J.Chem.Phys.***93** (1991) 6932.
[3]   C. T. Cambell, G. Ertl, H. Kuipers and J. Segner, *J.Chem.Phys.***73** (1980) 5862.
[4]   G. Blyholder, *J. of Chem.Phys.***68** (1964) 2772.
[5]   M. Boudart and G. Djéga-Mariadassou, *Kinetics of Heterogeneous Catalytic Reactions* (Princeton University Press, Princeton, NJ, 1984).
[6]   B. E. Nieuwenhuys, V. Ponec, G. van Koten, P. W. N. M. van Leeuwen and R. A. Santen, Bonding and elementary steps in catalysis, Chapter 4 in *Studies in Surface Science and Catalysis* **79** (Elsevier Science Publisher, B. V. Amsterdam, 1993).
[7]   A. C. Pavão et al., *J. of Molec. Struct. (Theochem)* **458** (1999) 99.
[8]   Kurt W.Kolasinski, *Surface Science-Foundations of Catalysis and Nanoscience,* (John Wiley &Sons, 2002).
[9]   E. M. McCash, S*urface Chemistry* (Oxford University Press ,2002)
[10] I. Langmuir, *Trans. Farad. Soc.***17** (1922), 621.
[11] C. N. Hinshelwood, *The kinetics of Chemical Change,* Clarendon Press, Oxford, 1940.
[12] T. Engel and G. Ertl , *Adv. Catal.***28** (1979)1.
[13] G. Ertl, *Langmuir* **3** (1987) 4.
[14] J. S. Wang , *Proc .R. Soc. London, Ser. A* **161** (1937) 127.
[15] D. L. Adams, *Surf.Sci.***42** (1974) 12.
[16] D. A. King , *Surf.Sci.***47** (1975) 384.
[17] D. D. Eley and E. K. Rideal, *Nature* **146** (1946) 401.
[18] C. C. Cheng e*t al.*, *J. Am Chem. Soc.* **114** (1992) 1249.
[19] K. R. Lykke and B. D. Kay, in *Laser Photoionization and Desorption Surface Analysis Technique-SPIE Proceedings, Volume 1208,*ed. N/ S. Nogar (SPIE, Bellingham, WA,1990) p.18.
[20] C. T. Rettner, *Phys. Rev. Lett.* **69** (1992) 383.
[21] H. Over, Y. D.Kim, A. P. Seitonen, S. Wendt, E. Lundgren, M. Schmid, P. Varga, A. Morgante, and G.Ertl ,*Science* **287** (2000)1474.
[22] P. Mars and D.W. van Krevelen, *Spec. Suppl. to Chem.Eng.Sci.***3** (1954) 41.
[23] B. L. M. Hendriksen and J. W. M.Frenken, *Phys. Rev.Lett.***89** (2002) 046101.
[24] B. L. M. Hendriksen, S. C. Bobaru and J.W.M.Frenken, *Surf.Sci.***552** (2004) 229.
[25] M.L. D. Ackermann *et al.*, *Phys. Rev. Lett.* **95** (2005) 255505.
[26] M. L. D Ackermann *et al.*, to be published
[27] S. K. Scott, *Oscillations, waves and chaos in chemical kinetics,* (Oxford University Press, 1994.)
[28] R.Imbihl, *Prog. In Surf.Sci.* **44** (1993) 185.
[29] M. M. Slin'ko and N. I. Jaeger, *Oscillating heterogeneous catalytic systems,*(Elsevier, 1994.)

Chapter 3

CO oxidation over palladium surfaces

In this Chapter we describe and interpret Scanning Tunneling Microscopy and Mass Spectrometry experiments on CO oxidation at ambient pressure and elevated temperatures over three palladium surfaces: Pd(100) ,its vicinal surface Pd(1.1.17) and Pd(553). We show that all three surfaces can be oxidized under sufficiently oxygen-rich conditions, which is accompanied by a change in reaction kinetics. On two of these three surfaces we observe reaction oscillations.

3.1 Motivation

As a catalyst palladium is known to be highly effective for various oxidation reactions such as the complete oxidation of hydrocarbons in automotive exhaust gas and methane combustion in advanced, low NO_x gas turbines. Palladium-based alloys are actively investigated for applications in fuel technology. Palladium's ability to absorb and re-emit hydrogen depending on temperature and pressure conditions makes it an efficient material to filter hydrogen. Palladium is also a critical catalyst in the manufacture of polyester and in the removal of a number of toxic and carcinogenic substances from ground water [1-7]. Other important reactions for palladium catalysts are the hydrogenation of olefins and aromatic nitro compounds. Self-sustained oscillations in the reaction rate have been observed during CO oxidation over palladium crystals. Since the understanding of the mechanism behind the self-sustained oscillations has great importance in physics, chemistry, biology and technology, palladium is also a popular model catalyst in fundamental catalysis research [8-10]. In addition, palladium is used to make springs for watches, surgical instruments, electrical contacts and dental fillings and crowns. And palladium is also compatible with human tissue and it is used, in a radioactive form, in the medical industry for the treatment of cancer [1].

3.2 Relation between the efficiency and the crystal structure of a palladium catalyst: a literature overview

Experimental studies have revealed that the catalytic combustion over Pd catalyst is a structure sensitive reaction (the rate depends on the detailed geometrical structure of the surface atoms of the catalyst) [11-13]. Structure sensitivity usually manifests itself as a dependence of the rate per surface atom on the average size of the catalyst particle. For example, Henry et al.,

who showed that the average CO chemisorption energy increases strongly with decreasing particle size, have demonstrated the structure sensitivity for CO adsorption on small Pd particles [14]. The high efficiency of palladium has been ascribed to its ability to dissociate oxygen molecules by forming a surface oxide [15]. Also the oscillations in the CO and CH_4 oxidation rates [16-20] and the extreme sensitivity of the CH_4 oxidation rate to catalyst history [3-5,20] have been attributed to a transition between the metallic and the oxidic state. In the light of these observations it is no wonder that numerous studies have been initiated in order to characterize the oxidation and reduction mechanism of Pd surfaces on the atomic scale using a variety of surface science techniques. For example, E.H. Voogt and co-workers have studied the interaction of oxygen with Pd(111) and with a palladium foil by use of ellipsometry, LEED, AES and XPS in the temperature range of 300 to 770 K and at pressures up to 1 Pa [21]. They have reported the formation of a surface oxide at higher temperatures (T>470 K) and pressures (P>10^{-4} Pa), ascribed to a square lattice with a=7.5±0.5Å and domains in six orientations. It was not possible to match this structure with a simple overlayer structure on the (111) plane or with an unreconstructed crystal plane of PdO. G. Zeng and E.I Altman have examined the oxidation of Pd(111) [22] and Pd(100) [23] by means of TPD, LEED and in-situ, variable-temperature STM. The oxidation of Pd(111) was observed to proceed in three stages, involving four distinct oxygen phases, all stages showing a strong dependence on the oxygen coverage. In the third stage corresponding to oxygen coverages higher than 2.2 ML the formation of a bulk PdO oxide was observed. The same was found for Pd(100) with the difference that bulk oxidation proceeded on this surface through four stages involving up to five surface phases. On both surfaces, bulk PdO formation is accompanied by surface roughening. The more open Pd(100) surface has shown a higher reactivity towards O_2. Density Functional Theory (DFT) calculations have suggested that for Pd, thin surface oxides can be stable at atmospheric pressure, in oxygen-rich flow [24]. In summary there is enough experimental and theoretical evidence for the formation of palladium oxides under certain reaction conditions. In spite of this large amount of information there is no consensus concerning the role played by these oxides in the chemical reactions. In the next section of this chapter we will provide direct experimental proof that the surface palladium oxides are intermediate products of the reaction, which act as active catalysts for the oxidation of CO at atmospheric pressure.

3.3 Electronic and structural information about Pd

Before showing the experimental results we mention a few bulk properties of our model catalyst material. Palladium is one of the late 4d transition metals. It has 46 electrons per atom and an almost complete 4f shell. The

equilibrium crystal structure of Pd is a face-centered cubic Bravais lattice, with one atom in the primitive unit cell. The lattice constant at room temperature is a_{exp}=3.89 Å and the nearest-neighbour distance between Pd atoms is 2.75 Å. The Pd(100) surface has a square symmetry, Fig.3.1. The step height is 1.96 Å. The Pd(1.1.17) has (100) terraces of 8.5 atoms wide separated by (111) monoatomic steps (not shown in Fig.3.1). The Pd(553) surface is vicinal to the (111) low-index surface and consist of (111) terraces with a width of 5 atoms (10.3 Å) separated by monoatomic, (111)-type steps.
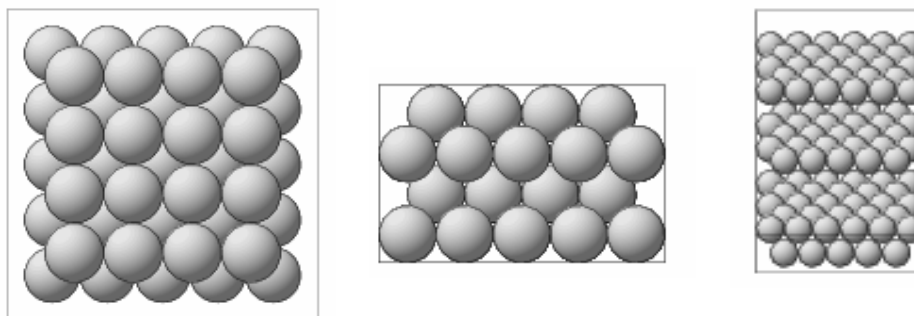

Figure 3.1: *The profile and side view of the (100) surface of a palladium crystal, and the Pd(553) surface represented as a ball model.*

3.4 Experimental

The Pd single crystal was cut by spark erosion polished mechanically to within 0.1° from the (100) orientation [25]. After introduction into the UHV chamber, the sample was cleaned by repeated cycles of 600 eV Ar-ion bombardment at 300 K, followed by annealing at 900 K in 10^{-6} mbar oxygen, and by a short flash to ~1100K in UHV until a clear LEED pattern was obtained.

3.5 Results and discussion

Figure 3.2 displays the oscillatory behaviour of the $CO+O_2$ reaction over Pd(100) at a constant total pressure of 1.25 bar and a temperature of 408 K. In figure 3.2 a the partial pressures of the reactant gases CO and O_2 and the reaction product CO_2 are depicted. The experiment started at t = 0 s in a CO-rich flow. At t = 188 s we switched to an O_2-rich flow (indicated by the dashed line). In response, the reaction rate, which can be read off from the partial pressure of CO_2, initially increased, passed through a maximum at t = 610 s and then decreased as the CO pressure was slowly lowered further. This behaviour is fully consistent with Langmuir-Hinshelwood kinetics (Chapter 2). At t = 3615 s there was a sudden step up in the CO_2

pressure (indicated by arrow number 1) and spontaneous oscillations followed. Coinciding with the upward step in the reaction rate we see a downward step in the CO partial pressure. We attribute the sudden increase in the reaction rate to a transition from a metallic surface with low catalytic activity to a surface oxide with higher catalytic activity [26-28]. In Chapter 2 of this thesis we have already mentioned that the CO oxidation over an oxide does not proceed via the "classic" Langmuir-Hinshelwood mechanism. The reaction occurs via the Mars van Krevelen mechanism, which requires the presence of a surface oxide and involves reactions between CO molecules from the gas phase and oxygen atoms from the surface oxide. Later in this section we provide further evidence for this scenario by use of STM images simultaneously recorded with the reaction kinetics. The oscillations in Fig.3.2 (a) have a block-wave character. At the beginning of the oscillation the times spent at the upper and lower reactivities were comparable (110 s and 90 s, respectively). At later times, i.e. for lower P_{CO}, the surface spent significantly less time in the metallic phase (31 s) while the time spent in the oxide phase decreased only slightly (72 s). This made the shape of the oscillations gradually changes from the initial square wave pattern to a series of (negative) peaks. While the CO partial pressure dropped, the CO_2 production rate in the metallic phase remained more or less constant, while the rate in the oxidic phase decreased, until at ~6500 s the difference between the two could no longer be observed. At t = 6909 s we have manually added a small amount of CO in the reactor. Simultaneously with the resulting increase in CO signal the reaction rate briefly dropped (marked by arrow 2 in the Fig.3.2 (a)) and immediately increased again. At this point, we have no explanation for this temporary dip in the reaction rate. At t = 8283 s (indicated by arrow number 3) the reaction rate again spontaneously increased stepwise, simultaneous with a decrease of the CO pressure and the catalytic system started again to spontaneously oscillate. This shows that the surface switched to the oxide phase and that immediately before 8283 s it must have been in the metallic state. The new series of oscillations evolved in time almost identically to the first oscillation series. At t = 10854 s we have switched to a CO rich flow. After a tiny, initial dip, the reaction rate passed through a significant maximum. Although we again have no explanation for the small dip, the maximum in the CO_2 production is easily recognized as Langmuir-Hinshelwood behaviour, starting with a low production on a surface dominated by adsorbed oxygen atoms (*not* an oxide), passing through a maximum-rate when the coverages of the two reacting species are equal ($\theta_{CO} = \theta_O = 0.5$), to end up at a dramatically decreased rate when the partial pressure of CO is high enough to make CO poison the surface. When we again increased the O_2 partial pressure at t = 17673 s, the reaction rate initially increased, then passed through a maximum, after which it decreased again. This is the same sequence of Langmuir-Hinshelwood kinetics in reversed order. After this we

observed a sequence of oscillations, starting at t = 20953 s, that was very similar to the first two series of oscillations. We now have a more detailed look at the first series of oscillations, which we plot in Fig.3.2 (b) as the CO_2 pressure (P_{CO_2}) as a function of CO pressure (P_{CO}). All data in this plot fall on two reaction branches, reflecting the bistability of the system. These two branches have been identified before for Pt(110) [26]. The lower branch corresponds to the Langmuir-Hinshelwood reaction on the metallic surface (R_{metal}), the higher branch to the Mars-van-Krevelen reaction on the oxide surface (R_{oxide}). What is different from the case of Pt(110) is that the present catalytic system of CO oxidation on Pd(100) is unstable and the system oscillates between the two states of the surface. We have observed that the reaction rate on the oxide branch is proportional to P_{CO} while the reaction rate on the metallic surface depends on both P_{CO} and P_{O_2}. In Fig.3.2 © we have the same type plot for the second oscillation series, to illustrate that this series is almost identical to the first series of oscillations. In the sequence of Fig.3.2 (a) the surface has been brought into and taken out of oscillation three times. The ratio $P_{CO}/\sqrt{P_{O_2}}$ at which the metal surface switched to the oxide and started to oscillate amounted to 0.040 $\sqrt{bar}$, 0.039 $\sqrt{bar}$ and respectively 0.037 $\sqrt{bar}$. From the small but statistically significant reduction in this ratio we see that after every series of oxidation-reduction oscillations, the surface oxidizes at a somewhat lower $P_{CO}/\sqrt{P_{O_2}}$ ratio. Combined with our observation that the oxidation-reduction cycles slowly makes the surface more and more rough (see below), this suggests that the $P_{CO}/\sqrt{P_{O_2}}$ ratio at which the surface oxidizes depends on the surface roughness and is thus sensitive to the 'history' of the model catalyst.

All our experiments concerning the oscillatory oxidation of CO over Pd(100) exhibited hysteresis in the CO_2 production rate (upon variation of P_{CO}) with a counter-clockwise orientation in the P_{CO_2}-versus-P_{CO} plot. In other words the oxide was formed on the Pd(100) surface at a higher P_{CO} value than that at which it was later reacted away. This observation is consistent with previous experimental studies performed by other researchers in the field of oscillatory CO oxidation on palladium surfaces, which also indicate the requirement of counter-clockwise hysteresis for the occurrence of oscillations [9, 16].

The upper part of Figure 3.3 shows a series of STM images, which were recorded simultaneously with the self-sustained oscillation plotted in the lower panel. Image A has been acquired immediately before the first oscillation. It shows the metallic surface with (rounded) square adatom islands, reflecting the symmetry of the (100) plane. The measured height of the adatom islands is equal to the monoatomic step height of Pd(100) of 1.96 Å. Image B was acquired at the same position, immediately after image A. Despite the low resolution one can recognize a noticeable difference in the morphology of the surface compared to image A. The adatoms islands have

disappeared or have been replaced by a high density of cluster structures. Image B was recorded immediately after the step up in the reaction rate.
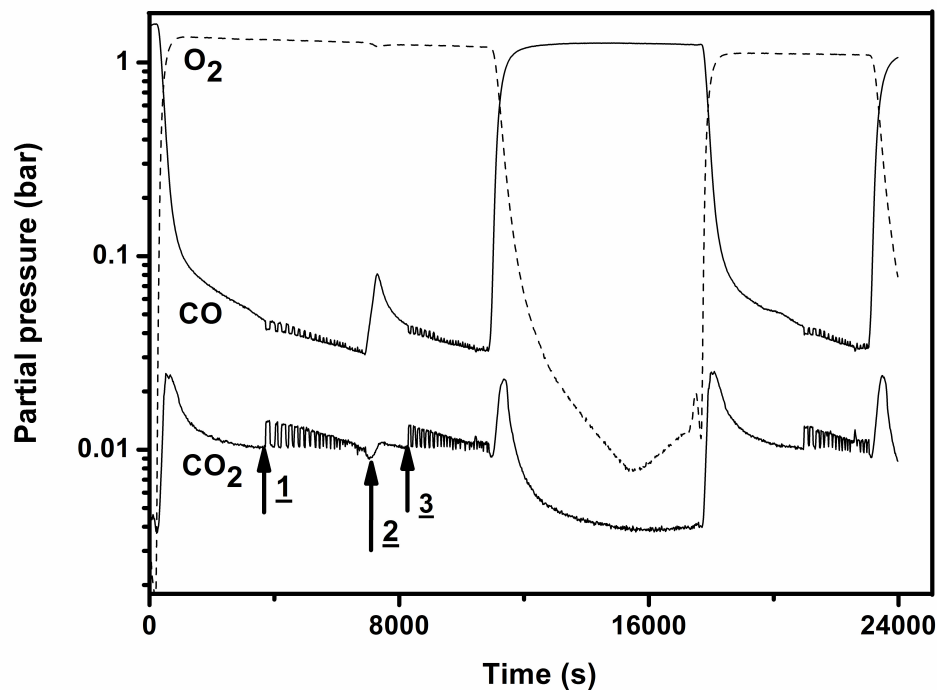
(a)
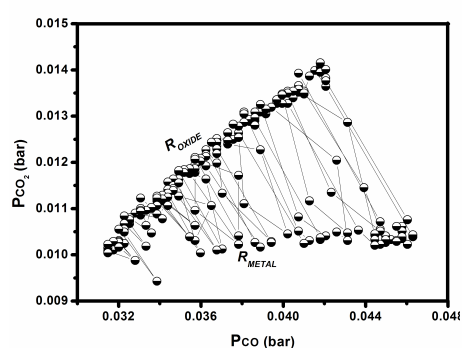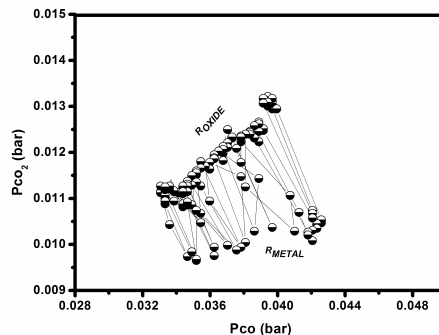
(b)   **(c)**

Figure 3.2: (a) Partial pressures of CO, O_2 and CO_2 on Pd(100) at T = 408 K and P_{tot} = 1.25 bar. The CO and O_2 pressures were regulated (upstream), while the CO_2 reflects the catalytic conversion rate. The first and second series of oscillations in these measurements have been re-plotted in panels (b) and (c) respectively as P_{CO_2} against P_{CO}.

The sudden increase in the reaction rate correlated with the change in the surface structure in an oxygen-rich environment suggests that the surface switched from a metal to an oxide with higher reactivity towards CO oxidation, similar to what has been found previously on Pt(110) [26]. The

changes in the surface structure associated with the variations in reactivity are better illustrated by images C and D. They were acquired during the third and the fourth periods of the first series of oscillations. In both images, the surface spontaneously switched between a structure with monolayer deep protrusions and depressions with square symmetry (lower part of images C and D), corresponding to the metal, to structures with a rougher appearance and with non-integer height differences, corresponding to the oxide (upper part of the images). Images illustrate that the self-sustained oscillations are spontaneous metal-oxide phase transitions.
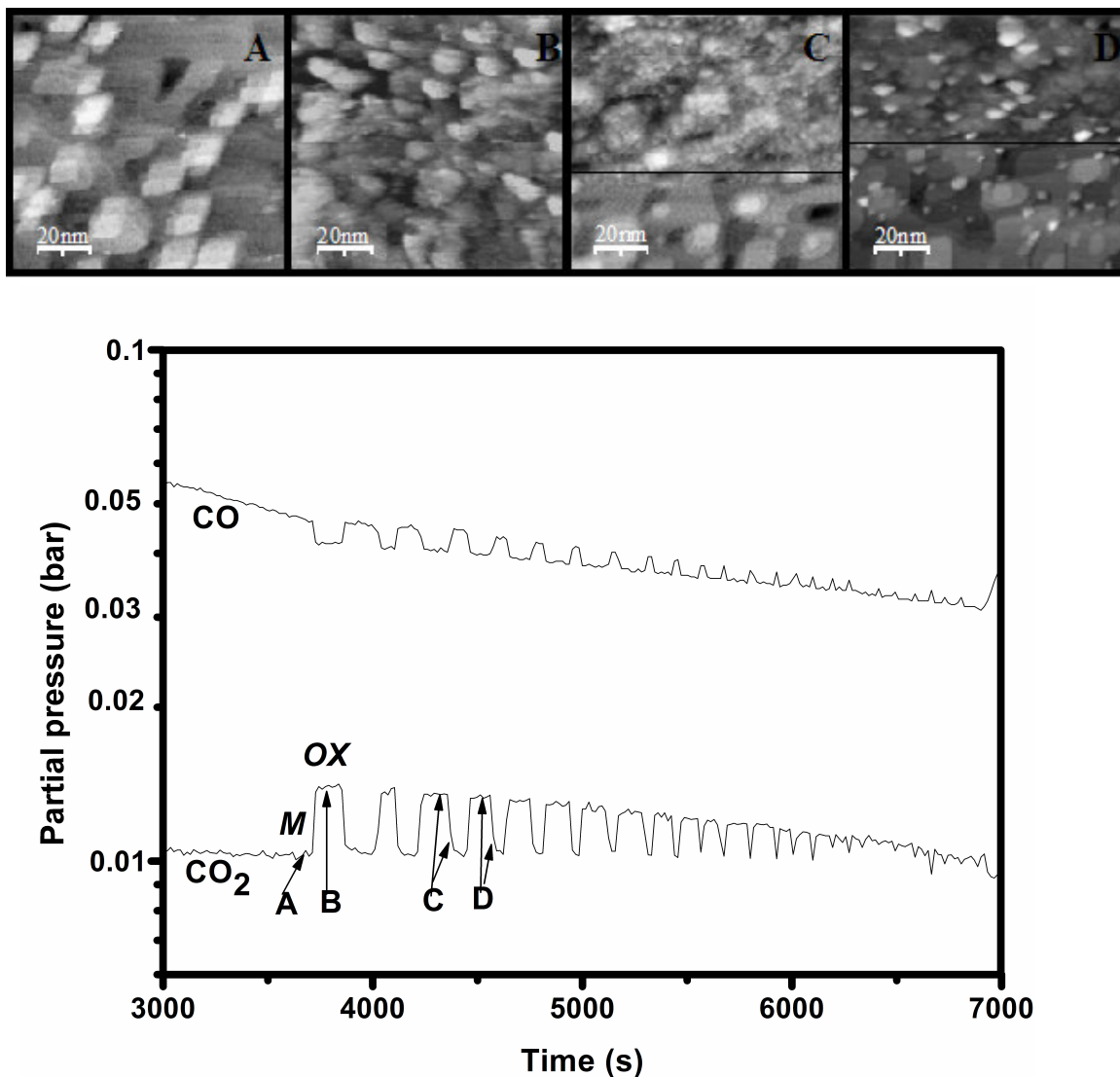
Figure 3.3 STM images (upper part; 100 nm × 100 nm) simultaneously recorded with the kinetics of the reaction (lower panel) under oscillation conditions. Letters A-D in the lower panel indicates the time at which the images have been taken. The letter M from the kinetics graph stands for the metallic surface, while Ox corresponds to the oxidic surface. The tunnelling conditions were: Vt = 100 mV, I_t = 0.2 nA.

25

The acquisition of the STM images under reaction conditions where the oscillations occurred has been very difficult. The CO oxidation reaction is highly exothermic. The switching in the reactivity was accompanied by small changes in sample temperature, reflected in the thermal drift visible in the images. Due to the repeated phase transitions between the oxide and the metal the surface diffusion made the tip unstable.

Figure 3.4 displays oscillations in the reaction rate during CO oxidation over Pd(100), acquired at a constant total pressure of 1.25 bar and three different temperatures. In Fig.3.4 a two series of oscillations can be seen at 408 K. Figure 3.4 b shows two periods from the second series. The oscillations are regular and their shape is almost identical. The oscillations in Fig .3.4 c and d were acquired at 413 K and 403 K respectively. The shape and the period of the oscillations vary upon the variation in the temperature as illustrated in fig. 3.4.

(a)   (b)

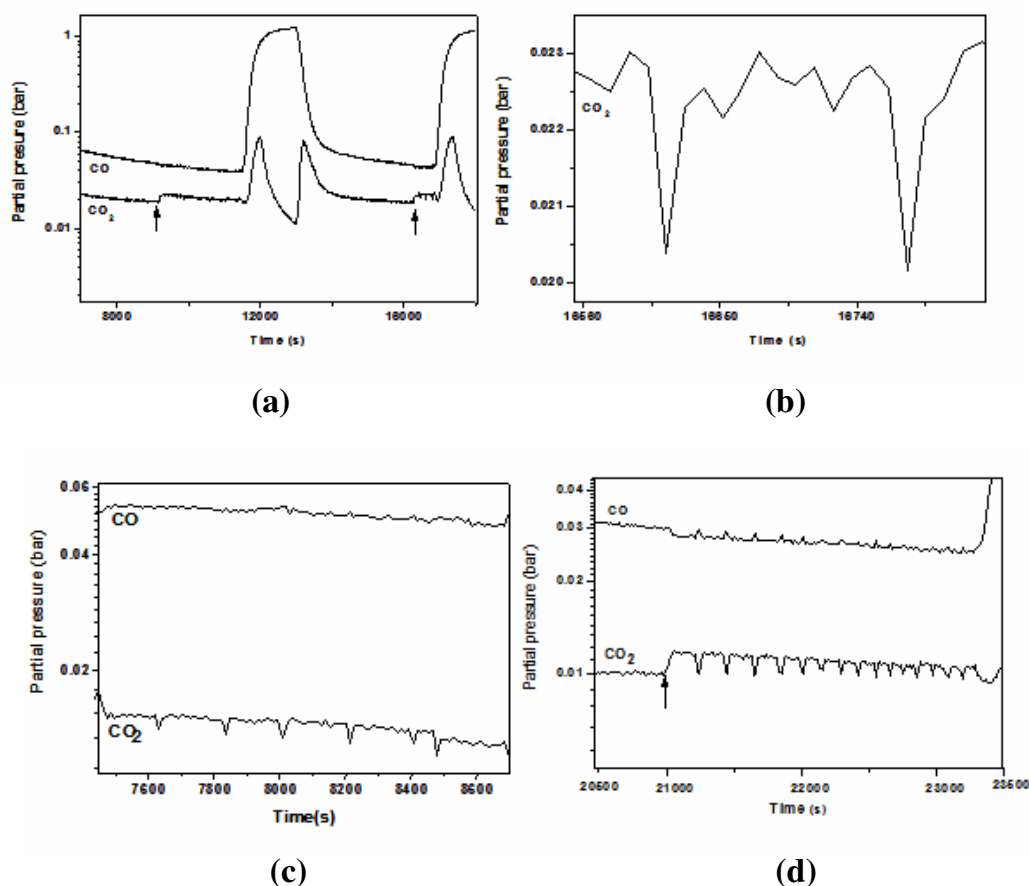(c)   (d)

Figure 3.4: *Oscillatory behaviour of CO oxidation over Pd(100) at a total pressure of 1.25 bar and temperatures of (a) 408 K, (b) 408 K, (c) 413 K and (d) 403 K.*

26

3.6 Summary for CO oxidation on Pd(100)

Oxidation of CO on a Pd(100) surface has been studied at atmospheric pressure and various temperatures around 410 K. Under these reaction conditions the reaction rate exhibits bistability, hysteresis and oscillations. The traditional Langmuir-Hinshelwood reaction runs on the metallic form of the palladium surface. At high partial pressures of O_2 the palladium forms a surface oxide, which introduces a Mars-van-Krevelen reaction mechanism and is the most active form of this model catalyst. Our experimental results show that it is essential for the hysteresis in a P_{CO_2}-versus-P_{CO} plot to be counter-clockwise for spontaneous reaction oscillations to occur.

In combination with these "in situ" STM experiments, we have also performed "in-situ" surface X-ray diffraction measurements at the European Synchrotron Radiation Facility (ESRF) in Grenoble which have confirmed the formation of a surface oxide on Pd(100) under similar reaction conditions and have resolved its atomic-scale structure. The X-ray results show that the oxide is typically 1.5-3 nm thick and slowly grows in time and that the structure is that of nearly completely relaxed PdO(001) oriented with its c axis parallel to the [011] axis of the Pd substrate [29]. Another important observation made with by both techniques, STM and SXRD, is that during the reaction on the oxide the surface continuously roughens due to the Mars van Krevelen mechanism. When the reaction rate oscillated, the Pd(100) surface was observed to periodically evolve back and forth between a smoother and a rougher morphology, roughness building up on the oxide surface and reducing again on the metal surface. In the next chapter, we will use this observation of variations in surface roughness as the basis for a new feedback mechanism, which we propose to be responsible for the oscillations between a smoothening, low-reactivity metallic surface and a roughening, surface oxide with higher reactivity.

Having investigated the oxidation of CO on the low-index (100) surface of Pd, we turn to CO oxidation on high-index surfaces in the next section.

3.7 CO oxidation over high-Miller-index palladium surfaces

3.7.1 Motivation

It is well known that industrial catalysts are not perfectly flat, low-Miller-index single crystal surfaces. The investigation of chemical reactions on surfaces with different types of intrinsic defects, such as steps, kinks, vacancies or adatoms, represents an important step to overcome the materials gap between traditional academic studies and industrial 'reality'. There is ample evidence in the literature that defects such as steps play a significant role in many reactions at the solid-gas and solid-fluid interfaces,

for example by acting as the preferred adsorption sites for reactant molecules. The morphology of a surface plays an important role not only in processes related to heterogeneous catalysis, but also in other physical and chemical phenomena, e.g. involving the stability of crystal shapes and the diffusion dynamics of a crystal, film growth, corrosion, etc. Due to their special structural and electronic properties the so-called vicinal or stepped surfaces are the perfect candidates for investigations of these effects. A short introduction to the subject is given in the next pages, followed by a detailed description of our experimental results concerning CO oxidation over two different vicinal palladium surfaces.

3.7.2 Vicinal surfaces - an introduction

A crystal surface cut at a small angle with respect to a high-symmetry plane [h k l] is called a vicinal surface. Such a 'miscut' surface consists of terraces of the high-symmetry plane, separated by parallel atomic steps running across the sample in a direction dictated by the cut. Therefore, vicinal surfaces are also known as stepped surfaces [30-31]. Due to their structure vicinal surfaces introduce additional properties compared with flat surfaces [32]. The structure around a step atom is different from that of around a terrace atom, simply because of the reduced number of neighbours (lower coordination number). Step atoms generally relax further away from regular lattice positions than terrace atoms. There are two reasons for this. Usually the entire surface is under stress [33], often tensile, and at the steps the atoms can respond to this stress by translating over a small fraction of lattice spacing. But also at an unstressed surface there are relaxations. One of the primary causes for this is that the electrons of the solid react to the presence of the step and attempt to minimize the energy of the defect by spreading out in a way that makes the discontinuity at the step less abrupt. This so-called Smoluchowski smoothing [34] generates an electrical dipole moment, which, in turn, makes the step atoms shift. Since the electronic structure of the steps differs from that of terraces, one may expect their chemical reactivity to be different as well. In particular, in view of the reduced coordination of the step atoms, step sites often provide extra strong binding to adsorbates. Steps are the locations where crystals tend to grow and where adsorbates tend to accumulate. One should keep in mind that the upper and lower sides of a step are different. This is illustrated by the so-called Erlich-Schwoebel effect (ESe), which describes the asymmetry between the diffusion barriers for atoms to attach to a step when they approach from the upper and from the lower terrace [35-36]. Often, vicinal surfaces do not have a completely regular array of steps and kinks. Most vicinal surfaces undergo a roughening transition already below room temperature, which introduces randomness in the distribution of step and kink distances and introduces extra, i.e. 'unnecessary' kinks [37]. From the perspective of crystal growth, vicinal surfaces are known to suffer from two types of

instabilities, step bunching and meandering, which may arise either as a consequence of step-step interactions or by high step energy [38]. Bales and Zangwill first pointed out the meandering instability in 1990 [39], which is the phenomenon that the steps are morphologically unstable during growth in the presence of an ESe (i.e. when it is more difficult for atoms to attach to the step from the upper terrace). The instability is due to the fact that the step velocity of the growing surface will be larger in regions of positive step curvature due to the geometrical increase of the adatom capture zone. A second form of transport-driven morphology change has been observed in 1989 by Lathyshev *et al.* [40], who showed that electromigration leads to step bunching on Si(111) vicinal surfaces. To simplify the step bunching process can be attained by the means of changing the temperature (a thermodynamically field) or chemical potential (due to the adsorption of molecules on the surface).

In the presence of adsorbates stepped surface often undergo structural phase transitions, e.g. faceting. For example, in the presence of oxygen, Ni(977), Pt(554), Rh(775), Rh(332) and other vicinal surfaces show a reversible doubling of the average terrace width and step height [41-44].

In order to address the effect of steps, we have investigated two vicinal palladium surfaces, one vicinal to a (100) orientation, namely Pd(1.1.17), and the other with a vicinal to the (111) orientation, namely Pd(553). In both cases the steps are close-packed, i.e. they run along a [110]-direction, or, equivalently, they can be viewed as one atom wide (111)-type terraces. In the remainder of this chapter we show the behavior of these two surfaces under the conditions of high-pressure CO oxidation.

3.7.3 CO oxidation over Pd(1.1.17)

Interaction of CO and O$_2$ with the stepped Pd(1.1.17)

The left panel of Figure 3.5 shows the starting point of our experiment on Pd(1.1.17). After cleaning the surface by repeated cycles of Ar ion bombardment and annealing, similar to the recipe for Pd(100), we imaged the surface with the Reactor-STM. Although the vacuum in the Reactor-STM is rather poor, we observe a pattern of narrow terraces and steps, with the average terrace width of 2.05 nm and the 0.22 nm step height corresponding to the expected structure of the clean Pd(1.1.17) surface at room temperature. The right panel of Fig.3.5 shows the effect of exposing this surface for 2 h to 1.25 bar of CO at a temperature of 420 K. The STM image shows an increase in the average terrace width by a factor of 2.

Also exposure to oxygen had a major impact on the vicinal Pd(1.1.17) surface. Figure 3.6 shows the surface in an oxygen rich flow at 413 K, after having been pre-exposed to CO. We observe terraces with 4 to 5 times the width of terraces on clean Pd(1.1.17) and a substantial density of kinks. Of

course, the step heights have increased by the same factor as can be seen from the two height profiles in Fig.3.6. Although we have not performed a separate experiment where the surface was first freshly prepared in UHV and then exposed to pure O_2, we assume that the structure in Fig.3.6 reflects the equilibrium structure of the vicinal surface in the oxygen (or, more accurately, oxygen-rich)atmosphere.
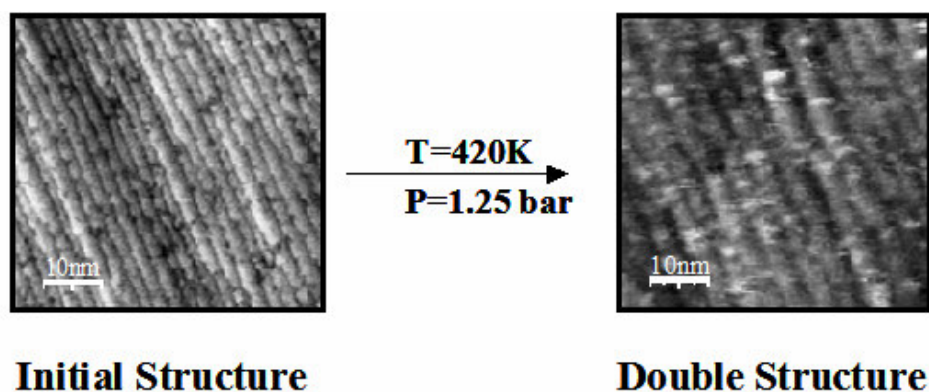

Figure 3.5: *Doubling of Pd(1.1.17) terrace width due to exposure of the surface to CO. Left panel: starting surface at room temperature in (poor) vacuum (10^{-2} mbar). Right panel: surface after 2 h at 420 K in 1.25 bar of CO. Both images measure 50 nm × 50 nm. V_t=0.4 V, I_t=0.2 nA.*
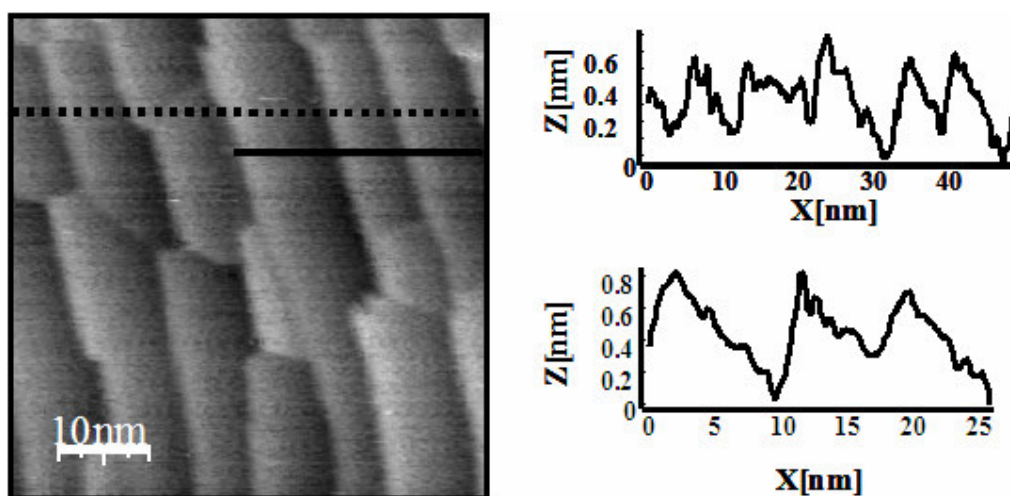

Figure 3.6: *Pd(1.1.17) after a single oxidation-reaction cycle at total pressure of 1.25bar and 413K. The average terrace width is between 4 and 5 times the equilibrium terrace width on the clean surface. The two height profiles run along the dotted and continuous lines in the STM image (50 nm x 50 nm) and illustrate the changes in the terrace width and height.*

This notion is further substantiated by the observation that each of the subsequent reduction-oxidation cycles of CO- and O_2-exposure returned the surface to the same structure. The single-terrace-width structure of clean Pd(1.1.17) was recovered only after repeated cycles of sputtering and annealing in UHV. The double-terrace-width structure was obtained only after exposing a freshly prepared surface to pure CO.

Oxidation-reduction process

Figure 3.7 shows a combination of the partial pressures of the reactant gases CO and O_2 and the reaction product CO_2 measured during one reduction–oxidation cycle and a selection of simultaneously recorded STM images. In the upper panel of the Figure 3.7 the reaction kinetics is depicted. At $t = 0$ s we changed the composition of the gas mixture from CO-rich to O_2-rich. In response, the reaction rate, which is again reflected in the measured CO_2 partial pressure, passed through a maximum at $t = 208$ s, similar to the reaction kinetics of CO oxidation on Pd(100) described in the first part of this chapter. This behavior is consistent with the Langmuir–Hinshelwood mechanism of competing adsorption by CO molecules and O atoms with a maximum reaction rate under conditions of equal coverages of reactants ($\theta_{CO} = \theta_O = 0.5$). After the maximum at $t = 208$ s the reaction rate monotonically decreased in time, following the decrease in CO partial pressure. At $t = 4867$ s (indicated by the arrow in Figure 3.7) the reaction rate suddenly increased by a factor 1.6. Simultaneously with this increase in the CO_2 signal, the mass spectrometer recorded an equally large decrease in the CO partial pressure.

The changes in reaction rate and kinetics strongly suggest that the surface was oxidized and that the reaction switched to the more efficient Mars-van-Krevelen mechanism. The catalytic system maintained its higher reactivity until $t = 5733$s, at which point we increased the CO partial pressure. This led to an immediate downward step in the reaction rate consistent with the removal of the surface oxide. After this, the reaction rate increased and passed through a maximum at $t = 6334$ s, corresponding to Langmuir-Hinshelwood kinetics on the metallic surface. After the maximum, the reaction rate dropped as the surface became increasingly poisoned with CO.

The lower panel of figure 3.7 displays a selection of images from the STM movie recorded simultaneously with the kinetics described above. Image A was recorded at $t = 3000$ s, in the oxygen rich flow at low reaction rate. As expected from the kinetics, the image shows the oxygen-covered metallic Pd(1.1.17) surface, containing flat terraces with a 4- to 5-fold increased width, separated by steps with a 4- to 5-fold increased height. Image B was acquired just before the reaction rate suddenly increased. Although the image suffers somewhat from a double tip effect, it shows that

the surface is still in the same state as in image A. Image C was recorded consequently after image B. The step up in CO_2 partial pressure happened during one scan line at the beginning of image C. Interestingly, in image C the steps can still be distinguished, even though there is a definite change in surface morphology (roughening) compared to image B.
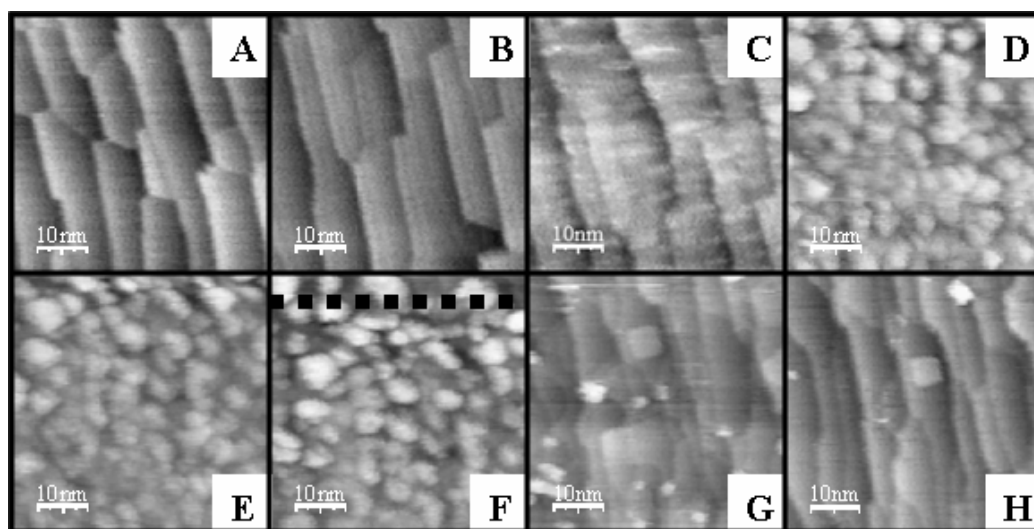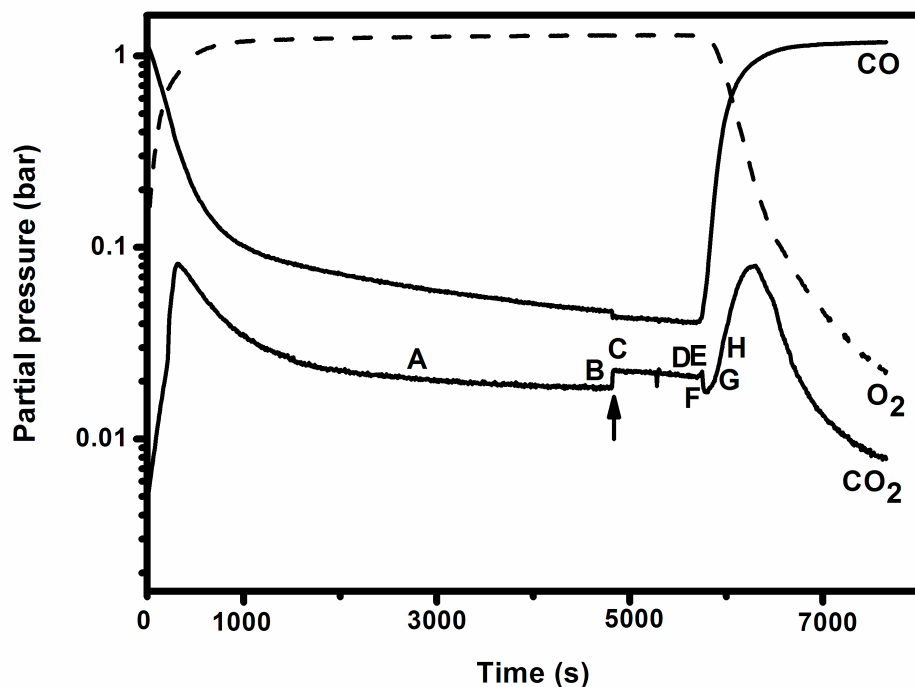

Figure 3.7: *STM images and mass spectrometer signals measured simultaneously during a cycle of CO oxidation, from a CO-rich mixture to O_2-rich and back to CO-rich, on the Pd (1.1.17) surface at T=413 K and P_{tot}=1.25 bar.*

32

Images D and E have been acquired after the surface had been kept in the high-reactivity state for approximately 14 minutes. The initial roughness visible in image C has developed into cluster-type structures. Such structures have been observed before and have been referred to as the "cauliflower structure" [45]. We will return to the evolution of this morphology in more detail below.

The changes in the surface structure, correlated with the stepwise increase in the reactivity are very similar to what we have observed in earlier experiments on Pt(110) and Pd(100) under atmospheric pressures of oxygen-rich CO/O_2 mixtures at elevated temperatures [28-29] and confirms our earlier suggestion that also Pd(1.1.17) undergoes a surface phase transition from a metal with a low reactivity to an oxide with higher reactivity. From the statistics of images D and E we obtain a density of 85 ± 10 clusters per image of 50 nm × 50 nm, with a diameter in the range of between 4 ± 2 nm. During image F the reaction rate stepped down. The lower part of the image still shows the surface oxide. The reduction in reaction rate took place at the location of the dotted line, above which a modest change can be observed in the appearance of the surface: the cluster density is lower (the smaller clusters have disappeared) and a few steps are faintly visible. Also, the tip seems to have changed. In the image acquired immediately after this (G), most cluster structures have disappeared, and the structure with terraces and steps, characteristic for the metal surface, is clearly visible. The remaining cluster structures have heights corresponding to multiples of the interlayer distance of Pd(100). The largest island has a square symmetry, reflecting the geometry of the (100) plane of palladium. Due to the coarsening of the adatom islands and their coalescence with the steps, the surface smoothens further, as can be observed by comparing images G and H.

In order to obtain additional information about the surface evolution, we have extracted the step density from the selected images in Fig.3.7. The result is shown in figure 3.8. The step density has been calculated as the sum of all the steps length divided by surface area. As long as the surface is in the metallic state, i.e. from image A to B and after image E, the step density decreases. When the surface is oxidized, between images B and C, the step density is increased suddenly by a factor of 1.6. As long as the surface stays in its oxidic form, the step density slowly increases further. We find that the step density of the metallic surface immediately after the oxide has been removed is higher than that just before the oxide is formed, consistent with the presence of decaying clusters in the first minutes after the oxide is reacted away.
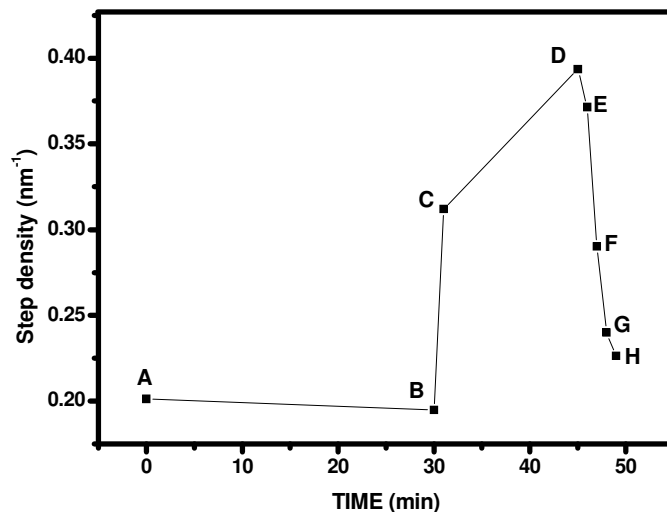
Figure 3.8: *Evolution of the roughness (step density) on the Pd (1.1.17) surface during the reduction-oscillation cycle of Fig. 3.7. The letters indicate the times of the individual STM images shown in Fig. 3.7.*

The oxide evolution in time

As already mentioned above, the initial oxidation of the vicinal surface was responsible for a modest roughening visible in image C in Fig.3.7 (e.g. the bright stripy structures, which developed from the step edges into the terraces). Since image C from Fig. 3.7 was the first image acquired in the high-activity phase we infer that at the beginning of the oxidation process the vicinal metal surface is covered by a thin oxide layer that covers the entire surface and that steps play a role as nucleation centres for the subsequent growth of the oxide clusters that make up the "cauliflower" structure. In order to illustrate this point we display in Figure 3.9 the STM images recorded between image C and an image showing a structure similar to the one in image D. The six images shown below have been acquired consecutively one after one. The recording time for an image was 46 s so image C_5 has been acquired at approximately 6 minutes after image C. As one could see the morphology of the surface changed rapidly due to high O_2 exposure. These images reveal how the (oxide) clusters develop from height variations in the initial thin oxide film (indicated in the image C by ellipses) that appears to originate from the steps and protrude into the terraces. It has been shown by Xu and Yates that for Pt(533) the lowest-energy adsorption site for CO and O_2 is at the step, whereas the highest probability of reaction is between CO molecules adsorbed on the terrace and oxygen atoms adsorbed on a step [46]. If we would replace the oxygen adsorbed on a step with the oxide which forms at the steps, and correlate this with the observation that the oxide has higher reactivity, their theory might ally also for CO oxidation on Pd(1.1.17).
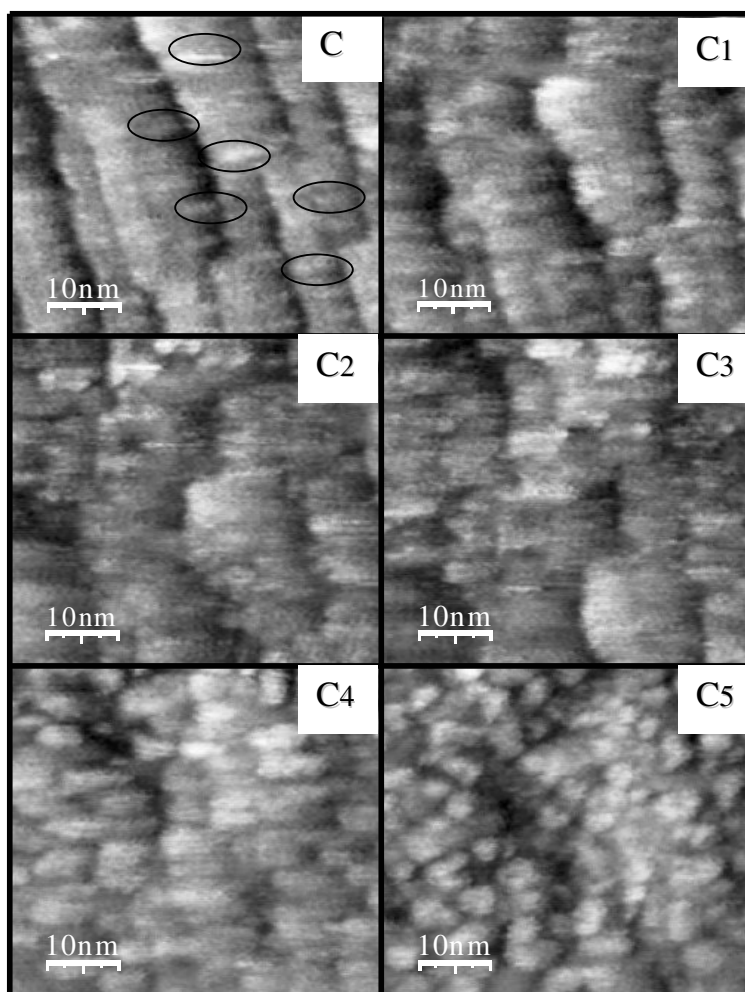
34

Figure 3.9: STM *images (50nmx50nm) illustrating the nucleation and growth of the palladium oxide clusters. At the beginning of image C, the reactivity had already stepped up, indicating that the entire surface had already formed a thin oxide. The sequence of images shows that the initial stages of cluster formation are assisted by the presence of steps.*

The development in time and the stability of the palladium surface oxide has been investigated in a different experiment performed at the same pressure of 1.25 bar, but a slightly different temperature of 417 K. Figure 3.10 displays the STM images and the simultaneously recorded reaction rate. Image K has been acquired immediately after the upward step in the reaction rate indicated by arrow 1 in the lower panel. Images K-N show that the oxide clusters structures have an imperfect square shape. Clear vertical lines are also observed within these images. After some time the fine lines disappeared and the number of clusters increased (image O and P). Finally the oxide clusters evolve to a more rounded shape, forming the "cauliflower" structure mentioned above (images R-W).

In order to check the stability of the oxide, we intentionally exposed the oxide surface to short pulses of CO. Image S has been recorded just

before the first CO pulse. Then the valve to the CO bottle has been opened for 10 s. Image T has been recorded during the first increase in the reaction rate marked by the arrow 2. The surface shows very similar oxide clusters to those in image S. Images U and V have been acquired during the second and third CO pulses respectively, indicated in the figure by arrows 3 and 4. Although there is some loss of resolution in these images, due probably to a change in the tip, the morphology of the surface seems to have remained largely unchanged.

The reaction rate exhibits downward spikes during the increases in CO_2 production. We will show later in this manuscript that the spikes are in fact oscillations. Similar to the case of Pd(100), the vicinal surface switches spontaneously between its metallic state and the surface oxide. The time spent in the metallic phase is too short compared to our scanning speed to show up clearly in the STM images. For this reason we are able to see only the oxidic phase.
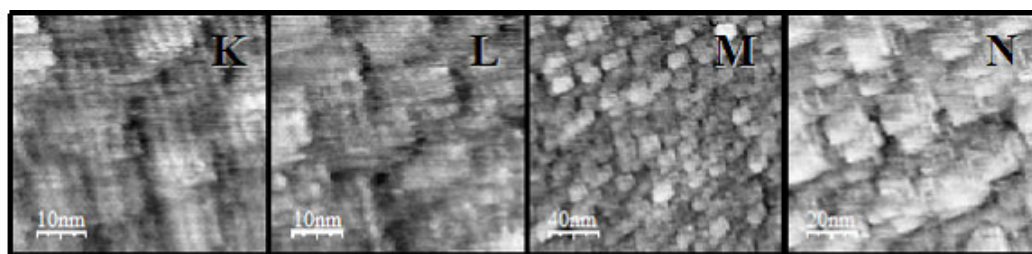
| t=0 min | t=5 min | t=11 min | t=21 min |

| t=26 min | t= 32 min | t= 50 min | t=90 min |

| t=104 min | t=115 min | t=137 min | t=161 min |
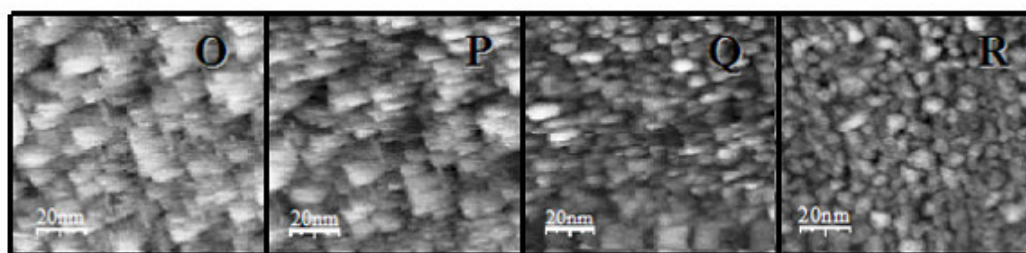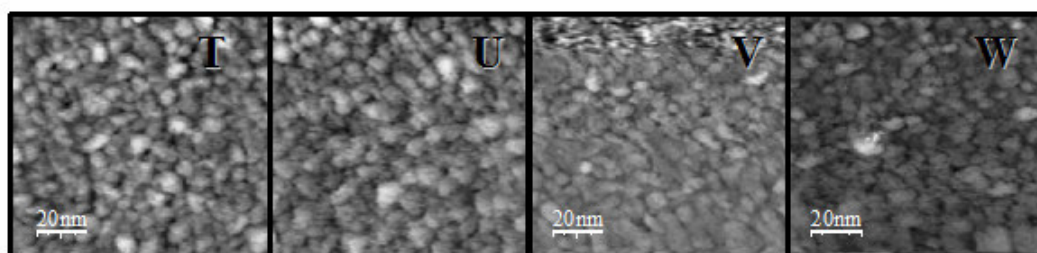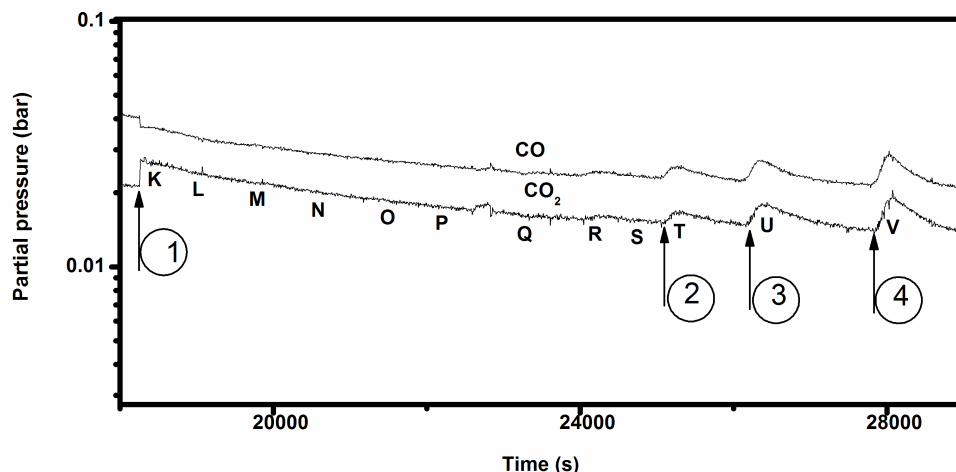
Figure 3.10: *STM images and simultaneously recorded reaction rate on Pd(1.1.17) at*
P_{tot} =1.25 bar and T = 417 K. Arrow 1 indicates the spontaneous upward step in
reactivity that is associated with the formation of the surface oxide. Arrows 2, 3 and 4
mark the times where the CO pressure was manually increased to 0.025 ,0.027 and
0.029 bar for a short duration of 10, 15 and 30 s. the size of the STM images is
50nm×50nm (K-L),200nm×200nm (M) and 100nm×100nm (N-W). V_t=1 V and
It=0.2 nA.

Oscillations and kinetics

If we plot the partial pressure of CO_2 as a function of the CO partial
pressure, while the partial pressure of O_2 is kept constant, all the data from
the experiment described above fall on two branches, as seen in figure 3.11.
This is similar to what has been observed on the other surfaces introduced in
this thesis. One branch corresponds to the oxidic surface with higher
catalytic activity. The other branch corresponds to the metallic surface, with
lower reactivity. For this particular experiment the catalytic system exhibits
bistability and the system oscillates between an oxide and a metallic surface
covered with an oxygen-dominated mixed overlayer of CO molecules and O
atoms. In contrast to Pd(100) the oscillations on the vicinal surface do not
have the square waveform shape and their period is very short. Experiments
performed at a constant total pressure of 0.5 bar showed the same behaviour,
with the data separating again in two branches.

At a total pressure of p = 1.25 bar the surface switched from the metal to
the oxide (high reactivity) at a ratio $P_{CO}/\sqrt{P_{O_2}}$ equal to 0.034 √bar. The phase
transition back to the metal happened at a ratio equal to equal to 0.030 √bar.
For the lower pressure of 0.5 bar the surface switched to the higher catalytic
activity branch at higher ratio $P_{CO}/\sqrt{P_{O_2}}$=0.038 √bar, while the switching
back to the lower catalytic activity branch took place a ratio $P_{CO}/\sqrt{P_{O_2}}$ equal
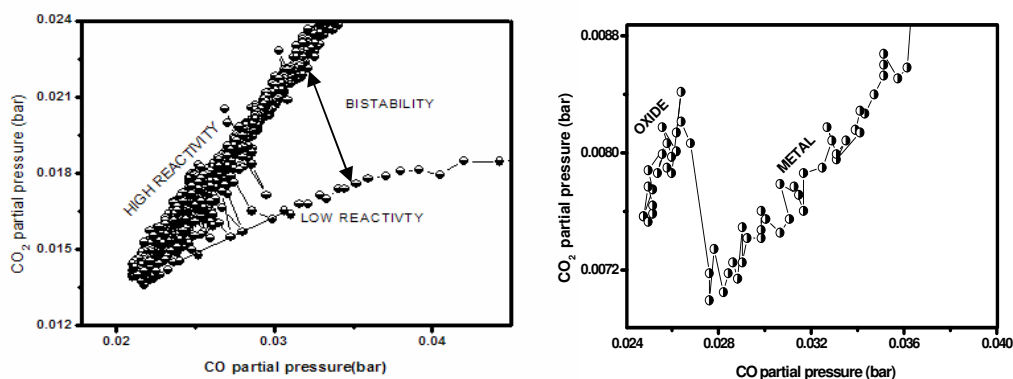to 0.036 √bar.

37

Figure 3.11: *Partial pressure of CO_2 (reaction rate) as a function of the CO partial pressure at a constant O_2 partial pressure of 1.25 bar (left panel) and 0.5 bar (right panel) at a temperature of T = 417 K. In both cases we observe two separate branches that we identify as the low-reactivity metallic surface, covered by an oxygen-dominated mixture of CO and O_2, and the high-reactivity oxide surface. The line connects the data points in the order in which they have been measured. The lines that cross over, back and forth, between the two branches indicate spontaneous reaction rate oscillations.*

Both data sets show in the CO_2 production rate (upon variation of P_{CO}) a hysteresis with a counter clock-wise (ccw) orientation. As explained previously in this chapter for Pd(100), the ccw hysteresis means that the oxide on Pd(1.1.17) was formed at higher P_{CO} value compared to the partial pressure of CO at which the oxide was reduced again. The ccw orientation of the hysteresis satisfies an important requirement for the existence of spontaneous reaction oscillations [47].

3.7.4 CO oxidation on Pd(553)

In Fig. 3.12 we show the usual combination of the time evolution of the three partial pressures of CO, O_2 and CO_2 and a series of selected STM images obtained during this evolution. The experiment was performed at a constant total pressure of 1.25 bar and a temperature of 410 K. At the beginning of the time sequence in Fig. 3.12 we switched from a CO-rich flow to an O_2-rich flow and at the end we switched back to a CO-rich flow. In both cases we see the rate of CO_2 production go through a maximum, corresponding to the behavior expected for the Langmuir-Hinshelwood reaction on a metallic palladium surface and similar to our observations on Pd(100) and Pd(1.1.17). While in the oxygen-rich flow the catalytic system switched two times to a higher reactivity; first at t = 5061 s for a short time interval (indicated by arrow 1), and a second time at t = 6114 s for a longer period (arrow 2). In both cases simultaneously with the increase in the reaction rate we notice a decrease in CO partial pressure. The critical values

for the CO partial pressures at which the catalyst switched to the higher reactivity were 28 mbar for the first increase and 26 mbar for the second. In analogy with our observations on Pd(100) and Pd(1.1.17), we associate the reactivity changes with the formation of an oxide on the palladium surface.

Image A in Figure 3.12 and the first part of image B (below the dashed line) are characteristic for the metallic Pd(553) surface. The dashed line in image B marks the point in time where the partial pressure of CO_2 stepped up the first time. In the upper part of image B and in image C, which was measured directly after B and corresponds to the maximum in the reaction rate, we observe a clear roughening of the surface, as we have observed also on the other surface orientations of Pd during CO oxidation on the oxide phase of the surface. Image D was recorded immediately after the step down in the reaction rate, and it shows again the morphology of the metal surface. Due to the fact that the density of steps is very high on the (553) surface the oxide cannot become very rough and that the metal returns to its equilibrium smooth state very quickly. Images E-J in Fig. 3.12 show the sequence of surface morphologies recorded on Pd(553) just before and after the second switch to the higher reactivity.
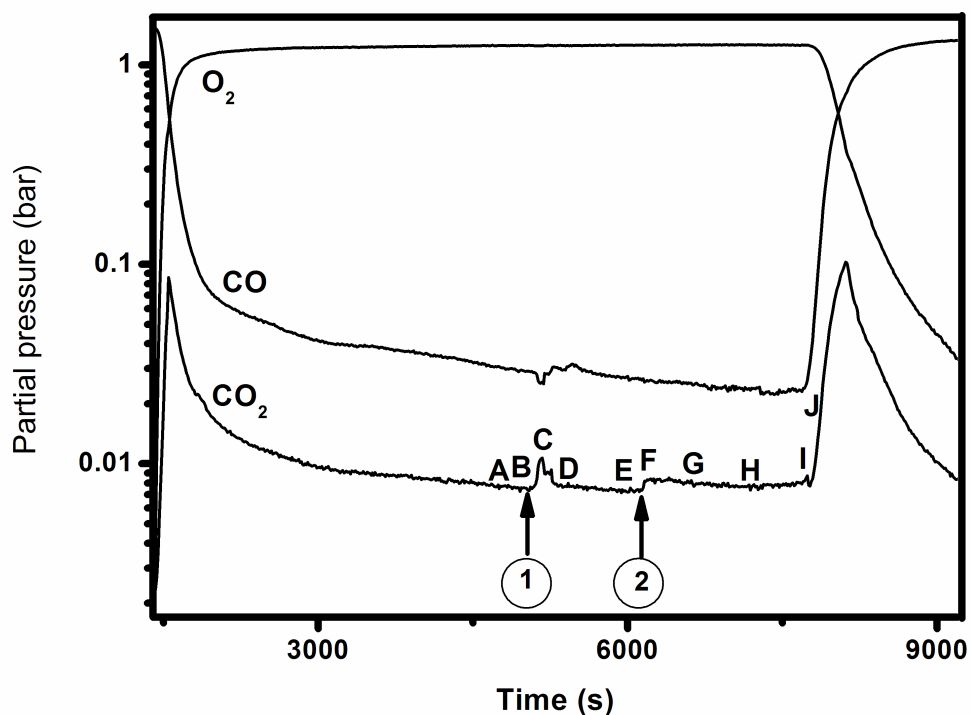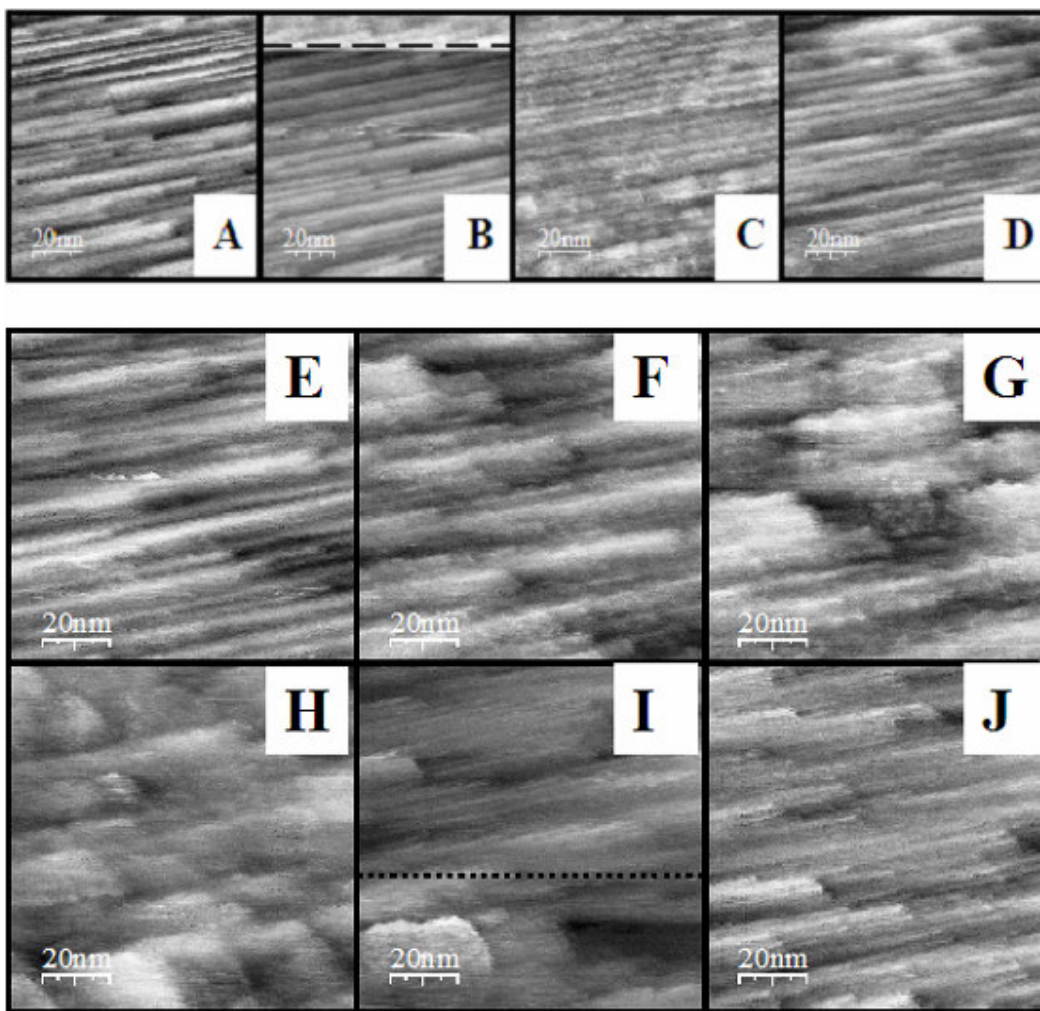
Figure 3.12: *Partial pressures of CO, O2 and CO_2 and STM images(100nm×100nm) measured during CO oxidation and a total pressure of 1.25 bar and a temperature of 410 K on Pd(553), while the gas mixture was cycled from a CO-rich mixture to an O_2-rich mixture and vice versa. $V_t= 0.1V$ and $I_t=0.2$ nA.*

Image E shows the metallic surface. The recording of image F took place after the reactivity stepped up (arrow 2 in top panel Fig. 3.12). Images F, G and H show a modest increase in roughness with time. The oxide features evolved from small protrusions to larger cluster-type structures, similar to the development of the oxide on Pd(1.1.17). The upper part of image I and the subsequent image J describe the appearance of the surface after the oxide had been reduced, due to the increase in CO partial pressure. This time, we do not observe any formation of adatom and vacancy islands, after the removal of the oxide. It is plausible that such roughness has been present after the removal of the oxide but that the timescale for the removal of this roughness is very short on the (553) surface as a consequence of the small terrace width.

3.8 Conclusions

We have investigated the "in situ" the CO oxidation at ambient pressures and elevated temperatures over two high Miller indexes surfaces of palladium. Pd(1.1.17) is vicinal to the (100) orientation, while Pd(553) is vicinal to the (111) single surface. Both surfaces revealed the formation of an oxide in oxygen rich flow. The oxide has higher reactivity compared to the metallic surface. On the oxide the reaction follows the Mars van Krevelen mechanism, while on the metallic surface it follows the Langmuir-Hinshelwood mechanism. Spontaneously oscillations in the reaction rate have been observed for CO oxidation over Pd(1.1.17). Similar to Pd(100) the oscillations can be interpreted as phase transition between a smooth and a rough surface. No oscillatory behaviour has been observed for Pd(553)

3.9 Reference:

[1]   http://www.stillwaterpalladium.com

[2]   http://education.jlab.org

[3]   S. M. Vesecky, D. R. Rainer, D.W.Goodman, *J. Vac. Sci. Technol. A* **14** (1996) 1457.

[4]   M. Lyubovsky, L. D. Pfefferle, *Appl. Catal. A Gen.* **173**(1998) 107.

[5]   M. Lyubovsky, L. D. Pfefferle, *Catal. Today* **47 (**1999) 29.

[6]   M. Lyubovsky, L. D. Pfefferle, A. Datye. J.Bravo, T. Nelson, *J. Catal.* **187** (1999) 29.

[7]   R. J. Farrauto, M.C. Hobson, T Kenelly, E. M. Waterman, *Appl .Catal. A Gen* **81** (1992) 227.

[8]   S. K. Scott, *Oscillations, waves and chaos in chemical kinetics,* (Oxford University Press, 1994.)

[9]   M. M. Slin'ko and N. I. Jaeger, *Oscillating heterogeneous catalytic systems,* (Elsevier, 1994.)

[10]   P. Gray and S. K. Scott, *Chemical oscillations and instabilities, non-linear kinetics,* (Oxford University Press, 1994).

[11]   G. A. Somorjai, *Introduction to Surface Chemistry and Catalysis* (Wiley,New York,1994).

[12]   M. Boudart, *Adv.Catal.***20**(1996)153.

[13]   B. Hammer, O. H. Nielsen, and J. Nørskov,*Cat.Lett.***46** (1997)31.

[14]   C. R. Henry, C. Chapon, C. Goyhenex and R. Monot, *Surf. Sci.***272** (1992)283.

[15]   Y .Li and J. N. Armor, *Appl. Catal. B* **3**(1994) 275.

[16]   S. Ladas, R.Imbihl, G.Ertl, *Surf. Sci.* **219** (1989) 88.

[17]   M. R. Bassett, R.Imbihl, J.Chem.Phys.93 (1990) 811.

[18]   V. Bondzie, P. Kleban, D.J .Dwyer, *Surf.Sci.***347** (1996).

[19]   V. Bondzie, P.Kleban,D.A.Browne, *J.Vac. Sci.Technol.***A 11** (1993) 1946.

[20]   J.G.Mcgarty, V.L.Wong, Y.F.Chang,*Scr.Metal.Mater.***31** (1994) 115.

[21]   E.H. Voogt, A.J.M.Mens ,O.L.J. Gijzeman, J.W.Geus, *Surf.Sci.***373** (1997) 210.

[22]   G. Zheng, E. I. Altman, *Surf.Sci.***462** (2000) 151.

[23]   G .Zheng, E.I .Altman, *Surf.Sci.***504** (2002) 253.

[24]   K. Reuter and M. Scheffler ,*Appl. Phys.A* **78**,(2004)793.

[25]   www.surf-prep-lab.com

[26]   B. L. M. Hendriksen and J. W. M.Frenken, *Phys. Rev.Lett.***89** (2002) 046101.

[27]   B. L. M. Hendriksen, S. C. Bobaru and J.W.M.Frenken, *Surf.Sci.***552** (2004) 229.

[28]   M.L. D. Ackermann *et al.*, *Phys. Rev. Lett.* **95** (2005) 255505.

[29]   M. L. D Ackermann *et al.*, to be published

[30]   B.Lang, R.W. Joyner and G.A.Somorjai, *Surf.Sci.***30** (1972) 440.

[31]   C. Barreteau, F. Raouafi, M. C. Desjonqueres, and D. Spanjaard J.*Phys.:Condens.Matter* **15** (2003) S3171.

[32]   H. C. Jeong and E. D. Williams,*Surf. Sci.Rep.***34** (1999) 1971.

[33]   H. Ibach and W. Schmickler, *Surf.Sci.***573** (2004) 24.

[34]   R. Smoluchowski, *Phys.Rev.***60** (1941) 661.

[35]   G. Ehrilch and F. G. Hudda , *J.Chem.Phys.***44** (1966) 1039.

[36]   R. L. Schwoebel and E. J. Shipsey, *J.Appl.Phys.***37** (1966) 3682.

[37]   M. S. Hoogeman, L. Kuipers, D. C. Schlößer, and J. W. M. Frenken, *Surf. Sci* **447** (2000) 25.

[38] O. Pierre-Louis, G.Danker,, J.Chang ,K. Kassner,C.Misbah, *J.of Cryst.Growth* **275** (2005) 56.

[39] G. S .Bales, A. Zangwill, *Phys.Rev. B* **41** (1990) 5500.

[40] A. V. Latyshev,et al., *Surf.Sci* .**213** (1989) 157.

[41] L. Niu, D. D. Koleske, D. J. Gaspar, S. F. King, S .J. Sibener, *Surf.Sci.***356** (1996) 144.

[42] B. Lang, R. W. Joyner and G. A. Somorjai, *Surf.Sci.***30** (1972) 454.

[43] D. G. Castner and G .A. Somorjai, *Surf.Sci.***83** (1979) 60.

[44] G. Hoogers and D. A. King, *Surf. Sci.* **286** (1993) 306.

[45] J. Han, D. Y. Zemlyanov, F. H. Ribeiro, *Surf. Sci.* **600** (2006) 2730.

[46] J. Xu and J. Y. Yates,Jr., *Surf. Sci.***327** (1995) 193.

[47] M. Ehsasi, M. Berdau, A. Karpowicz, K. Christmann and J. H. Block, *New frontiers in catalysis,* Elsevier Science Publishers B.V.,1993.

Chapter 4

New insights into the oscillatory behaviour of CO oxidation over platinum group metals

In this Chapter the most popular models described in the literature regarding the oscillatory behaviour of catalytic reactions such as CO oxidation are discussed. In order to explain the experimental observation introduced in Chapter 3, of oscillations between a metallic surface and a surface oxide, a new model is proposed This new model involves two key features: (1) the observation that the oxide surface gradually roughness under reaction conditions and that the metal surface gradually smoothens and (2) the relation between the surface roughness and the CO partial pressure at which the surface switches between metal and oxide (and vice versa).

4.1 Introduction

The discovery by Belousov that during reactions involving $HBrO_3$, bromomalonic acid and the redox couple Ce^{3+}/Ce^{4+} in solution, the colour of the solution changed periodically under otherwise stable conditions, such as a constant temperature, has constituted the starting point of research of oscillatory chemical reactions [1]. Oscillatory behaviour of chemical reactions is a fascinating phenomenon, which can help in understanding the reaction mechanism of a catalyst and the mechanism of communication between different parts of a catalyst. Knowledge about the oscillatory mechanism may also be useful when trying to prevent potentially dangerous situations in practical, e.g. industrial processes, due for example to the periodic increase in the heat released by the reaction [2]. In addition, oscillations are sometimes deliberately forced onto a catalytic system by varying the reaction conditions. In this way sometimes better average conversion rates or selectivities can be obtained [3]. Sustained oscillatory behaviour has been observed in a large number of oxidation reactions catalysed by transition metals of Groups VIII and I B [4-9]. This behaviour is very well documented for the platinum catalysed oxidation of carbon monoxide [10], hydrogen [11], ammonia [12], ethylene [13], propylene [14], and other hydrocarbons. Oscillations during CO oxidation on Pd and Pt have been observed for a variety of catalyst configurations, e.g. in the form of a single crystal [15], a wire [16], a foil [17] or supported on a pellet [18], under a variety of conditions, involving low and high gas and catalyst

temperatures and (partial) pressures ranging from UHV [19,20] to atmospheric pressures [7,20-22]. In the course of previous attempts to explain the origin of reaction oscillations a large number of mathematical models has been suggested in the literature. In spite of the large number of studies there is no agreement yet on the chemical source of the behavior. It is also not clear whether all observations of catalytic oscillations share the same origin [23]. From the mathematical point of view the description of the oscillatory evolution of the gas concentrations and other relevant aspects of the reaction system can be described by means of an appropriate set of differential equations [24-27]. Often, these differential equations are not linear. As a consequence the oscillatory catalytic systems have been classified as *non-linear* [24-27]. It is well established in the literature that in order to meet the conditions for oscillations the catalytic system should be sufficiently far from thermodynamic equilibrium [28]. In the previous chapter the concept of *bistability* has been introduced. In a system exhibiting bistability, we can have oscillations between the two levels of the reaction rate. A requirement for such oscillations is the existence of a *feedback* mechanism, which allows the periodic transition of the system between the two states [27-30].

In some catalytic systems the oscillatory process is even more complicated. By adjusting the reaction parameters the system can make the transition from one to two to four to eight, etc. levels, which introduces several doublings of the oscillation period. This scenario is illustrated in figure 4.1, which represents the Feigenbaum diagram or *Feigenbaum scenario* to chaos [31]. It shows the rate of the reaction as a function of some suitable reaction parameter λ, which could be the temperature or a ratio of concentrations. The left side of the diagram contains only one branch, corresponding to the conventional situation in linear kinetics. There the reaction system is not too far from the equilibrium state and there is one rate of reaction for each set of reaction conditions. If the system deviates from equilibrium to the point where the reaction parameter exceeds a critical value, the system becomes unstable and oscillates between two states, for example between the two surface structures (reconstructed and unreconstructed) of Pt(110) during CO oxidation. If the reaction parameter exceeds a next critical value, the number of available branches for the rate doubles again and the reaction cycles between four levels. The final transition on the right-hand side of the Feigenbaum diagram is to an infinitely long period and infinitely many levels, a situation referred to as chaos [31].

4.2 Traditional models for reaction oscillations

Since this thesis is mainly devoted to CO interaction with various Pd and Pt single-crystal surface in this section we will summarize the models proposed

46

previously, in particular for the oscillatory behaviour of CO oxidation over various platinum-group catalysts.
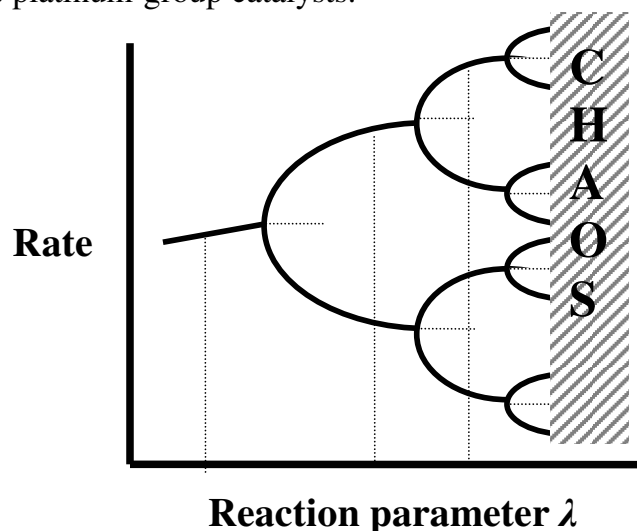

Figure 4.1: *Schematic representation Feigenbaum diagram: if the reaction parameter λ deviates sufficiently from equilibrium conditions, the rate of the reaction may develop oscillations between two, four, eight, … levels. At high deviation from equilibrium the system may behave chaotically. After [29].*

Adsorbate-induced surface structural transformation

This model, also known in the literature as the reconstruction model is based on the facts that the topmost metal layers of a single crystal can reconstruct and that different reconstructions show different adsorption behavior. The first kinetic oscillations linked to an adsorbate-induced surface structural transformation have been observed for the (100) surface of platinum. Clean Pt(100) exhibits a quasi-hexagonal reconstruction, which can be transformed into the bulk like, unreconstructed (1×1) structure by the adsorption of a variety of gases. CO oxidation over Pt(100) will be described in detail in Chapter 6. Here, we illustrate the reconstruction model using the example of Pt(110). A freshly prepared, adsorbate-free Pt(110) surface shows the (2×1) periodicity of the so-called "missing row" reconstruction [32-34]. CO adsorption lifts this reconstruction and a phase transition to a (1×1) structure occurs. In spite of the fact that this unreconstructed surface is CO covered and has a low reaction rate, its sticking coefficient for oxygen atoms is twice as high as that on the reconstructed surface. In other words oxygen will adsorb even though CO to some extent inhibits the process. Under oscillation conditions the increased consumption of CO can now make the surface flip to become predominantly O-covered. With no CO to stabilize the surface against the missing-row reconstruction, the surface will reconstruct again. In turn, this surface has a low sticking coefficient for

oxygen. This situation enables CO to take over, so that the surface becomes again CO-covered and it switches back to the unreconstructed phase. This completes one oscillation cycle and sets off the next one [32-34].

Faceting model

Faceting is a process, which causes an initially flat, single-crystal surface to separate into two (or three) other surface orientations [35]. This process has been studied intensively on Pt(110) [36-38]. By exposing the surface under appropriate conditions to a constant CO+O_2 flow, structural transformations of the surface have been observed. The experimental data (diffraction patterns) revealed that the structure of the facets consists of steps with a (100) orientation and (110) terraces [37]. The facetting of Pt(110) is associated with an increase in catalytic activity ,which is connected with the formation of (100) steps in the facetting process, since these exhibit a higher sticking coefficient for oxygen compared to the flat (110) surface [28,39]. There is a high temperature limit for facetting, at about 530 *K* above which no facetting can take place (depending on partial pressures). A CO covered (1x1) surface constitutes the starting point of an oscillation cycle. On this surface the reaction rate is low and the facets grow slowly. These facets have a high sticking coefficient for O_2, and at a certain point the surface becomes oxygen-covered. This destabilizes the facets and they are removed by surface diffusion of Pt atoms. The surface becomes CO-covered again and the cycle starts all over [28, 40].

Carbon model

A different mechanism for the oscillations was first suggested by Burrows *et al.* [41] and further developed by Collins, Sundaresan, and Chabal in 1985 [42]. In short, in this model the adsorption sites on the catalyst surface are blocked by carbon impurities. Two sources for carbon impurities have been suggested. The first one refers to the diffusion of atomic carbon from the bulk metal, while the presence of hydrocarbons in the gas stream constitutes the second source. According to the carbon model the oscillations result from the cyclic activation and deactivation of adsorption sites, by atomic carbon impurities.

Subsurface oxygen model

Some authors have proposed that the origin of the oscillations in a catalytic system is the formation of a different oxygen species, called "subsurface oxygen". The subsurface oxygen model was first put forward to explain the oscillatory behaviour of Pd(110) [43]. At low Pco some fraction of the oxygen atoms of an oxygen-covered surface are thought to penetrate below

the outermost atomic layer of the Pd catalyst. The subsurface oxygen species is thus in thermodynamic equilibrium with the chemisorbed oxygen on top. Experimental evidence for the existence of subsurface oxygen has been acquired by TDS, XPS, ion scattering, and titration techniques [44]. The oscillation mechanism can be rationalized as follows: starting with an active oxygen-covered surface (high reaction rate branch) oxygen starts to penetrate into the subsurface region. This leads to a deactivation of the surface as the surface becomes CO-covered (low reaction rate branch). But as soon as subsurface oxygen begins to diffuse back to the surface and reacts with CO, the decreasing subsurface oxygen concentration leads to a reactivation of the surface and the initial situation is established again.

Oxidation-reduction model

In 1981, Sales, Turner and Maple have explained their experimental observation of kinetic oscillations in CO oxidation on polycrystalline Pt, Pd and Ir at atmospheric pressure by a model in which they have included the formation of a surface oxide [7, 45]. The basic idea of their model is that the slow oxidation and reduction of the metal surface layer can induce transitions between the two branches of a Langmuir-Hinshelwood reaction. The model is based on the following assumption: the oxide formation blocks the site with respect to CO and O_2 chemisorptions; the rate of the oxide formation is proportional to the concentration of adsorbed oxygen and the fraction of free sites for oxide formation in the subsurface layer; the oxide reduction is assumed to proceed via the interaction with adsorbed CO [28, 45].

4.3 Comparison with experimental observations

Most of the models reviewed above, with exception of the oxidation-reduction model of Sales, Turner and Maple, are based on experimental results obtained under UHV conditions. The importance of investigating these phenomena under more realistic conditions has been emphasized before in this thesis. The high-pressure STM experiments in Chapter 3 have revealed that during CO oxidation over Pd(100) and Pd(1.1.17) the reaction rate spontaneously oscillates between two states, one with high reactivity and the other with low reactivity. In the next chapter we show similar behaviour for CO oxidation over Pt(111). In this section we confront the models discussed above with these experimental results. We will see that none of these models apply. In order to substantiate this point, we recall the main conclusions of our observations in Chapter 3. At atmospheric pressures and elevated temperatures CO oxidation on Pd(100), Pd(1.1.17) and Pd(553) can occur in two different modes. On the metal surface the reaction follows the classic Langmuir-Hinshelwood mechanism, with CO molecules and O

atoms competing for adsorption sites and with the reaction rate going through a distinct maximum as a function of the partial pressure of either CO or O_2. At sufficiently high oxygen partial pressure and/or sufficiently low CO partial pressure the surface undergoes a first-order phase transition to a surface oxide. Evidence for the oxidation was seen in the STM images and confirmed by SXRD. The simultaneously performed kinetic measurements show that the oxide exhibits a higher reactivity to CO oxidation than the original metal surface. On the oxide the reaction follows the Mars van Krevelen mechanism, according to which a CO molecule reacts with an oxygen atom from the oxide lattice. The resulting oxygen vacancies are refilled with oxygen from the gas phase. During the reaction the temporarily uncoordinated Pd atoms sometimes diffuse out of the surface layer forming pits and protrusions. As a consequence the roughness of the oxide surface gradually increases. The metallic surface observed immediately after the oxide has been removed shows a high step density due to the formation of adatom and vacancy islands. Surface diffusion is seen to smoothen the metallic surface, making it evolve towards the initial, flat metallic surface that formed the starting configuration, before the oxidation process. Another important outcome of the experiment is the observation of spontaneous oscillations in the reaction rate, which were shown to go back and forth between the metal (with LH kinetics) and the oxide with (MvK kinetics). We have observed such oscillations for Pd(100) and its vicinal surface Pd (1.1.17). No oscillations have been observed during CO oxidation on Pd(553). Figure 4.2 illustrates the oscillation of the CO oxidation reaction on Pd(100) in a constant reactant flow at ambient pressures. We clearly see how the reaction rate spontaneously switches periodically between two levels, labelled R_{oxide} and R_{metal}. The oscillations in CO_2 production are in anti-phase with the variations in CO pressure, as a result of the difference in the CO consumption at the two reaction rates. The accompanying STM images that were acquired simultaneously show that during the periods with the low reaction rate the height variations of the surface are all multiples of the Pd(100) step height and a square symmetry is visible in the step orientations, which is the geometry that we have recognized before (Chapter 2) as the metallic state. All images during the high rate show the disordered, rough character of the surface oxide. Even during the few minutes of a reaction oscillation period we observe that the surface roughness increases in the oxide phase and decays in the metal phase. As already explained in the previous chapter the oscillations are periodic switches between the low-activity metal phase and the high-activity oxide. The terrace and step configurations of the metallic phase are reflecting the geometry (square symmetry) and the step height of Pd(100), while the oxide phase has a disordered, rough appearance. Despite the fact that metal-oxide and oxide-metal transitions take only a fraction of a second, the period of an oscillation can be several minutes.
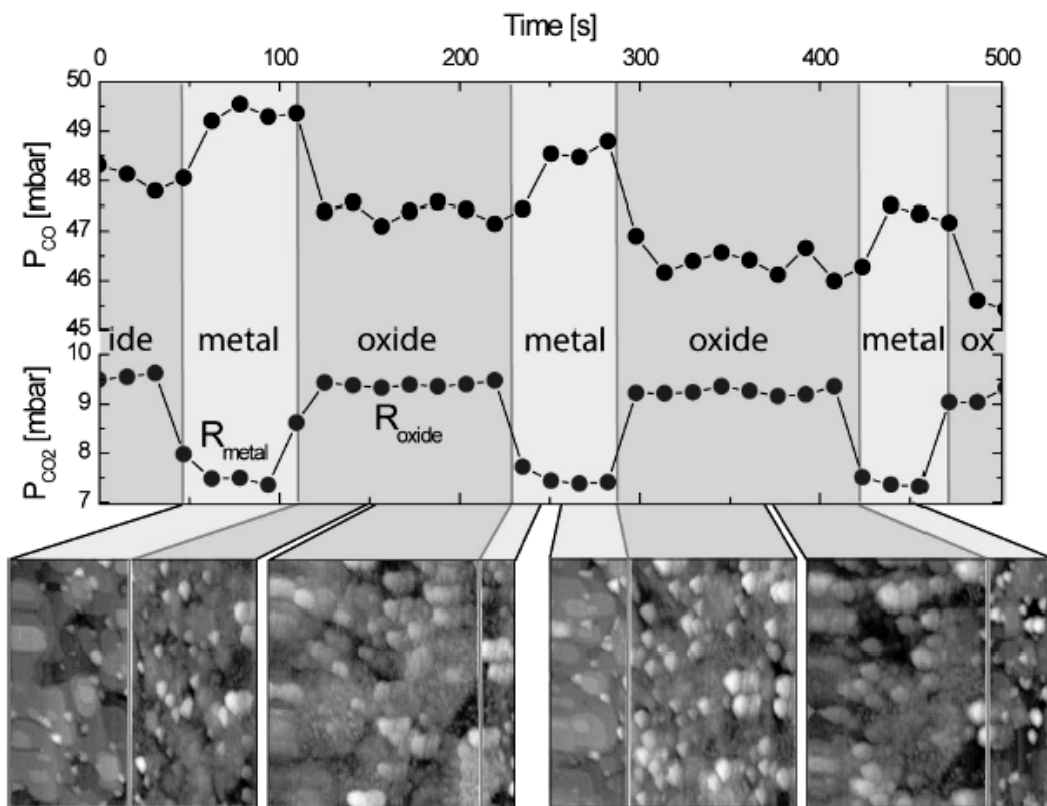
Figure 4.2: Spontaneous oscillations in the CO oxidation rate on Pd (100) at a constant oxygen pressure of 1.25 bar and temperature of 408 K. The combination of the reaction rate and simultaneously recorded STM images (100 nm × 100 nm) shows that the oscillations are the periodic oxidation and reduction of the surface. V_t=100 mV, I_t=0.2nA.

As will be discussed below, we attribute the long oscillation period to the slow variation of the surface roughness. Indeed, even during the short times in Fig.3.2 that the surface stays in the metal phase, we observe a decrease in surface roughness, while the roughness can be seen to increase somewhat in the oxide phase.

Since clean Pd surfaces and Pt(111) do not reconstruct, kinetic oscillations attributed to adsorbate-driven transformations of the surface structure, such as (de)-reconstruction, are unlikely. Contrary to Pt(110) [36-38], the Pd(110) surface does not undergo faceting during CO oxidation, so also the faceting scenario can be ruled out as the cause for reaction oscillations on the palladium surfaces. Although it would be difficult to exclude the possibility of sub-surface oxides, based on the STM observations alone, our SXRD measurements provide additional, strong evidence for the formation of a surface oxide, rather than a mere sub-surface

layer of oxygen [46]. So, we are forced to also disqualify the sub-surface oxygen model. The SXRD observation of surface oxides on Pt and Pd surfaces makes the oxidation-reduction model of Sales, Turner and Maple (STM) a very interesting, potential explanation for the oscillations observed during high-pressure CO oxidation over palladium model catalysts. However, there is one striking difference between this model and our measurements. STM model assumes that the surface oxide formed at ambient pressures shows no reactivity at all. By contrast, our combined "in situ" STM and SXRD measurements clearly prove that the formation of the surface palladium (platinum) oxides are associated with higher catalytic activity than that on the metal.

We have arrived at the conclusion that none of the existing models for reaction oscillations apply to our observations on Pd(100) and Pd(1.1.17). In the next we introduce a new mechanism that is fully consistent with all our observations for reaction oscillations during CO oxidation.

4.4 The role of roughness

On the basis of the experimental results that have been discussed in the previous chapter plus additional results obtained with SXRD [46], Hendriksen *et al.* have proposed a new model for the origin of oscillations on palladium surfaces [47]. There are two new elements in this new scenario that combine to cause the oscillatory behaviour of CO oxidation on Pd surfaces. The first essential ingredient is the continuous roughening of the oxide surface and the smoothening of the metal surface observed under reaction conditions. The other key element is a one-to-one relation between the roughness (step density) of the surface and the conditions, e.g. the partial pressure of CO, at which the transition metal-oxide takes place.

The idea that the roughness of a catalyst plays an important role in the dynamic behaviour of a chemical reaction is not new. There is a lot of literature containing experimental observations about oscillatory phenomena associated with oxidation reactions on unsupported catalytic surfaces as wires and gauzes on a variety of materials, such as Pt, Pd, Ni and their alloys. Summarizing the experimental results reported in the literature, we identify three aspects that stand out [48]:

i) Completely smooth wires do not readily ignite, but must "activated" by heat treatment, which roughens the surface [49-52]

ii) Smooth wires do not exhibit reaction oscillations and analysis of the simple models confirms that such oscillations should not be possible [53]

iii) Roughened wires oscillate for a rather wide range of catalysts and reactant gases, and these oscillations tend to be very complex (a complete overview of these observations has been given in reference [48].

We now show how surface roughness can play an important role also in the oscillations of oxidation reactions on single crystals. Figure 4.3 summarizes the four stages of our oscillations model.
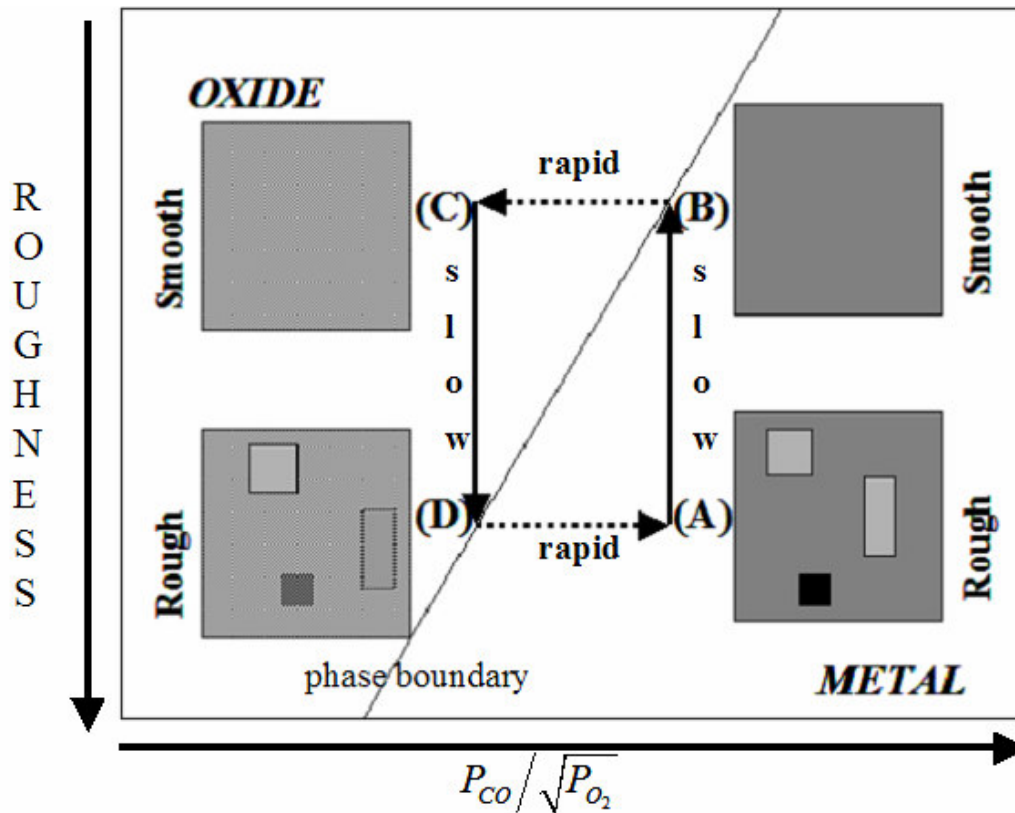

Figure 4.3: Schematic representation of an oscillation cycle. The starting point is a rough metallic surface. In the metallic phase, the surface smoothens. When the step density has reduced sufficiently, the surface suddenly oxidizes. The reaction on the oxide makes the surface increasingly rough. When the roughness is strong enough the oxide is suddenly removed and the surface is back to metallic and rough. The difference in reaction rate on the metal and the oxide leads to a noticeable difference in P_{CO} in the reactor.

We start our description of an oscillation cycle with a rough metal surface (situation A in Fig. 4.3). As explained previously the reaction on the metallic surface follows the Langmuir-Hinshelwood mechanism (gas adsorption and reaction, followed by desorption of the product) and results in a low reaction rate R_{metal}. The first part of the cycle (A)→(B) is the observed *smoothening* of the rough metal surface (cf. Fig. 4.2). The second part of the cycle (B)→(C) is the sudden *metal-oxide transition*. It takes place when the step density has become low enough. While the surface is in the oxidized state, the reaction follows the Mars-van-Krevelen mechanism with a high reaction rate R_{oxide}. In the third stage (C)→(D) the oxide becomes progressively *rough*. We have explained previously that this is due to the

Mars-van-Krevelen mechanism, which leads to temporarily undercoordinated metal atoms that become mobile for a brief period of time. Finally, the fourth part of the cycle (D)→(A) is the *oxide-metal transition.* When the oxide has become sufficiently rough the system switches back to a (rough) metal surface with lower reactivity R_{metal}.

The self-sustained cycle proposed in Fig. 4.3 is possible by virtue of a dependence of the critical CO pressure – or, more accurately, the ratio $P_{CO}/\sqrt{P_{O_2}}$ – at which the surface switches between metal and oxide or vice versa and the roughness (step density) of the surface. Indeed, such a one-to-one correspondence has been measured in high-pressure SXRD experiments [46]. There are several ways in which such dependence can be introduced. For example, when the difference in adsorption energy between CO molecules and O atoms is stronger at the steps than on the terraces of a Pd surface, the free energy of a surface with steps will reduce more quickly as a function of the CO partial pressure than that of a step-free surface. If this effect is stronger on the metal surface than on the oxide, this shifts the critical CO pressure down for rougher surfaces.

There are several qualitative features to our roughness model that can be checked immediately. For example, the timing of the oscillations should exhibit strong temperature dependence. In particular, we may expect that the time required for the metal surface to smoothen is reduced at higher temperatures due to the faster diffusion. This trend seems to be consistent with the data in Fig. 3.9, but more measurements will be necessary over a wider range of temperatures in order to really prove this point. Also, the steps introduced deliberately by turning to vicinal surfaces in Chapter 3 should have a significant effect. First of all, they should shift the critical P_{CO} to lower values than that on the low-index (100) surface, which appears to be consistent with our observations in Chapter 3. Secondly, the steps of the vicinal surfaces very much reduce the typical distance over which metal atoms need to diffuse in order to smoothen the surface, thus noticeably shortening the time that the surface spends in the metallic phase. The shape of the oscillations should therefore change for vicinal surfaces to relatively long periods of oxide phase with relatively brief interruptions by a short-lived metallic phase. Also this change in character can be recognized in the experimental data in Chapter 3 for the Pd(1.1.17) surface. Finally, when the step density is very high, the variation in roughness introduced by the oxide and metal phases becomes very small, which should make the oscillation period rather short and it should make the window of conditions over which the reaction oscillates very narrow. This seems to be the case for the Pd(553) surface, which we have not been able to bring into oscillation.

A complete description of the roughness scenario, including full mathematical details of the rate equations behind the model, will be provided in a future publication [46-47].

4.5 Conclusions

Regarding the oscillatory behaviour of catalytic systems we have briefly reviewed the most well-known models in the literature. We have also indicated where they fail to explain the experimental data introduced in Chapter 3. A new model has been proposed that provides a natural explanation of our data. The model involves two key quantities and a phase boundary between the two states of the catalyst (metal with low activity and oxide with higher activity). One of the key quantities is the partial pressure of CO. During oscillations, changes in this quantity always drive the system away from the phase boundary. The other quantity is the surface roughness. During the oscillations, the variations in roughness are such that they drive the system back to the phase boundary. Our model is fully rooted in experimental observations. The qualitative features predicted by the roughness model are consistent with the oscillations measured on Pd(100) and Pd(1.1.17).

The mechanism introduced in this chapter is not necessarily restricted to the oxidation of CO on Pt-group metals. We speculate that similar scenarios could be behind oscillations of other catalytic reaction systems.

4.6 References:

[1] B. P. Belousov, *Sb. Ref. Ridiats*. Med. Za. (1958), 1 (1959), 145
[2] C. A. de Wolf, PhD thesis, Leiden University, 2001
[3] F. Schüth, B. E. Henry, L. D. Schimidt, *Adv. Cat.***39** (1993) 51.
[4] P. K. Tsai, M.G. Wu, N. M. Maple, *J. Catal.***127** (1991), 512
[5] L. Loban, D. Luss, *J. Phys. Chem* 93 (1989), 6530
[6] H .G. Lintz, T. Weisker, Apl. Surf. Sci. 24 (1985), 251
[7] J. E. Turner, B. C. Sales, M. B. Maple, Surf. Sci. 109 (1981), 591
[8] N. I. Jaeger, P. J. Plath, E. van Raaij, Z.Naturforsch.36A (1981), 395
[9] C. A. de Wolf and B. E. Nieuwenhuys, *Catal. Today* **70** (2001) 287.
[10] E. McCarty, J. Zahradnik, G. C. Kuczynski, and J. J. Carberry, *J.Catal.***39**, (1975), 29
[11] J. E. Zuniga, and D. Luss, *J. Catal*. **53** (1978), 312
[12] M. F. Stephanopoulus, L. D. Schmidt, and R. Caretta, *J. Catal.* **64,** (1980), 346
[13] C. G. Vayenas, B.Lee , and J. Michaels, J. Catal. 66 (1980), 36
[14] M. Sheintuch, and D. Luss, J. Catal. 68 (1981), 245
[15] M. Eiswirth, P. Möller, K. Wetzl, R. Imbihl and G. Ertl, *J.Chem.Phys.* **90** (1989) 510.
[16] P. K. Tsai, M.G. Wu and M. B. Maple, *J. Catal.* **127** (1991) 512.
[17] R. T. Plichta and R. A. Schmitz, *Chem. Eng. Commun.* **3** (1997) 387.
[18] W. Keil and E. Wicke, *Ber. Bunsenges. Phys. Chem.* **84** (1980) 377.
[19] M. P. Cox, G. Ertl, R. Imbihl and J. Rüstig, *Surf. Sci.***134** (1983) L517.
[20] *Catalysis Today,* Vol.**105,** Issue 2 (2005)-Oscillatory Behaviour of Heterogeneous Catalytic Reactions , ed.by M.M. Sliknko and J. N. Jaeger
[21] B. L. M. Hendriksen, S. C. Bobaru and J.W.M.Frenken, *Surf. Sci.* **552** (2004) 229.
[22] B. L. M. Hendriksen, S. C. Bobaru and J.W.M.Frenken, *Catal. Today* **105** (2005) 243.
[23] M. Sheintuch, *J. Catal.* **96** (1985), 326
[24] N. N. Boutin and E. A. Leontovich, *"The Methods and Technique of the Theory of Bifurcation of Dynamical Systems on a Plane"* Nauka, Moscow, 1976 (In Russian).
[25] A. A. Andronov, E. A. Leontovich, I. I. Gordon and A. G. Maier *"Theory of Bifurcation of Dynamic Systems on a Plane"* Wiley, New York, 1973.
[26] A. A. Andronov, E.A. Vitt and S. E. Khaikin, *"Theory of Oscillations"*, Pergamon Press, Oxford, 1966.
[27] P. Gray and S. K. Scott , *"Chemical Oscillations and Instabilities: Nonlinear Chemical Kinetics"*, Oxford University Press, Oxford, 1990.
[28] M. M. Slin'ko, and N. I. Jaeger, *"Oscillating heterogeneous catalytic systems"*, Elsevier, Amsterdam, 1994.
[29] V. P. Zhdanov, *Surf. Sci. Rep.* **55** (2004) 1.
[30] R. Imbihl, and G.Ertl, *Chem. Rev.*, **95** (1995) 697.
[31] M. J. Feigenbaum, *J. Statist. Phys.* **19** (1978) 25.
[32] G.Ertl, P. R. Norton, and J. Rustig, *Phys. Rev. Lett.* **49** (1982) 177.
[33] M. M. Slin'ko et al., *Surf. Sci.* **264** (1992) 157.
[34] K. Krischer, M. Eiswirth, and G. Ertl, *J. of Chem. Phys.* **90** (1989) 510.
[35] G. Ertl, *Adv. Catal.* **37** (1990) 213.
[36] S. Ladas, R. Imbihl, and G. Ertl, *Surf. Sci.* **198** (1988) 42.
[37] S. Ladas, R. Imbihl, and G. Ertl, *Surf. Sci.* **197** (1987) 153.

[38] R. Imbihl, S. Ladas, and G. Ertl, *Surf. Sci.* **206** (1987) L 903.

[39] R. Imbihl, J. Falta, D. Kaletta, and M. Henzler, *J. Vac. Sci. Technol.* **A9** (1991) 1749.

[40] R. Imbihl, M. Sander, and G. Ertl, *Surf. Sci.* **204**, (1988) L701 .

[41] V. A. Burrows et al., *Surf.Sci.* **160** (1985) 122.

[42] N. A. Collins, S. Sundaresan, and Y. J. Chabal, *Surf. Sci.* **180** (1987) 136.

[43] S. Ladas, R. Imbihl, and G. Ertl, *Surf. Sci.* **219** (1989) 88.

[44] R. Imbihl, *Prog. in Surf. Sci.* **44**, 185.

[45] B. C. Sales, J. E. Turner, and M. B. Maple, *Surf. Sci.* **114** (1982) 381.

[46] M. L. D. Ackermann et al., to be published

[47] B. L. M. Hendriksen et al., to be published

[48] K. F. Jensen, and W. H. Ray, *Chem. Eng. Sci.* **35** (1980) 2439.

[49] C. G. Rader, and S. W. Weller, *A I Ch E J* **10** (1974) 272.

[50] W. M. Edwards, J. E. Zuniga, F. L. Worley and D. Luss, *A I Ch E J* **20**(1974) 571.

[51] C. L. Parson, *Ind. Engng. Chem.* **11** (1919) 541.

[52] L. D. Schmidt, and D. Luss, *J. Catal.* **22**(1971) 269.

[53] W. H. Ray, A. Uppal, and A. B. Poore, *Chem. Eng. Sci.* **29** (1974) 1330.

Chapter 5

CO oxidation on Pt(111):overlayers, oxidation and reaction oscillations

In this Chapter we describe in-situ STM observation of Pt(111) during the catalytic oxidation of CO at atmospheric pressure (1.25) bar and elevated temperatures. Similar to the palladium surfaces of Chapter 3 we observe the presence of two reaction branches, one corresponding to a metallic surface and the other to a surface oxide. Oscillations between these two branches are also observed.

5.1 Introduction

As explained in the introductory chapter the most important three criteria that need to be met before a metal can be regarded as a "good" catalyst for any reaction are: good selectivity for the specific reaction, high activity for that reaction and long active life. Platinum based catalysts have many applications. We mention here the catalytic combustion of hydrocarbons and CO, in the treatment of vehicle exhaust gases and in the purification of hydrogen for use in fuel cells. Platinum is also a good catalyst for the production sulphuric acid and for the production of nitric acid via NH_3 oxidation to NO_2. Another application is the conversion of alcohol to formaldehyde [1]. Moreover platinum is a catalyst in the production of biodegradable elements for household detergents [2]. It is also one of the most used materials in electrocatalysis.

In Chapter 2 and 3 we already mentioned that self-sustained oscillations in reaction rate have been observed during CO oxidation over platinum crystals [3], similar to those on palladium surfaces. Interestingly, in previous work by our group on Pt(110) no reaction oscillations have been observed. In this chapter we turn to the (111) surface of Pt. We will see that, similar to Pt(110) and the Pd surfaces investigated in the previous chapter, the Pt(111) surface is oxidized at sufficiently high oxygen pressures. Again we observe the existence of two distinct reaction branches. By contrast with Pt(110) we do observe reaction oscillations on Pt(111). We will discuss the similarities and differences in structure, reactivity and oscillation behaviour with the other Pd and Pt surfaces. We will start this chapter with a brief description of Pt(111) and with summaries of previous work on platinum oxides and on the interaction of Pt with CO at high pressures.

5.2 Structure of clean Pt(111)

The crystal structure of platinum is face-centred cubic with a lattice parameter at 20°C of 0.392 nm. Among the low-index surfaces of platinum, the (111) plane is preferred by the majority of the researchers, due to its flatness and its low surface energy. Atoms in the (111) plane have 9 nearest neighbours, which should be compared with their regular coordination number of 12 in the bulk. Pt(111) surface has a step height of 2.2 Å. Figure 5.1 shows a ball model of this unreconstructed, close-packed surface.
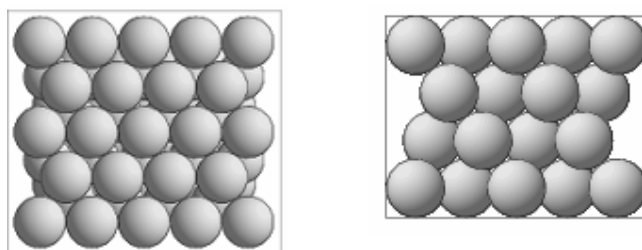

Figure 5.1: *Plan and profile views of (111) of platinum surface using a hard-sphere model.*

5.3 Previous work on Pt(111)

5.3.1 Existence and stability of surface platinum oxides - a literature survey

Since platinum is one of the elements that are well known for their chemical inertness to oxidation, the existence and stability of surface platinum oxides have been extensively studied for a long time. Nevertheless, the structures and properties of the surface platinum oxides have been poorly characterized and sometimes their existence has even been questioned. In an early study Moore and Pauling reported that PtO is probably isostructural with PdO and PtS [3]. Galloni and Roffo have used X-ray diffraction to find a body-centered cubic lattice for Pt_3O_4 [4]. Reinterpreting these diffraction data, however, Shishakov et al. have concluded that the actual composition of this oxide was not Pt_3O_4, but Pt_3O_8 [5]. In the work by Ariya et al., Pt_3O_4 has been described as a tetragonal lattice with unit cell dimensions of $a_o = 7.98$ Å and $c_o = 5.44$ Å [6]. The hexagonal structure of PtO_2 has been determined by Busch et al. [7]. According to these authors, at low temperatures only an amorphous oxide is formed. Only after a heat treatment at 350ºC the hexagonal lattice was visible. In 1968 Müller and Roy have investigated the Pt-O system using X-ray powder diffraction at high oxygen pressures (up to 3.500 bar) and temperatures ranging from

400ºC to nearly 900ºC. They identified three platinum oxide phases: the hexagonal α-PtO_2 with $a_o = 3.10$ Å and $c_o = 4.8$ Å, a new phase β-PtO_2 ($CaCl_2$ structure) with $a_o = 4.486$ Å, $b_o = 4.537$ Å, $c_o = 3.138$ Å, and Pt_3O_4 [8].

Using the tools of surface science the formation of platinum oxides on low-index surfaces of single-crystalline platinum and on polycrystalline platinum has been studied under conditions ranging from UHV to ambient pressures. Berry has studied the multilayer surface oxidation of polycrystalline Pt wire using a high-precision electrical resistance technique. His observations have shown that the oxide growth commences within 3 h after the Pt is exposed to about 1 bar of O_2 at 450ºC; once started, the oxide growth will continue at temperatures in the range of 450-560ºC [9]. From their Auger electron spectroscopy studies of the oxidation of Pt(111) Bonzel and co-workers have concluded that not platinum, but oxidized Si impurities are responsible for structures that would have been mistaken for a surface "platinum oxide" [10]. In an extensive study Salmeron *et al.* have used LEED to identify the oxide structure formed on Pt(111), Pt(332) and Pt(110) under UHV conditions. All structures found could be related to hexagonal planes of PtO_2 [11]. Studying the oscillatory CO oxidation on a supported catalyst, EuroPt-1, at atmospheric pressure, Hartmann and co-workers found the existence of a mixture of PtO and Pt_3O_4 [12].

5.3.2. Interaction of Pt(111) with CO

The adsorption system carbon monoxide on Pt(111) is without any doubt one of the "Drosophilae" of surface science and a large database on this interaction has been acquired under UHV conditions. Trying to bridge the so-called "pressure gap", several research groups have recently extended these studies to intermediate and high pressures.

Structural and energetic information about the adsorbed CO layer in equilibrium with the gas phase has been obtained using a variety of techniques. From LEED investigations under UHV conditions Ertl and co-workers have concluded that the heat of adsorption of CO on Pt(111) is strongly coverage dependent [13]. A ($\sqrt{3}$x$\sqrt{3}$)-R30º pattern was identified up to θ_{CO}=1/3, which transformed into a c(4x2) structure at θ_{CO}=1/2. As a saturation value of θ_{CO}=0.68 was approached a hexagonal close-packed CO layer was formed. The atomic resolution introduced by the STM has enabled the imaging of the CO overlayer structures, also under ambient conditions, which has initiated a debate about the inequivalence between the structures found in vacuum and under atmospheric pressures. Jensen and collaborators [14] have investigated a stepped and a flat Pt(111) surface in a CO-rich atmosphere at room temperature. At pressures higher than 200 torr a hexagonal, close-packed layer of CO was identified. The layer is incommensurate with the Pt(111) substrate, showing an intermolecular

separation of 3.7 Å and a Moiré pattern with a period of 12 ± 1 Å. According to Jensen et al., no ordered CO structure was observed at pressures lower than 1×10^{-4} bar. Kruse Vestergaard et al. investigated Pt(111) under 1 bar of CO at room temperature. These authors found two rotational domains of a hexagonal Moiré pattern with a period of 11.8 ± 0.4 Å, rotated over $24 \pm 2°$ with respect to the structure of the underlying Pt substrate [15]. The unit cell of this new structure was identified as (√19x√19) R23.4°-13CO. At low pressures (10^{-6} Torr) and low temperatures (170 K) the same Moiré pattern was observed. Based on their measurements Kruse Vestergaard et al. have concluded that increasing the pressure is equivalent with decreasing the temperature, which is to be expected on the basis of thermodynamics, provided that the kinetic barriers can be overcome at the lower temperature so that equilibrium is established on an acceptable timescale. The results in Ref. [15] are in good agreement with earlier low-temperature LEED studies and "in situ" electrochemical studies (STM combined with IRAS) [16].

5.4. Experimental

The experiments presented in this paper have been performed using the home-built combined flow Reactor-STM described in detail in the introductory chapter. This combination allows us to image the surface of a model catalyst during a reaction at atmospheric pressures. Simultaneously, we can determine the catalytic activity by analysis of the gas flow leaving the reactor using a quadruple mass spectrometer. Connected to the Reactor-STM we have a dedicated gas system especially made for high-pressure use, which allows us to independently mix the high purity gases in the desired ratios, set the pressure in the reactor and control the flow rate.

The Pt single-crystal (Czochralski grown, 5N purity) was purchased from Surface Preparation Laboratory [17], where it was spark eroded to a cylindrical shape with a diameter of 10 mm and a thickness of 2 mm and where its surface was mechanically polished to within 0.1° from the (111) orientation. In our UHV system, the surface was further prepared by repeated cycles of Ar^+ ion sputtering and O_2 (1×10^{-6} mbar) treatment at 800-900 K, followed by annealing in UHV at ~1100 K. The cleanliness and crystalline order of the surface has been checked with LEED and with the STM.

5.5 Results and discussion

5.5.1 CO adsorption on Pt(111) at ambient pressure

Images A and B in Figure 5.2 have been recorded in 1 bar of CO at room temperature. They show the Moiré pattern, previously identified by Kruse

Vestergaard et al. [15]. After this observation, we heated the sample for 2 hours to 393 K in a 1.18 bar flow of CO (the partial pressure of O_2 has been low 4.6×10^{-4} mbar). Image C was recorded under these conditions. Even though the resolution in image C is not as good as that in images A and B (due to the thermal drift the Moiré pattern seems stretched) the ($\sqrt{19} \times \sqrt{19}$) R23.4°-13CO overlayer can be recognized.
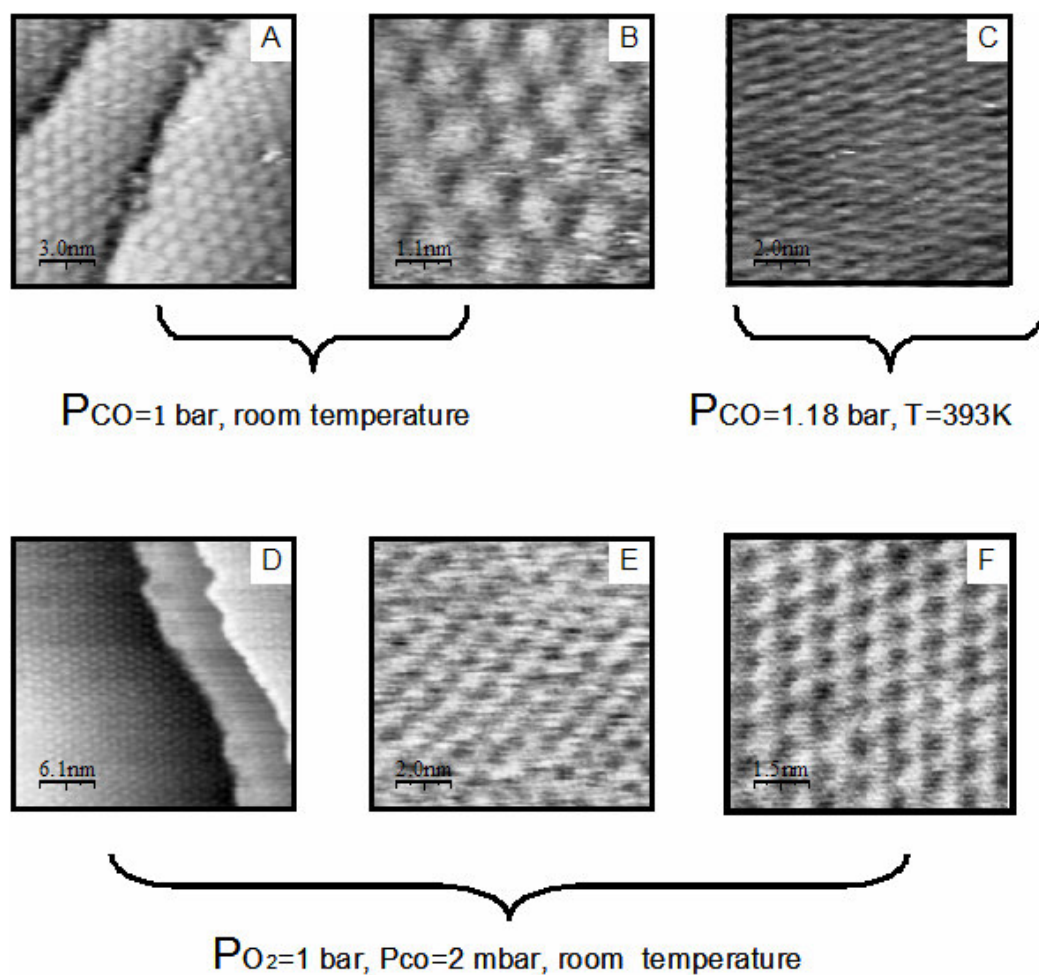

Figure 5.2: STM images illustrating the formation and stability of the Moiré pattern of a dense, ($\sqrt{19} \times \sqrt{19}$) R23.4°-13CO overlayer of CO molecules on Pt(111) under different gas compositions and temperatures. Images A (15 nm × 15 nm) and B (7.6 nm × 7.6 nm) were acquired in 1 bar of CO at room temperature, image C(9.8 nm × 9.8 nm) at 393 K in 1.18 bar CO rich flow and images D (30 nm × 30 nm), E (9.8 nm × 9.8 nm) and F (7.6 nm × 7.6 nm) at room temperature and 1 bar of oxygen, with a low, approximately 2 mbar residual component of CO. I_t=0.2nA and V_t=0.1V.

The survival of the Moiré pattern after the sample temperature had been raised above 100°C indicates that at the high partial pressure of CO, the

63

impingement rate of CO was sufficient to maintain the saturation overage of the CO overlayer, i.e. it was higher than the desorption rate of CO from the surface at that temperature. Immediately after we switched to an oxygen-rich flow the CO overlayer pattern disappeared. We interpret this as the result of the rapid removal of the adsorbed CO molecules by the reaction with the oxygen, after which the surface became oxygen covered.

Images D-F were recorded after exposing the sample to 1 bar of oxygen at 423 K, under which conditions it oxidized (see below), and subsequently cooling it down to room temperature, still in 1 bar of oxygen. To our surprise, the images no longer exhibit the characteristics of an oxide but instead they contain the Moiré pattern associated with a close-packed CO overlayer. This shows that the low residual pressure of CO (only 2mbar; to be compared with the O_2 pressure of 1 bar) is sufficient to poison the model catalyst surface at room temperature. In the light of this observation we can conclude that in order to obtain information on the structure and composition of the surface that truly applies to the situation under actual reaction conditions it is important not just to increase the pressures of the reactants into the practical regime but to also investigate the surfaces at sufficiently high temperatures, in order to avoid poisoning. Another argument to work at elevated temperatures is that the kinetic barriers for one or more of the processes may be high enough to dramatically slow down or even block the catalytic cycle. For the complete characterization of a catalytic system *temperature does matter!*

5.5.2 STM images combined with reaction kinetics

The results of a typical experiment under reaction conditions, i.e. with mixtures of CO and O_2 and at elevated temperatures, are summarized in Fig.5.3. In the upper panel a selection of images is displayed from an STM movie, showing the surface structure during the catalytic oxidation of CO on Pt (111). The lower panel depicts the partial pressures of the reactant gases CO and O_2 and the reaction product CO_2, as measured by mass spectrometry simultaneously with the STM movie. The CO_2 signal is proportional to the reaction rate. The experiment reported here started in an oxygen-rich flow of a mixture of O_2 and CO at a total pressure of 1.25 bar and a temperature of 423 K. Image G corresponds to the smooth platinum surface with large, flat terraces, separated by monatomic steps. At $t = 0$ s the CO pressure was slowly decreased and the CO_2 pressure followed this decrease until t = 750 s, where we observed an abrupt upward step by a factor 1.4 in CO_2 production rate (indicated by the arrow in the lower panel). The step in reaction rate occurred during the acquisition of image H. Above the dashed line in the upper part of image H we notice a dramatic change from the original, flat surface to a disorganized, rough surface. The sudden appearance of the rough structure coincided with the upward step in reaction rate. The analogy with Pt(110) and the Pd surfaces discussed in the previous chapter strongly

suggests that a surface oxide is formed, which is more reactive than the metallic surface. Image I shows the further build-up in time of rough structures that we associate with the platinum oxide. At $t = 2500$ s we increased the CO pressure. This resulted in an abrupt change back to a surface with flat terraces and steps with the step height of Pt(111). Initially, several Pt vacancy islands were left behind, as seen in image J that decayed with time. Following the increasing in CO pressure the reaction rate signal passed through two subsequent maxima.
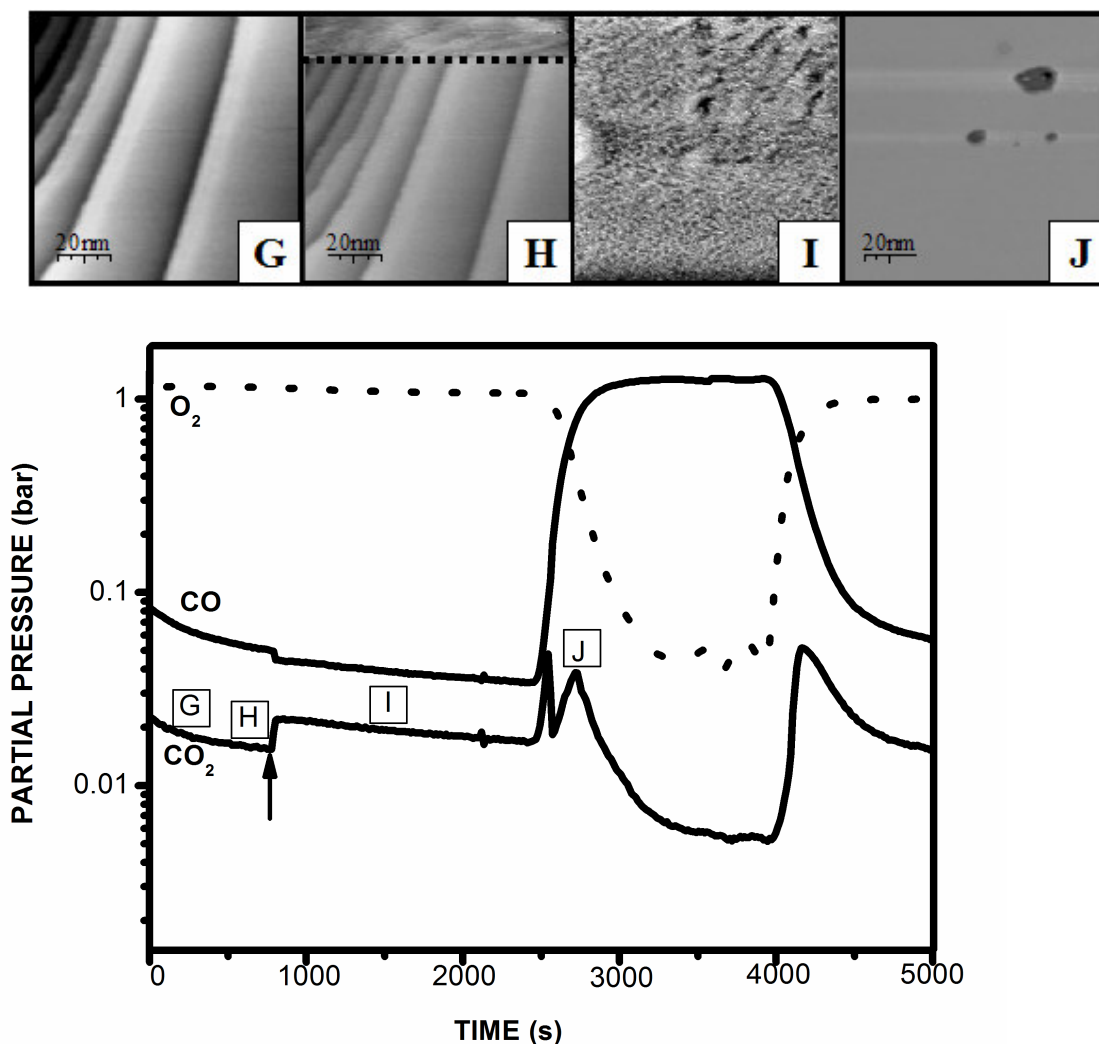

Figure 5.3: STM images and mass spectrometer signals measured simultaneously during CO oxidation on the Pt(111) surface in a flowing mixture of O_2 and CO at a total pressure of 1.25.bar and a temperature of 423 K.

The first one has the shape of a continuous rise in CO2 signal, starting at $t = 2500$ s, and a sharp downward step somewhat later. The next maximum, around $t = 2750$ s is broader and has no sharp features. The first peak results from the fact that the reaction rate initially follows the increase in CO partial pressure. When P_{CO} exceeds a critical value and the oxide is suddenly removed and the reactivity steps down to the lower level characteristic for

65

the metal surface. Indeed, this downward step coincides with the sudden change back to the flat, i.e. metallic, surface in the STM images. The second peak has the characteristics of the maximum rate in Langmuir-Hinshelwood kinetics. The presence of a peak actually implies that when the oxide surface is reduced to the metal surface, oxygen forms the dominant species adsorbed on the surface. When the partial pressure of CO is further increased, the CO coverage grows and at the maximum we have $\theta_{CO} = \theta_O = 0.5$. When P_{co} is increased further, the reaction rate drops because carbon monoxide poisons the catalyst surface. At t = 4000 s we switched again to an oxygen-rich flow. The reaction rate increases, passes again through the maximum of Langmuir–Hinshelwood kinetics, at t = 4142 s, and then decreases again, more or less proportional to the CO pressure, as oxygen becomes the dominant surface species.

For a more detailed understanding of the above results we will go through our interpretation step-by-step and provide additional information to support our conclusions. A series of images from a different STM movie with higher resolution is shown in figure 5.4 in order to underline the changes in the surface due to exposure of high pressures reactive gases.
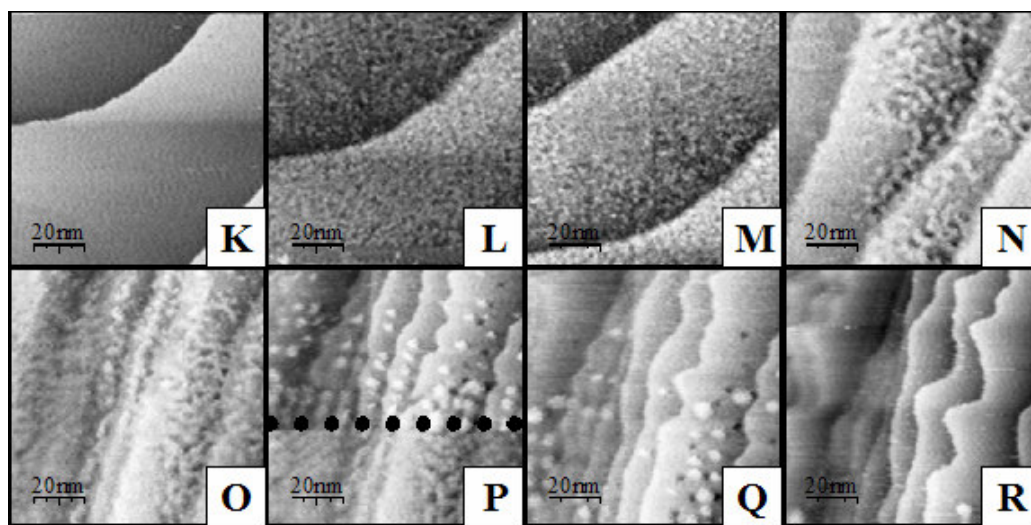

Figure 5.4: *STM images recorded in a flowing mixture of O_2 and CO at 413 K and a constant total pressure of 1.25 bar. Images K-O have been acquired in an oxygen-rich flow. Image K corresponds to the metallic Pt (100), with large flat terraces. In image L acquired immediately after image K small protrusions are visible. We assign this change of the surface to the formation of a thin platinum oxide with higher reactivity, which gradually develops cluster-type structures (images L-O and lower part of P). The upper part of image P and images Q-R correspond to the metallic surface after the oxide was removed, due to the exposure to a CO-rich flow. This removal is seen to lead to the formation of vacancy and adatom islands. In time these structures decayed and the flat surface of Pt (111) was restored. The size of the STM images is 100 nm × 100 nm. I_t=0.2 nA and V_t=0.2V.*

The metal surface before oxidation:

Image G and the lower part of image H in Figure 5.3 as well as image K in Figure 5.4 show that in the initial gas mixture, the platinum surface had the same structure as a freshly prepared clean Pt(111) surface in UHV, with flat, large terraces separated by monatomic steps (d_{step}=2.2 Å). As argued above, the observation of a maximum in the Langmuir-Hinshelwood reaction rate on the metal surface as a function of CO pressure indicates that just prior to oxidation the metal surface was covered mainly by oxygen. Since prior to oxidation there was a modest CO_2 production, resulting corresponding to a partial pressure of CO_2 of 20 mbar, also a small amount of CO must have been present on the surface in spite of the high coverage of oxygen.

The oxide evolution in time:

We assume that the oxidation of the metal surface follows the next steps:
(1) O_2 molecules reach the metal surface and O atoms are chemisorbed.
(2) As soon as the concentration of chemisorbed oxygen reaches a critical level the surface oxidizes. The oxidation itself may involve the initial formation of oxide clusters followed by lateral growth and coalescence of these.
(3) Once the layer is closed, the oxide may continue to grow in thickness, i.e. in the direction perpendicular to the surface.

For a qualitative description of the oxidation process of a surface one would need to find answers to the following fundamental questions:

(1) What is/are the oxide structure(s) and how does it depend on the oxidation parameters (temperature, pressure and gas composition)? Does it depend on the surface morphology (steps, defects, etc.)?
(2) How does the oxide thickness develop with the oxidation time (oxidation kinetics)?
(3) What is the epitaxial relation between the metal substrate and the oxide surface film?
(4) What are the rate limiting factors in the oxidation process?
(5) Is the oxide film passivating or is it catalytically active?

In our case the lack of atomic resolution makes it difficult to obtain answers to all of these questions on the basis of the STM images alone, but valuable information about the oxide could still be extracted from them.

In Figure 5.3, the upper part of image H and image I and in Fig. 5.4, images K-O and the lower part of image P (below the dashed line) show the development in time of a structure that we attribute to a form of platinum oxide. In all cases, the surface is rougher than the metallic surface, prior to

oxidation. The roughness comes in the form of pits and protrusions. As we had already seen above, this surface exhibits a higher reactivity than the metallic surface. Our conclusion that the rough, higher-reactivity surface corresponds to a surface oxide film is supported by observations with complementary techniques. Preliminary Surface X-ray Diffraction measurements by Ackermann et al. have confirmed the formation of a thin (1-2 ML) film of platinum oxide, when Pt (111) is exposed to high pressures of oxygen at high temperatures [18]. Based on these measurements, the structure of the oxide has been identified to correspond to be relaxed PtO_2, azimuthally aligned but with lattice periods that are incommensurate with the underlying Pt(111) substrate. Similar to the case of Pt(110) [19], also on Pt(111) there is an alternative, oxide-like structure that is present in a certain range of partial pressures and temperatures when both CO and O_2 are present. In this context we also recall the work by Li and co-workers, whose results on high-pressure oxidation of Pt(110) has revealed the formation and co-existence of ordered surface oxide islands with chemisorbed reconstructed (12×2)-O structure [20].

Carefully comparing the partial pressures during 50 oxidation-reduction cycles, we come to the conclusion that at fixed O_2 pressure the oxidation takes place when the CO partial pressure is lowered to a critical value. For example, at $P_{O_2} = 1.14$ bar and $T = 418$ K, this critical CO pressure is $P_{CO} = 0.022$ bar. From image H (in Fig.5.3) and upper part of image K in Fig.5.4 we have concluded that the change from a smooth, metallic surface to a rougher, oxidized surface happens within the time of one single scan line, which amounted to 1line scan/s in the present experiment. We have analysed the height profiles on the (same) middle terrace in images K and L, i.e. directly before and after oxidation, and also we have compared the Z corrugation values for the same square region in both images. Careful analysis of the individual scans lines within which the surface oxidized shows that the local height increases abruptly by 1.2 ± 0.8 Å (e.g. difference between images K and L). The large error margin reflects the fact that the change in reactivity, caused by the oxidation, also results in a stepwise change of the thermal drift, which makes it difficult to extract a reliable number for the height change. These observations are a good indication that at the beginning of the oxidation process the surface was immediately covered with a thin but rough oxide layer. Figure 5.5 repeats panel M from Fig. 5.4 and shows an enlargement of the marked, central square.
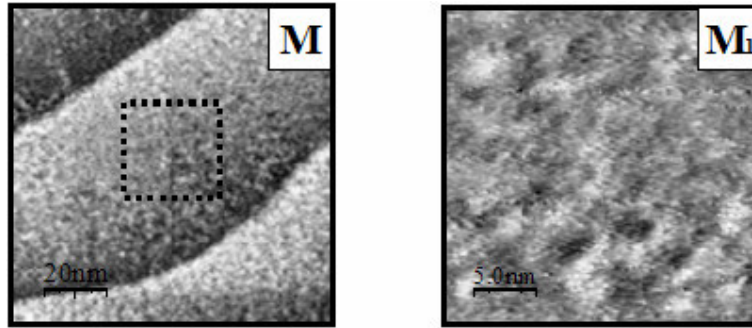
Figure 5.5: *The oxide surface immediately after oxidation (F). Image F_1 (25nm×25nm) is a zoom in on the middle terrace (dashed square) from image F (100nm×100nm). The oxide has small protrusions and pits with a typical lateral size of 2 nm and a typical height/depth of 1 ± 0.36 Å. I_t=0.2 nA and V_t=0.2V.*

In the next series of images (Figure 5.6) the development in time of the oxide roughness is shown from small corrugations of typically 1.25 ± 0.75 Å and short lateral length scales of typically 1.7 ± 0.2 Å to larger structures with typical dimensions of 2 ± 1 Å and 19 ± 0.5 Å in height and in width. It seems that this coarsening is not uniform over the surface and that it initiates primarily at steps, as can be seen in images M and H. The mechanism behind the preferential growth of the oxide patches might be similar to the one responsible for the formation of the denuded zones, as a result of oxygen outdiffusion during a high temperature-annealing step of a few hours, on silicon surfaces [21].
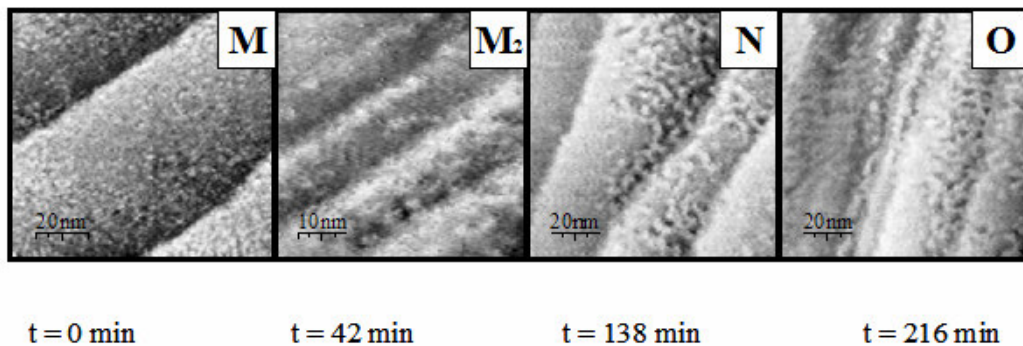

t = 0 min   t = 42 min   t = 138 min   t = 216 min

Figure 5.6: *Development of the oxide in time. After t = 138 min from the initial oxidation the features on the oxide surface have evolved from small protrusions (image M) to coarser structures (image N). This coarsening appears to initiate primarily close to steps. As the structures become coarser, the coarsening process slows down (images N, O). The size of image M is 50 nm × 50 nm, while the size of images M, N and O is 100 nm × 100 nm. I_t=0.2 nA and V_t=0.2V.*

If we zoom in on the second terrace in image N of the above series we clearly can distinguish the curved shapes of the cluster-like features and the depressions between them (figure 5.7). From the height profiles we

have found that the depths of those depressions varies between 1.45-3.2 Å, which does not correspond to the 2.2 Å atomic, step height of Pt (111).
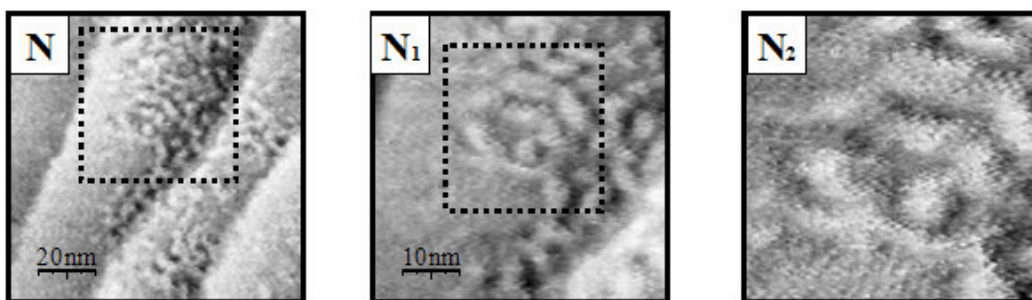

Figure 5.7: Series of STM images (N-N$_2$) were we have repeatedly zoomed in, starting with the second terrace of image N of Fig. 5.6. The height profiles of these images show height variations that are all different from multiples of the step height of Pt(111). I$_t$=0.2 nA and V$_t$=0.2V. The size of the images is 100nm×100nm (N), 50nm×50nm (N$_1$) and 25nm×25nm (N$_2$).

The metallic surface after the oxidation

When we increased the CO pressure again at t = 2520 s in Figure 5.3, the oxide was removed at a higher CO pressure of 54 mbar than the CO partial pressure of 44 mbar at which it had been formed. The metallic surface immediately after the reduction of the oxide showed a number of platinum adatom and vacancy islands (image J in Fig. 5.3 and the upper part of image P and images Q-R in Fig. 5.4). These observations are similar to those of Itaya and co-workers, who observed adatom and vacancy islands on the Pt(111) surface after cycles of an electrochemical oxidation-reduction process [22]. Figure 5.8 shows images of the metallic surface immediately after reduction of our high-pressure oxide, as observed in three different experiments performed at the same pressure (1.25 bar) but different temperatures. The imperfect hexagonal shapes of the platinum adatoms and vacancy islands reflect the triangular symmetry of Pt(111). The heights and depths of the adatom and vacancy islands correspond to one or few times (integer number) the atomic step height of Pt(111). The general trend in all experiments that we have performed is that after the removal of the oxide, if the surface is kept in a CO-rich flow, the platinum adatom and the vacancies islands disappear in time due to ripening or coalescence processes and the surface smoothens again.
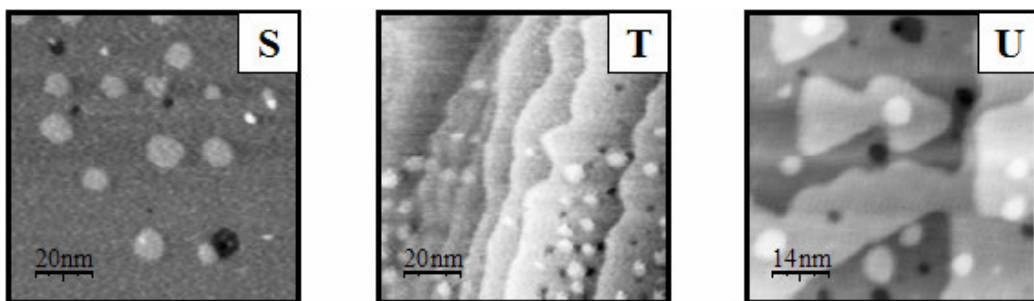
70

Figure 5.8: *STM images corresponding to the metallic surface, briefly after the oxide had been reduced, obtained in three different sets of measurements performed at the same pressure 1.25 bar and different temperatures. Image S (100 nm × 100 nm) was acquired at T = 373K, image T (100 nm × 100 nm) at T = 413 K and image U (70nm × 70 nm) at T = 420 K. The shape of the adatom and vacancy islands reflects the hexagonal (triangular) symmetry of Pt(111).*

5.5.3 I-V spectroscopy

In order to obtain additional information about the electronic structure of a surface one can make use of scanning tunnelling spectroscopy. We have performed scanning tunneling spectroscopy during switching experiments. The results are depicted in figure 5.9. The I-V curves corresponding to the low reactivity in the reaction kinetics were characteristic for a metallic surface (dashed lines in figure 5.9). The I-V measurements on the oxidic surface clearly showed semiconductor behaviour (continuous lines). In these measurements, the tunneling current was initially set at $I_t = 0.2$ nA at a tunnelling bias voltage of $V_t = 70$ mV for the metallic surface and $V_t = 1476$ mV for the oxide surface. The high bias voltage for the oxide surface was necessary in view of the measured band gap of the oxide. The I-V curves were measured by fixing the tip height and recording the tunnelling current as a function of tunnelling voltage over a sweep from -2 V to +2 V. Both on the metal and on the oxide surface, the I-V measurements were quite reproducible. From the I-V curves on the oxide surface we measure a band gap of 1.1 ± 0.1 eV. We have not measured systematic differences between I-V curves acquired at different locations on the oxide surface, but the I-V data were recorded only on the initial oxide, when the roughness was still small, both in height and in lateral length scale.

  Unfortunately there is only limited information in the literature about the band gap of platinum surface oxide. Naegele and Plieth identified by means of the Kramers –Kronig technique a band gap of 1.4 eV for a thin (2-6 Å) oxide formed on platinum during anodic polarization [23]. In electrochemical studies on platinum electrodes band gaps varying between 0.7 and 1.3 eV have been found for different species of platinum oxides [24]. Our value of 1.1 ± 0.1 eV falls comfortably within this range of band gaps.
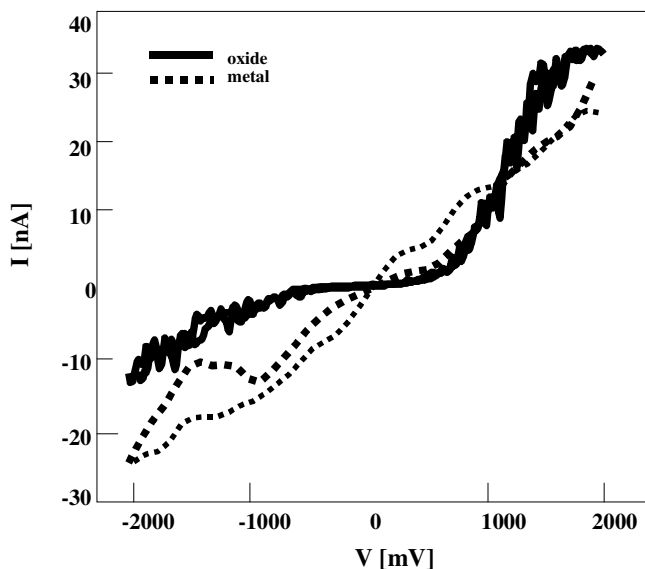
Figure 5.9: *Averaged I-V curves measured on the oxidic surface (solid line) and on the metallic surface (dotted line). The band gap measured for the oxide surface is 1.1 ± 0.1 eV.*

5.5.4 Bistability and oscillations in the reaction kinetics

As explained above, from the combined analysis of the STM images and reaction kinetics, we have concluded that during the oxidation of CO over Pt (111), a new structure is formed, which we have identified as a thin film of platinum oxide. The surface platinum oxide is formed at high partial pressure of O_2 (pressure e.g.1.12 bar) and (sufficiently) low CO partial pressure, e.g. 49 mbar in the above-mentioned experiment. In Fig. 5.10 we show that if we plot the reaction rate, measured in the form of the partial pressure of CO_2, of figure 4.3 as a function of the CO partial pressure at constant partial pressure of oxygen 1 bar), the experimental data separate into two branches. One branch corresponds to the high reactivity (oxide) and the other one to the low reactivity (the metal). Figure 5.11 summarizes the kinetics for a different set of data acquired at a total pressure of 1.25 bar and T=416 K.

Figure 5.11 (a) displays the partial pressures of the reaction product CO_2 and the partial pressure of the minor reactant CO, while the partial pressure of the major reactant O_2 was kept constant at 1.23 bar. At $t = 115$ s (indicated by the arrow) a stepwise increase in the reaction rate is recorded by the quadrupole mass spectrometer, accompanied by a step down in CO pressure. As explained earlier in this thesis, the upward step in CO_2 pressure indicates that the surface is oxidized.
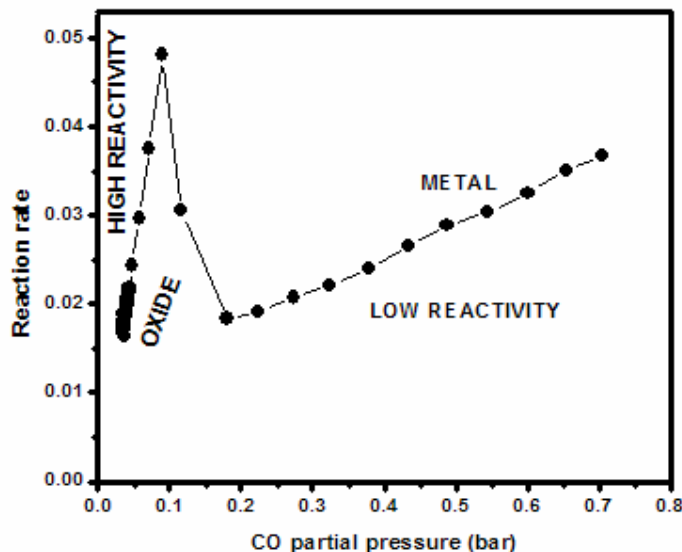
72

Figure 5.10: *The CO_2 pressure of figure 4.3 versus the CO pressure at a constant O_2 partial pressure of 1 bar and a temperature of 423 K. At low CO pressure the reaction rate shows two branches. The lower branch corresponds to the reaction on the metallic surface. The upper branch corresponds to the reaction on the oxide and shows a linear dependence of the CO_2-production on the CO-pressure.*

At t = 921 s, corresponding to a CO partial pressure of 0.032 bar, the system began to spontaneously oscillate. Accompanying the oscillations in CO_2 production there are clear oscillations in the CO partial pressure that have the opposite sign (i.e. P_{CO} goes down when P_{CO_2} goes up and vice versa). The period, amplitude and shape of the oscillations show a strong dependence on the CO pressure. For example, both the period and the amplitude of the oscillations decreased with decreasing the CO partial pressure. With reducing P_{CO}, the shape of the oscillations changed from the initial rectangular waveform to a 'spike' shape, with a more or less permanent high reactivity, interrupted by very brief low-reactivity excursions. Figure 5.11 (b) shows the same, oscillatory CO_2 production rate, plotted in the form of P_{CO_2} versus P_{CO}. From this graph it is clear that the reaction rate switched several times spontaneously back and forth between the familiar high (oxide) branch to the low (metallic) branch.

To some extent our measurements confirm the results of Colen and collaborators [25]. They have investigated the oxidation of carbon monoxide on Pt(111) at intermediate pressures (10^{-2} mbar of O_2). By manually varying the CO pressure the crystal has been "forced" to oscillate. Their observations showed that the reaction rate signal and the reactant CO are in antiphase and the rate oscillations occur above the bistable regime. Similar to our observations the oscillations had a rectangular waveform and a long period of several minutes.

73

Similarly to the behaviour of Pd(100) and vicinal Pd surface, discussed in Chapters 2 and 3, none of the models introduced previously to explain the oscillatory behaviour of CO oxidation on the platinum group metals (see Chapter 3) seems to apply to our data on Pt(111). Since Pt(111) does not have any reconstruction, the reconstruction model proposed as an explanation for the origin of the oscillations on platinum metals does not apply [26]. The faceting model is also inappropriate, since we do not observe any sign of faceting in our STM images [27]. The oxidation-reduction model proposed by Turner, Sales and Maple [28] seems to make more sense. In this model the reaction rate would oscillate between a low value, corresponding to the CO-covered metallic surface and a high value, corresponding to the mainly oxygen-covered metallic surface, via the formation of an oxide, which is considered to not be catalytically active itself. The disagreement between this model and our experimental observation is twofold. First, we do not observe the switching between two metallic versions of the surface, but only between a mainly oxygen-covered surface and an oxide. Second, the oxide is catalytically not *in*active but, in fact, it is more active than the metal.
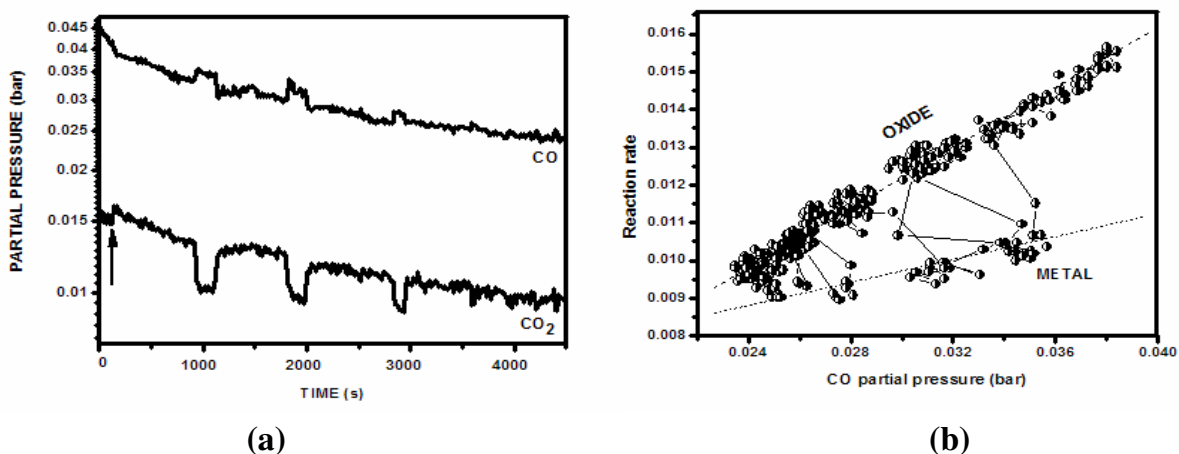

(a)   **(b)**

Figure 5.11: *(a) Partial pressures of CO and CO$_2$, during a slow, downward ramp of the CO partial pressure at T = 416 K. The O$_2$ pressure (not shown) was kept constant at 1.23 bar. The first metal-oxide transition occurred at t = 115 s. After this, spontaneous oscillations in the CO and CO$_2$-pressures were observed. (b) By re-plotting the same data in the form of P_{CO_2} versus P_{CO}, we see that the oscillations reflected the spontaneous switching between the familiar metallic and oxidic branches.*

It is important to highlight our observation that in most experiments on Pt(111) we have not observed oscillations and the hysteresis was "clockwise" (CW), meaning that the oxide was formed at a lower CO pressure than that at which it was removed. Our measurements showed that in the data sets containing oscillations, the hysteresis was always "counter

74

clockwise" (CCW). This is summarized in Table 4.1. The "direction" of the hysteresis might be a good indicator whether or not a catalytic system oscillates [29]. In previous studies performed in our group on CO oxidation at ambient pressure over Pt(110), spontaneous oscillations in the reaction rate have never been observed. By contrast, CO oxidation over Pd(100) showed oscillatory behaviour. The main differences between the two surfaces are: 1) the Pt(110) surface switched between an oxide and a metal surface that was mainly covered with CO, whereas Pd(100) switched between an oxide and an oxygen covered surface, similar to Pt (111) and 2) for the Pt(110) surface "clockwise" hysteresis was observed in all measurements, similar to Pt (111) for most of the experiments, while the Pd(100) surface had "anti-clockwise" hysteresis in agreement with the oscillatory data set for Pt(111). At this point, we can only speculate what parameters are responsible for the "direction" of the hysteresis. From experimental observations it has been concluded that in the case of Pd(100), the reaction-induced formation of roughness on the palladium oxide combined with a specific preference of CO for binding at the steps on the metallic surface are responsible for the "counter clockwise" orientation of the hysteresis and for the reaction oscillations on this surface (see Chapter 3). In those cases where reaction oscillations have been observed on Pt(111) the surface had been exposed to repeated cycles of oxidation-reduction, which might have created excessive roughness on the surface. Whether this can explain that oscillations sometimes but not always occur on Pt(111) remains to be investigated in more depth.

No.	P_t (bar)	T (K)	$P_{CO} \rightarrow$ M-Ox (mbar)	$P_{CO} \qquad \rightarrow$ Ox-M (mbar)	Hyst.
1	1.25	433	49	57	CW
2	1.5	433	45	110	CW
3	1.25	438	31	89	CW
4	1.25	433	47	65	CW
5	*1.25*	*408*	*47*	*28*	ACW

Table 5.1: The direction of the hysteresis, clockwise or counter clockwise and the values of the CO pressure at which the surface switched from the metal to oxide ($P_{CO} \rightarrow$ M-Ox) and vice-versa ($P_{CO} \rightarrow$ Ox-M) are indicated for five measurements performed at different pressures and temperatures.

5.6 Conclusions

We have studied the oxidation of CO over a Pt(111) model catalyst, using an in-situ STM combined with a flow reactor. This has allowed us to correlate the changes in the surface structure to reaction kinetics. At high CO

coverages a CO overlayer with a characteristic Moiré pattern was observed, both at room temperature and at elevated temperatures. The CO overlayer was stable under high pressures of O_2 at room temperature. Under reaction conditions two different structures have been observed, namely a (adsorbate–covered) metallic surface and an oxide. The two structures showed different reaction rates and reaction kinetics. The oxidation process has made the surface rough and the reaction has made the roughness develop further in time. The kinetics on the metallic surface followed the Langmuir-Hinshelwood mechanism, while on the oxide surface the kinetics could be explained by a Mars-Van Krevelen mechanism. Under conditions of slowly decreasing P_{CO} oscillations in the reaction rate have been observed. The mechanism responsible for making the oscillations present or absent was not fully elucidated, but our experimental observations indicate that the orientation of the hysteresis in the reaction rate might play an important role.

5.7 References

[1]   http://web1.caryacademy.org
[2]   http://wwww.unctad.org/infocomm/anglais/platinum/uses.htm
[3]   W. J. Moore, Jr. and L. Pauling, *J. Am. Chem. Soc*. **63** (1941) 7392.
[4]   E. E. Galloni and A. E. Ruffo, Jr., *J. Chem.Phys*. **9** (1941) 875.
[5]   N. A. Shishakov, V.V. Andreeva and N. K. Andrushchenko, *Stronie I Mechanism Obrazovaniya Okisnykh Plenok na Metallakh, Akad. Nauk.* SSSR, Moscow 1956, Chapter 6.
[6]   S. M. Ariya, M. P. Morozova, G. S. Markevich and A. A. Reikhardt, Sb. Stat. Obs. Khim. Akad. Nauk. SSSR, I (1953) 76.
[7]   R. H. Busch, E. E. Galloni, J. Raskovan and A. E. Cairo, *An.Acad.Brasil.Cienc.,* **24** (1952) 185.
[8]   O. Muller and R. Roy, J. *Less-Common Metals* **16** (1968) 129.
[9]   R. Berry, *Surf. Sci.***76** (1978) 415.
[10] H. P. Bonzel, A. M. Franken and G. Pirug, *Surf.Sci.***104** (1981) 625.
[11] B. Lang, R. W. Joyner, and G. A. Somorjai, *Surf. Sci.* **30**(1972) 454.
[12] N. Hartmann, R. Imbihl, and W. Vogel , *Catal. Lett.* **28** ((1997) 373.
[13] G. Ertl, M. Neumann, and K. M. Streit, *Surf. Sci.*64 (1977) 394.
[14] J. A. Jensen, K. B. Reider, M. Salmeron and G. Samorjai, *Phys.Rev.Lett.*80 (1998), 1228
[15] E. K. Vestergaard, P. Thostrup, T. An, E. Laegsgaard, I. Stensgaard, B. Hammer, and F. Bessenbacher, *Phys.Rev.Lett.*88 (2002) 259601.
[16]   I. Villegas and M. J. Weaver, *J. Chem. Phys.* 101 (1994) 1648.
[17] surf-prep-lab.com
[18] M. D. Ackermann et al, to be published
[19] M. D. Ackermann, T. M. Pedersen, B. L. M. Hendriksen, O. Robach, S. C. Bobaru, I. Popa, C. Quiros, H. Kim, B. Hammer, S. Ferrer, and J. W. M. Frenken *Phys. Rev. Lett.* **95** (2005) 255505
[20] W. X. Li, L. Osterlund, E. K. Vestergaard, R. T. Vang, J. Matthiesen, T. M. Pedersen, E. Laegsgaard,B. Hammer and F. Besenbacher, *Phys. Rev. Lett.* **93** (2004) 146104.
[21] G. Kissinger, J. Vanhellemont, G. Obermeir and J. Esfandyari, *Mat.Sci.and Eng*.**B73** (2000) 106
[22] K. Itaya, S. Sugawara, K. Sashikata and N. Furuya, *J. Vac. Sci. Technol.* **A 8** (1990) 515
[23] K.Naegele and W. J. Plieth, *Surf.Sci.***50** (1975) 64.
[24] H. Angerstein-Kozlowska, B. E. Conwayand, W. B. A. Sharp, *Electroanalytical Chemistry and Interfacial Electrochemistry* **43** (1973) 9.
[25] R. E. R. Colen, J. Christoph, F.Pena,and H. H. Rotermund, *Surf. Sci.* **408** (1998) 310.
[26] S. Ladas, R.Imbihl, and G.Ertl, *Surf.Sci.***198** (1988) 42.
[27] G.Ertl, P. R. Norton and J. Rustig, *Phys.Rev.Lett.***49** (1982) 177.
[28] J. E. Turner, B. C. Sales and M. B. Maple, *Surf.Sci.***109** (1981) 591.
[29] M. Ehsasi, M. Berdau, A. Karpowicz, K. Christmann and J. H. Block, New Frontiers in Catalysis,ed.L. Guczi et al., Elsevier Science Publishers, B. V.(1993).

Chapter 6

Oxidation of Pt (100)

In this chapter the structure, chemistry and catalytic activity of the (100) surface of platinum is discussed. From the structural point of view there is an important difference with the Pt(111) surface discussed in Chapter 5, since the Pt(100) surface exhibits a reconstruction. We show that the CO oxidation reaction on this surface has two regimes of bistability, rather than just one. The first corresponds to the transition between the metallic surface and a surface oxide, similar to the scenario on the palladium surfaces in Chapter 3 and on Pt(111). The second is the traditional bistability of the Langmuir-Hinshelwood reaction on the metal surface. The surface oxide is found to be stable only at extremely low CO pressures, where it leads to little advantage over the reaction rate on the metal surface. The Langmuir-Hinshelwood reaction turns out to have spectacularly high conversion rates.

6.1 The quasi-hexagonal reconstruction

Structure

A clean Pt(100) surface undergoes a structural transformation from a bulk like terminated Pt(100)-(1×1) structure to the so-called Pt(100) hex reconstructed phase [1]. This reconstruction is favoured because it minimizes the surface free energy in absence of adsorbates.
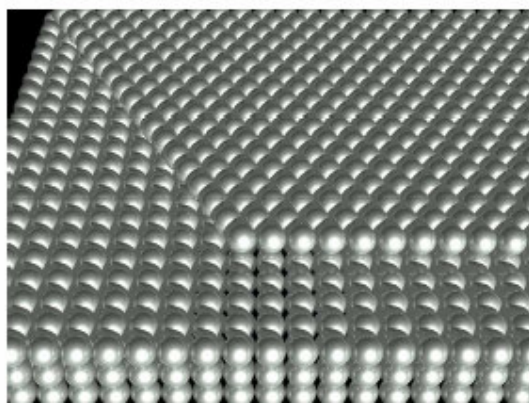

Figure 6.1: *The hex-reconstructed layer on top of the Pt(100)-(1x1) structure.*

The first reconstruction of a clean metal has been reported in 1965 for Pt(100) by Hagstrom et al. [2]. Since the LEED pattern showed the appearance of diffraction beams in (or near) multiples of the (1/5)-th order position, the authors called the new structure (1×5). In 1967, Fedak and

Gjostein observed a (1x5) reconstruction for Au(100) [3]. Soon after their observation these authors managed to resolve a splitting in the LEED spots for Au, indicating a (20×5) rather than (1×5) structure. Fedak and Gjostein have been the first to propose a hexagonal overlayer on the square substrate mesh as a model for the surface rearrangement [4]. A sharp (1×5) LEED pattern without splitting has been found for Ir(100) in 1969 by Grant [5]. In summary, the (100) faces of Au, Pt, and Ir have a surface reconstruction formed by a compact (quasi) hexagonal surface layer resting on top of the underlying square lattice. In each case the pattern exhibits a row-like structure, resulting from a regular structure in which every group of six top-layer atom rows covers the area of on five atom rows of the substrate.

In the case of Pt(100), two phases of reconstruction exists. Upon annealing to temperatures in the range of 400 K-1100 K, the unrotated phase designated as Pt (100)-hex is formed. Above 1100 K, a transformation occurs to a phase where the hexagonal layer is rotated 0.7° with respect to the underlying, square lattice, a structure referred to as Pt(100)-hex-R0.7° or, in matrix notation:

$$\begin{bmatrix} N & 1 \\ -1 & 5 \end{bmatrix}$$

where N is in the range of 12-14 [6].

The quasi-hex reconstruction of Pt(100) is lifted by adsorption of various gases (NO, CO, O2 and C_2H_4) resulting in adsorbate-covered (1x1) surface structures [7-16].

Origin

In order to explain the origin of the reconstruction one should take in consideration several interesting aspects of this platinum surface. First, this reconstruction is seen only at the end of 5d transition metal series, for the metals Ir, Pt, and Au, but not on their 4d counterparts (Rh, Pd, and Ag). Second, it has been shown that the (100) surfaces of the late 5d metals can be easily forced to switch between the reconstructed and unreconstructed phases by deposition and removal of small amounts of adsorbates, which indicates that the energy difference between the two phases is small. The (111) face of a face-centred crystal is usually the surface with the lowest free energy, so it may come as no surprise that the (100) surfaces prefer the reconstruction with a close-packed hexagonal overlayer. Of course, this argument completely ignores the unfavourable atomic stacking of a hexagonal layer on a lattice with square symmetry. In spite of the seeming

similarity between the hex-reconstructed Pt(100) surface and Pt(111), the work function on Pt(100) is lower than that on Pt (111) by as much as 0.5eV [17].

Ab initio calculations have suggested that the origin of quasi-hexagonal reconstruction lies in a relativistic effect. The calculations performed by Fiorentini et al. have shown that the reconstruction results from a delicate balance between surface-substrate mismatch and stress-related energy gain. Only in the case of 5d metals is the latter gain large enough to actually drive the reconstruction against the substrate resistance to misregistry, which is comparable for isoelectronic systems (e.g., Pd and Pt). The origin of the surface stress is the d-depletion at the surface accompanying the enhanced sp-hybridisation; the remarkable stress enhancement in 5d metals is due to the major relativistic effects in the 6s and 6p shells [18]. A similar effect drives the (110) surfaces of the same materials to the so-called missing-row reconstruction and stabilizes atomic chains of these materials in break-junction experiments [19].

6.2 Experimental

All the experiments described in this chapter have been performed using the Reactor-STM, which has been described in the introductory chapter. The surface has been prepared in UHV by cycles of 600 eV Ar^+ bombardment followed by annealing to ~800 K in 1×10^{-6} mbar O_2 and brief annealing in UHV around 1000 K. This procedure was repeated until a sharp LEED diffraction pattern was obtained, as illustrated in figure 6.2, reflecting the fivefold period of the Pt(100) hex-reconstructed surface. The cleanliness of the sample was checked with the STM. As shown in figure 6.3 atomically resolved, high-quality STM images have been obtained.
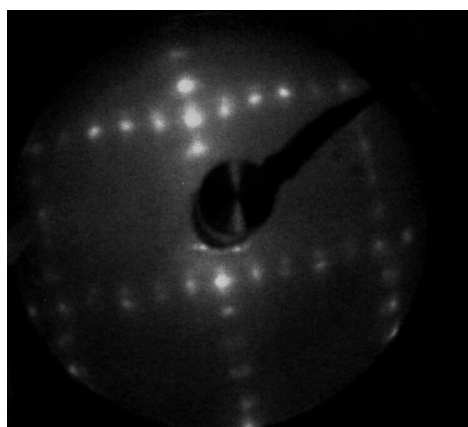

Figure 6.2: Room temperature LEED pattern of the clean, hex-reconstructed Pt(100) surface. The electron beam energy was 60 eV.
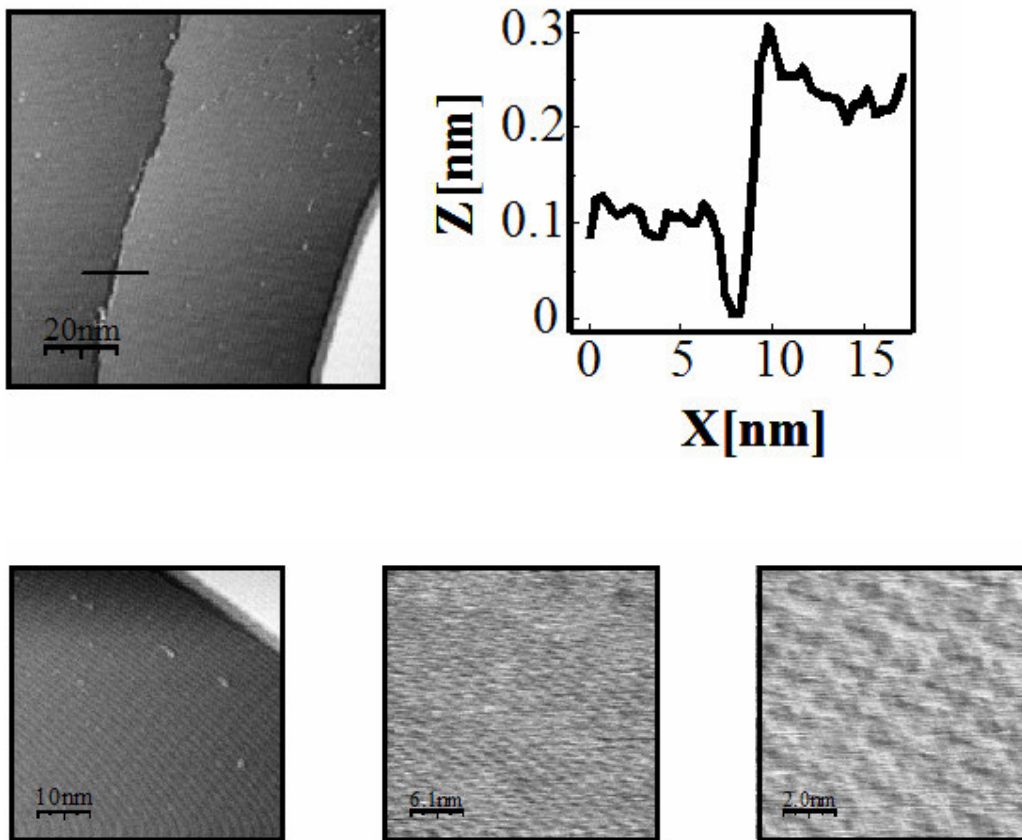
Figure 6.3: *Upper left: 100 nm × 100 nm STM image showing the clean Pt(100) surface in the poor vacuum of our Reactor-STM. The row-like features of the hexagonal reconstruction are clearly visible as stripes in the surface. Upper right: the cross-section along the line segment in the upper left image shows a step height of 2.0 Å, the expected value for Pt(100). Lower images: zooming in further, we have obtained STM images (50 nm× 50 nm, 30 nm × 30 nm, 10 nm × 10 nm) illustrating atomic-scale detail within the (5x20) unit cell of the hex-reconstructed Pt(100) surface. V_t=0.8 V, I_t= 0.2 nA*

6.3 Results and discussion

6.3.1 Interaction of CO with Pt(100)

As mentioned above, it is known that the hex-reconstruction is lifted by the adsorption of CO and several other adsorbates. Thiel et al. [20] have proposed the following mechanism for the removal of the reconstruction by CO adsorption at low temperature (400 K). This mechanism involves initial CO adsorption on the hex phase, which is followed by migration of CO, cluster formation, rapid hex→(1x1) conversion of the local substrate area, and trapping of the CO molecules on the resulting (1x1) patches. The

driving force for the CO-induced hex→(1x1) phase transition is the higher heat of adsorption of CO on the (1x1) phase compared to the reconstructed phase. Other STM studies have revealed that the transformation from the hex reconstruction to a CO-covered Pt(100)-(1x1) surface structure is indeed initiated by heterogeneous nucleation and that the growth of the (1x1) phase is highly anisotropic [15]. Figure 6.4 displays the (1x1) islands which have formed on the hex-reconstructed Pt(100) due to CO adsorption. The STM images have been acquired after the clean hex reconstructed surface was exposed to a 4:1 mixture of Ar and CO. The total pressure was 1.25 bar, and the temperature of the sample was 433 K. The height of the islands relative to the surrounding terrace was determined to be 2.0 Å, which is equal to the height of a monoatomic step as can be seen in the cross line profile from figure 6.4. From the STM images in figure 6.4 we see that the shape of the islands has a weak, square symmetry, showing that the hexagonal structure is indeed removed.
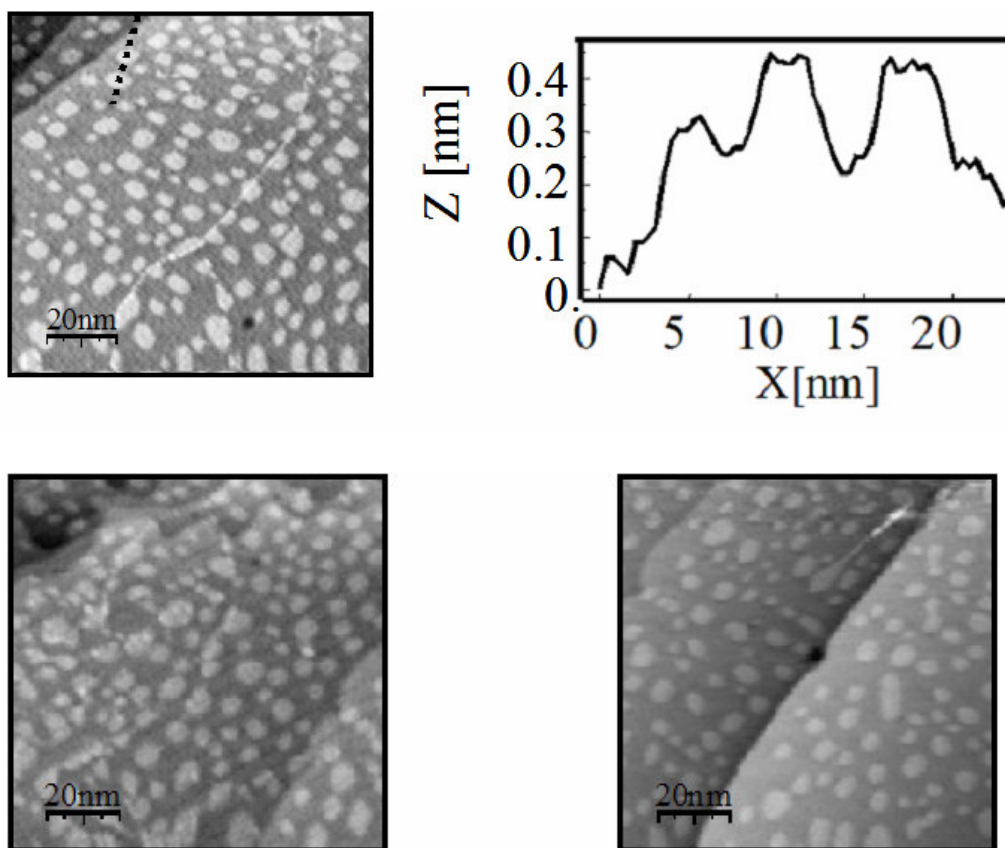

Figure 6.4: *STM images (100nm×100nm) illustrating the lifting of the hex-reconstruction due to CO adsorption at* P_{CO} *= 1.0 bar and at* T *= 433 K. The resulting (1x1) islands have a variety of sizes and different shapes with a weak, square symmetry.* V_t*=0.1 V,* I_t*= 0.2 nA*

Our measurements have shown that in a CO-rich flow the Pt(100) surface has a high mobility. The sizes and shapes of the adatom islands were observed to evolve in time, primarily via the coalescence dynamics resulting from spontaneous shape and position fluctuations of the islands. Once two islands had made contact with each other, they lowered their combined perimeter length and thereby their total free energy by fusing together into a single, compact island. In figure 6.5 we illustrate this process of rearrangements of the (1x1) adatom islands of the Pt (100) surface under a high CO partial pressure. If we compare image A with image G we see that many islands have changed their shape. The island sizes have remained almost unchanged, which indicates that Ostwald ripening is not strong under these conditions. In Figure 6.5 we also see that two coalescence events have occurred. The two adatom islands indicated in A by numbers 1 and 2 have coalesced, resulting in the formation of adatom island number 5 in image G. Similarly, islands 3 and 4 in image A have merged into adatom island number 6 in image G. In both cases two neighbouring islands fused together. The initial distances between their edges were 2.5 nm and 1.17 nm respectively. The island pairs have managed to bridge these distances and already evolve substantially towards a new, compact shape within the time interval between of approximately 10 minutes between images A and G. If we add the perimeters of islands 1 (12.7 nm) and 2 (26.6 nm) we obtain a sum of 39.3 nm that is substantially larger than the perimeter of the merged island 5 of 27.6 nm. A similar reduction in total perimeter length can be measured for the merger of islands 3 and 4. Images B-F show several intermediate stages in the encounter and coalescence of islands 3 and 4. In image B the two islands are still separated by 1.2 nm. Within a time interval of 3 minutes this distance has remained almost unchanged (C). After a further 2 minutes, the two islands have formed a connecting neck, resulting in the structure labelled 6 with a perimeter length of 34.0 nm, as seen in image D. This structure quickly reshaped itself. Within only 1 min the neck of the 6 structure has grown substantially in width as seen in image E, reducing the perimeter to a length of 31.3 nm. After an additional time of 2 min we arrived at image F in which structure 6 has an even more compact shape and a perimeter of 29.3 nm. The fact that the areas of the merged islands are not changing during their rearrangement to a more compact shape shows that also this part of the process does not involve exchange (evaporation and recondensation) of Pt atoms between the islands and their surroundings, but most probably this reshaping proceeds via edge diffusion of Pt atoms.
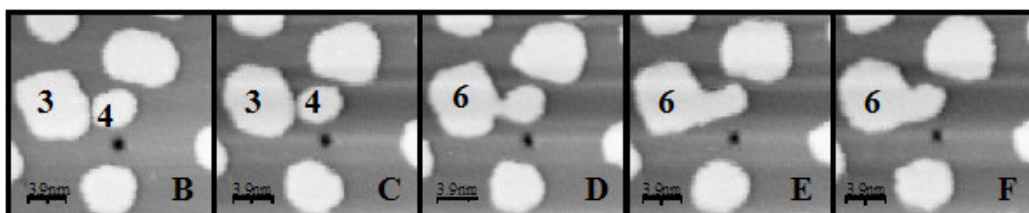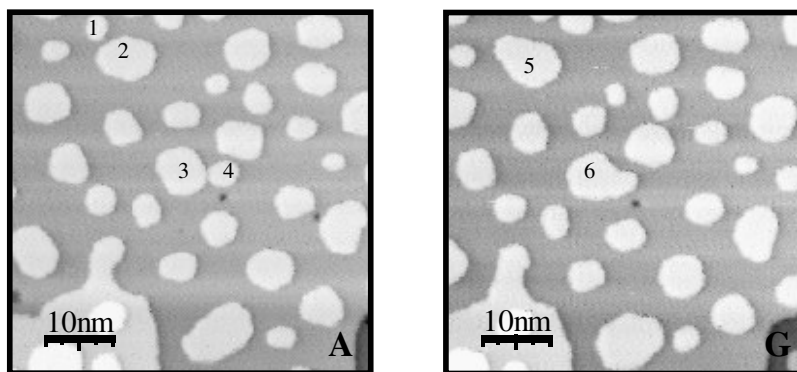
Figure 6.5: *STM images displaying the coalescence dynamics of adatom islands on an unreconstructed Pt(100) surface in CO-rich flow at atmospheric pressure (P_{CO} = 1.0 bar) and an elevated temperature of 368 K. V_t=0.1 V, I_t= 0.2 nA.*

Another example of the rapid dynamics of the unreconstructed Pt(100) surface is displayed in figure 6.6. In this case besides the coalescence process introduced above, we have also observed the opposite process: the break-up of a large structure into smaller-size features. Similar to the case introduced in figure 6.5 this process took place under CO-rich flow. Initially islands 2 and 3 coalesced with island 1 forming a complex structure with a very stretched and branched shape, as seen in image H2. This large structure decayed in time (images H3-H5) towards a more compact shape. Interestingly, the part formed by island 2 and most of island 1 was competing in this process with the part formed by island 3 and the lower left section of island 1. This competition actually led to a thinning and eventually even a rupture (image H6) of a narrow part that was originally within island 1. We might refer to this special type of event as 'coalescence-induced island break-up'. We stress that in this break-up process the total perimeter length was *not* increased. The stretched geometry made the total step length decrease when the island was separated into two more compact shapes.

In order to learn more about the smoothing process in a CO-rich flow we have calculated the step density in the images discussed above as well as images acquired at intermediate times (not shown). The result of this analysis is displayed in figure 6.7. The graph shows a clearly decreasing trend in the step density as a function of time.
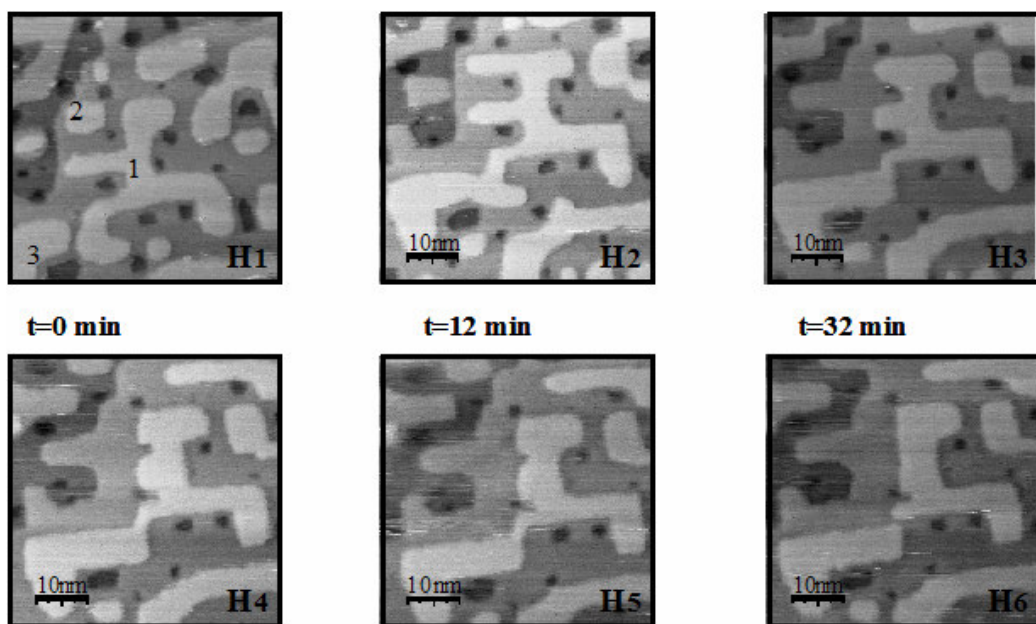
Figure 6.6: *STM images illustrating the evolution of a complex adatom island structure. As a consequence of the evolution towards a more compact shape, the central island breaks up into two smaller fragments. The size of the images is 50 nm × 50 nm. V_t=0.1 V, I_t= 0.2 nA.*
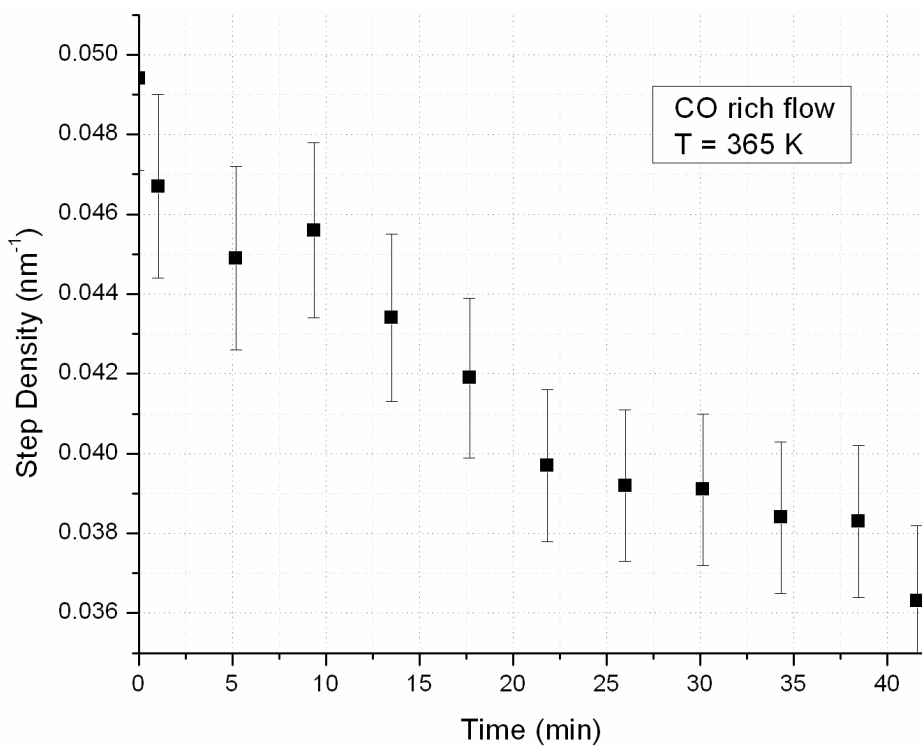

Figure 6.7: *The decrease of the step density in time in CO rich flow, measured from a series of STM images acquired in a flow of 1.25 bar of CO at a temperature of 365 K.*

Summarizing, based on the experimental evidence introduced in this section we conclude that exposure of the hex-reconstructed Pt(100) to atmospheric pressures of CO lifts the reconstruction. In this process, the excess Pt atoms expelled from the surface layer form adatom islands. Under the same conditions of high CO pressure and elevated temperature we observe that the adatom island pattern coarsens, mainly by coalescence dynamics, leading to a gradual smoothening of the surface.

6.3.2 Interaction of O_2 with Pt(100)

Since Pt(100) constitutes one of the low-Miller-index faces of platinum and the density of atoms on this surface is intermediate between those of the other two low-index surfaces, Pt(110) and Pt(111), we may expect that in an O_2-rich flow the (100) surface would show similar behaviour to these other surfaces (see ref. [21] for the (110) surface and Chapter 5 for the (111) surface). In particular, we expect the surface to oxidize at sufficiently high P_{O_2} and we expect this oxide surface to exhibit a higher reactivity towards CO oxidation.

Relatively little information is available in the literature about the interaction of O_2 with Pt (100), except for the fact that, similar to other gases, the oxygen lifts the hex- reconstruction. Early work by Griffiths and Norton [9,10] has revealed the existence of two surface phases depending on the atomic oxygen coverage. The first structure gives rise to a (3×1) LEED pattern and involves 0.51×10^{15} Pt atoms cm^{-2} that are displaced by 0.025 nm from bulk lattice positions. The other phase has a very complex LEED pattern, it shows a decrease in the work function compared with the (3×1) phase, and it involves 0.82×10^{15} Pt atoms cm^{-2} that are displaced by 0.025 nm. STM studies [15] describing the lifting of the reconstruction of Pt (100) –hex-R0.7° have suggested that the nucleation of the (1×1) islands may be initiated by the adsorption of oxygen molecules on the hex-R0.7° surface. The nucleation process is limited by the low sticking coefficient of oxygen on this surface, which is about four orders of magnitude lower than that for CO on the same surface. However, the oxygen sticking probability may be higher at step edges [22]. Figure 6.8 shows a STM images recorded on the CO-covered Pt(100) surface and its height profile histogram. From the histogram clearly can be seen that the step height from the adatom island down to the terrace is 2 Å corresponding to the step height of metallic platinum. When exposed to O_2 rich-flow the surface visibly roughness compared to the CO-covered surface as seen in STM images from figure 6.9. We have performed 30 additional cycles of exposure of the surface to a CO-rich gas flow and exposure to an O_2-rich flow and in each case find that the surface is significantly rougher in the O_2-rich flow than in the CO-rich flow.
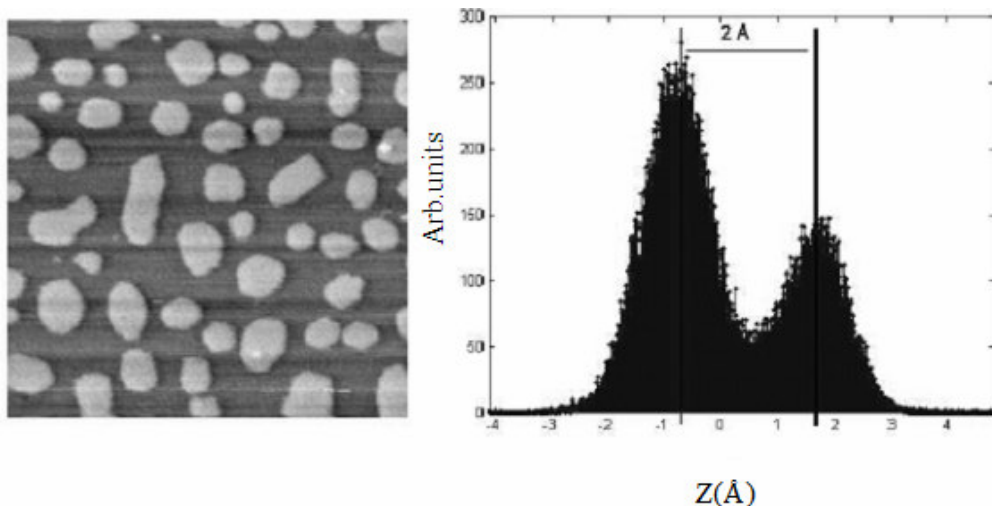
Figure 6.8: STM image (50nm×50nm) and its histogram in CO rich-flow (1.12 bar) at T=418 K.

As illustrated in figure 6.9 new structures are formed. In Fig. 6.9 we also show the height distribution for each image. The histograms show a variety of height differences, some of which may be close to multiples of the 0.20 nm step height of Pt(100) but others being completely different. We interpret the changes in the images and the new heights introduced upon exposure of the surface to high oxygen pressures as a strong indication that also this surface is oxidized, similar to Pt(110) and Pt(111).

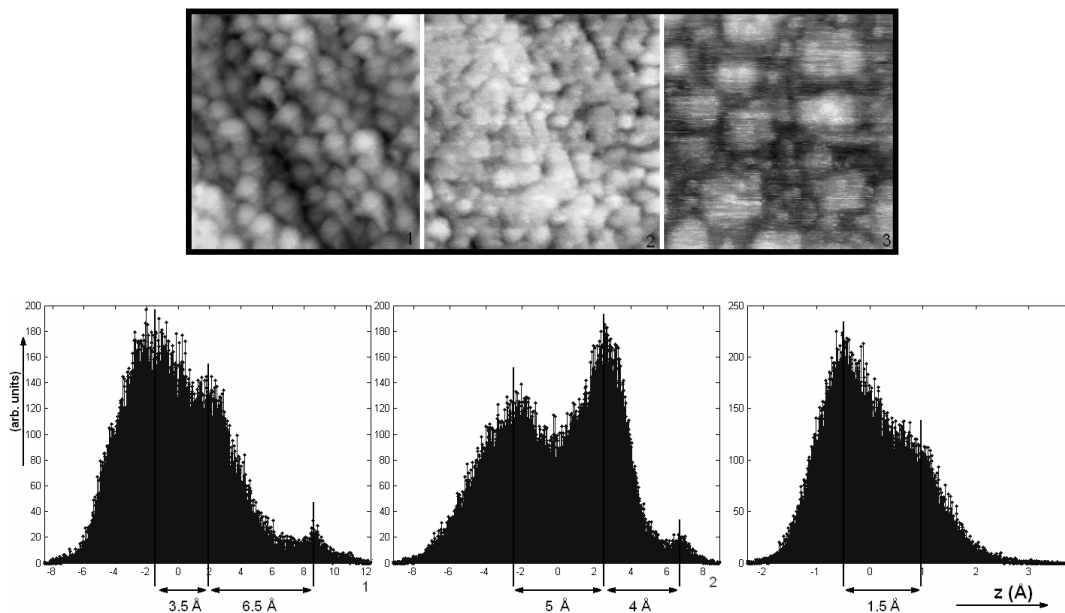*Figure 6.9: Various oxygen-covered states of Pt (100) surface and the corresponding histograms .The size of the first 2 images is 100nm×100nm , while the size of image 3 is 30.5nm×30.5nm. The first 2 images have been acquired at 1.25 total pressure (1.16 bar of O_2). Image 3 has been recorded in a ratio O_2:CO equal to 6. The temperature was 403 K (image1), 408 K (image 2) and 368K (image 3).V_t=0.1V and I_t=O.2 nA.*

An important aspect of the surface oxide is that, contrary to the CO-covered surface; the oxygen-induced structures hardly evolve in time. In oxygen atmosphere the surface is much less mobile than in a CO-rich flow, as illustrated by the images in figure 6.10. Between the recording of the first and the last image in the series a time interval of 2 h passed. The crosses in the images indicate the same location on the surface.
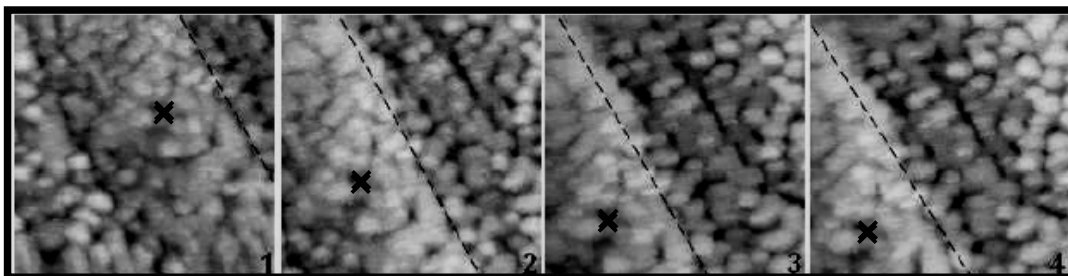

Figure 6.10: *STM images (100 nm × 100 nm) showing the absence of evolution in time of the Pt(100) surface in an O_2-flow of P = 1.25 bar at T =408 K.*

6.3.3 Pt(100) in a CO+O_2 mixture, during CO oxidation

Langmuir-Hinshelwood versus Mars-van-Krevelen reaction kinetics

Although the reversible oxidation and reduction of the Pt(100) surface in O_2 and CO atmospheres is strongly reminiscent of the behaviour of Pt(110) and Pt(111), there are also important differences between these low-index platinum surfaces. The most important difference is that only in a few experiments (3 out of 30) on Pt(100) we have measured a small, stepwise increase in CO_2 production rate and a simultaneous, modest step down in CO partial pressure at a sufficiently high partial pressure of O_2 and a sufficiently low pressure of CO. The kinetics of such an experiment, performed at P_{total} = 1.25 bar and T = 418 K is depicted in figure 6.11. First, the sample has been in a CO-rich flow. At t = 769 s we have switched to an O_2-rich flow. The CO_2 production rate followed the increasing trend of the oxygen partial pressure. The reaction rate passed through a maximum value at t = 769 s, after which it followed the decreasing trend of the CO partial pressure. As we have seen several times before in this thesis, this sequence is characteristic for the Langmuir-Hinshelwood reaction mechanism, for which the reaction rate is at its maximum when we have equal coverages of CO and O. At t = 3938 s (indicated by the arrow) we observe a sudden step up in the CO_2 production. The upward step in the reaction rate is accompanied by a small, downward step in the CO partial pressure, as can be seen in the enlarged graph in figure 6.11 (b). For the other platinum and palladium surfaces such steps in reactivity have been found to be associated with the formation of a new structure, namely a surface oxide. On these

surface oxides the oxidation reaction was found to follow the Mars van Krevelen mechanism: each CO molecule reacts with an oxygen atom from the surface oxide lattice.
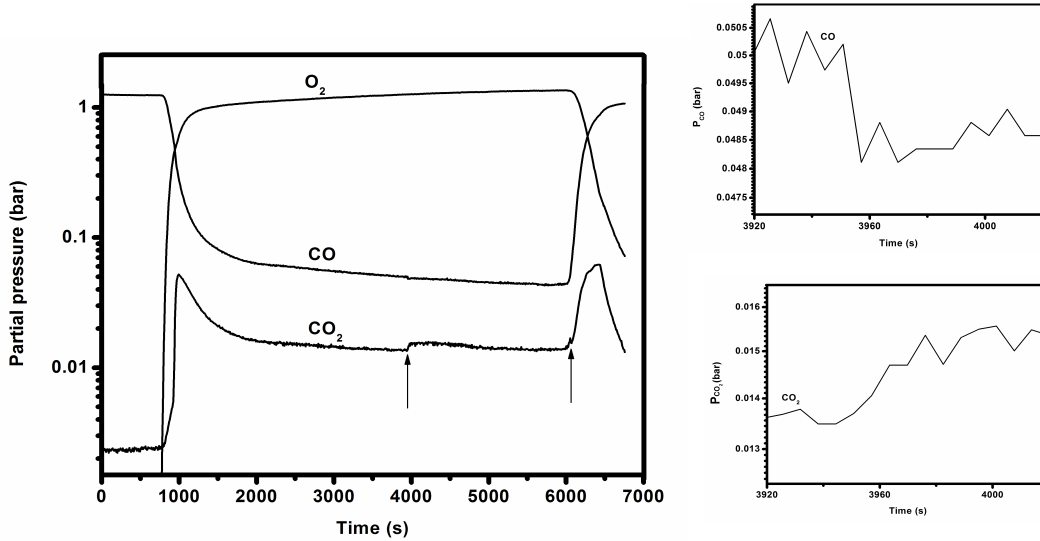

Figure 6.11: *CO oxidation reaction kinetics on Pt(100) at a total pressure of 1.25 bar and T= 418 K. The sequence shows Langmuir-Hinshelwood behaviour for times up to t = 3938 s and for times after t = 6091 s and Mars-van-Krevelen behaviour for intermediate times. The MvK behaviour is associated with the formation of a surface oxide.*

Figure 6.12 shows an attempt to fit the measured production rates of CO_2 with a simple model, based solely on Langmuir-Hinshelwood kinetics. The left panel shows a time sequence of the CO_2 partial pressures P_{CO_2} similar to that in Fig. 6.11, this time displayed on a linear pressure scale. The right panel represents the best fit to this data according to the LH mechanism, modeled by the following equations for the reaction rate R.

$$R = P_1 \frac{\sqrt{p_{O_2}}\, p_{CO}}{\left(P_2\sqrt{p_{O_2}} + p_{CO}\right)^2} \,, \tag{5.1}$$

in which we have defined

$$P_1 = \frac{k_3\sqrt{K_{O_2}}}{K_{CO}} \text{ and } P_2 = \frac{\sqrt{K_{O_2}}}{K_{CO}} \,. \tag{5.2}$$

In this calculation the partial pressures p_{O_2} and p_{CO} have been taken from the experiment and the constants k_3 and P_2 have been used as fitting parameters. Although the fit to the two LH peaks is not perfect, it is clear

that the model catches the essence of the LH behaviour. Obviously, the stepwise increase and decrease of the reaction rate at 9600 s and 10800 s respectively, which reflect the transition between LH-kinetics and MvK-kinetics associated with the oxidation of the surface, are not described by this LH-model.
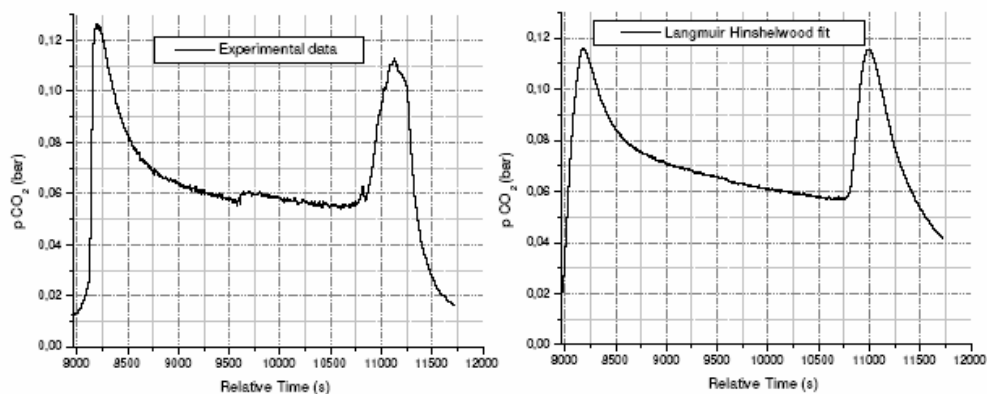

Figure 6.12: *Measured CO oxidation rate on Pt(100), as recorded by the mass 44 CO_2 signal from the mass spectrometer at P_{total} = 1.25 bar and 423 K (left panel) and the calculated reaction rate according to Langmuir-Hinshelwood kinetics (right panel).*

As mentioned already, the upward step in the reactivity, which is associated with the formation of the oxide, has been observed only in three experiments, in which we performed repeated cycles of exposure to CO and O_2. Interestingly, these three experiments were the *very first* experiments performed on a new, freshly polished and UHV-prepared Pt(100) sample. After these initial three experiments we have never been able to again provoke the increase in CO_2 production, even though we have fully reproduced the reaction conditions and the sample cleaning procedures of the initial experiments. This observation presents a strong indication that in this case the history of the surface plays a key role in the catalytic activity. In particular, the initial step density of the freshly prepared Pt(100) surface (Fig. 6.3) was lower than the step density after one or more cycles of oxidation and reduction of the Pt surface. We speculate that the Pt(100) surface exhibits a relation between step density and oxidation conditions, similar to what we have found on Pd(100) (Chapter 3), in the present case rapidly shifting the critical CO pressure for oxidation of the Pt surface at the temperatures and oxygen pressures used in our experiment to lower values. As we have seen before for other surfaces and as we will see for Pt(100), the step in reactivity, i.e. the difference in the production rate of CO_2 between the MvK and LH mechanisms, is smaller at lower CO pressures. In the present case the step in P_{CO_2} has been going down from a small value to basically zero, meaning that we can no longer use the measured reactivities

to be sure whether the catalytic system is operating on the LH branch or on the MvK branch.

Langmuir-Hinshelwood kinetics

Figure 6.13 depicts the partial pressure of the reactant gases CO and O_2, and the reaction product CO_2, as were measured by the mass spectrometer in an experiment that started at $t = 0$ s in a CO-rich flow at a total pressure of 1.25 bar and 368 K. At $t = 3716$ s the O_2 pressure was raised and the CO_2 signal initially increased accordingly, then reached a maximum value at $t = 4229$ s (indicated by arrow 1), after which it decreased, following the reduction in the CO pressure as we switched to an O_2 rich flow. Similar to the other platinum group metals, CO oxidation on Pt(100) follows the Langmuir-Hinshelwood mechanism over a certain regime of partial pressures. According to this mechanism the maximum value in CO_2 production corresponds to equal coverages of reactant gases $\theta_{CO} = \theta_O = 0.5$. At $t = 7931$ s we increased the CO pressure again. Consequently the CO_2 pressure also increased and again reached a maximum at t=8559s (arrow number 2), where we again assume to have equal coverages, $\theta_{CO} = \theta_O = 0.5$. At high CO pressures the CO_2 signal decreased in time due to the poisoning of the surface by the high coverage of CO.

Arrow 3 indicates a modest increase in CO_2 pressure that occurred when we increased the O_2 partial pressure at $t = 15333$ s to 0.22 bar. Since the total pressure is constant the CO partial pressure decreased hand in hand with the increase in O_2 pressure, the CO:O_2 partial pressure ratio becoming 3.5. Interestingly, 2107 s later, at $t = 17440$ s, we observed a spontaneous, big step in the reaction rate (arrow 4). Coinciding with the increase in CO_2 pressure we noticed modest reductions in the CO and O_2 partial pressures. After this big increase the reaction rate was steady as long as we kept the partial pressures of CO and O_2 unchanged. At $t = 19604$ s (arrow 5) we further increased the O_2 partial pressure. This resulted in a strong decrease in the reaction rate, similar to what we always measure at high oxygen pressures (e.g. the reduction after the LH-peak at arrow 1).
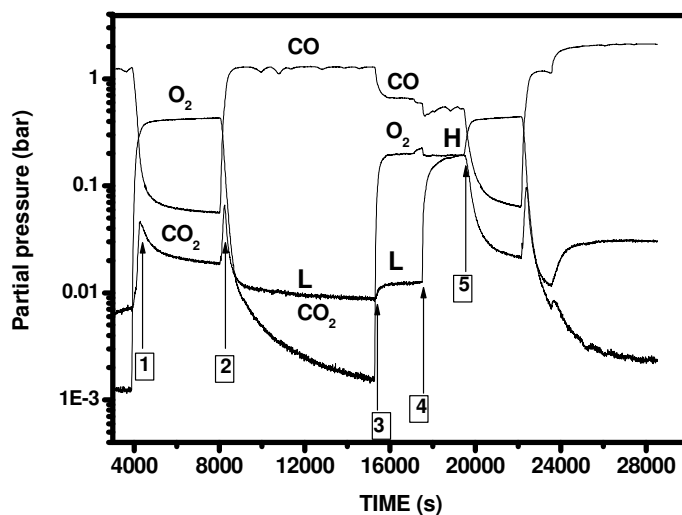
Figure 6.13: Reaction kinetics for CO oxidation at a total pressure of 1.25 bar and 368 K. The letters L indicate the regime where the reaction rate is low and the letter H corresponds to the maximum in the reaction rate.

The increase in the reaction rate at arrow 4 is quite spectacular. In the particular example of Fig. 6.13, a minor variation took place in the CO/O_2 partial pressure ratio in the 500 s prior to the sudden increase in reactivity. We have reproduced the stepwise increase in reactivity several times and have verified that the pressure variation of Fig. 6.13 does not form a necessary ingredient of this behaviour. In view of the previous results obtained with our high-pressure STM and SXRD experiments on CO oxidation catalysis, one would expect that the dramatic increase in reactivity would be accompanied by a sudden change in the surface structure. Figure 6.14 repeats a part of the time trace of the partial pressure of CO_2 from Fig. 6.13 and combines it with the structure of the surface as observed simultaneously with the STM. Apart from modest fluctuations of the island shapes, the images obtained prior to and after the change in reactivity are close to identical (images S, S_1, S_2); they all show the unreconstructed Pt(100)-(1x1) surface with adatom islands. Only when we exposed the surface to high oxygen pressures, towards the end of the time interval of Fig. 6.14, did the STM image change and show a pattern typical for a surface oxide (image S_3), but this was under conditions at which the reaction rate was low again.

93
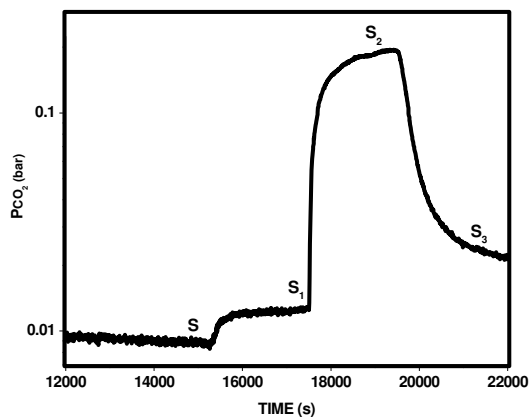
(a)
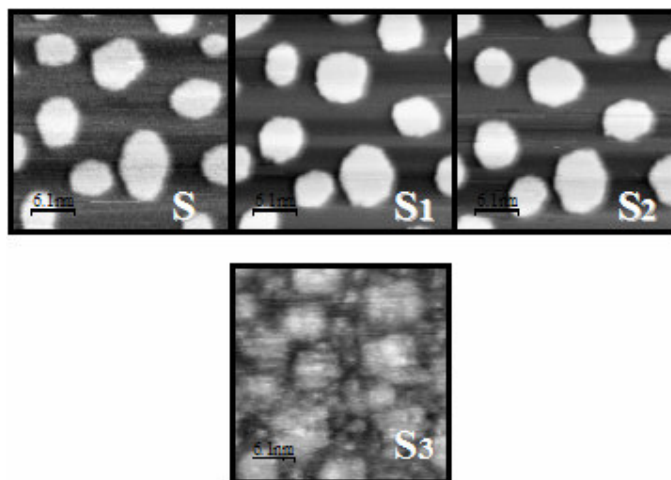
(b)

Figure 6.14: *Time sequence of the CO_2 production rate around the sudden increase in rate, taken from Fig. 6.13, combined with simultaneously recorded STM images (30.5 nm × 30.5 nm). Image S has been acquired in the initial, CO-rich flow. Image S_1 shows the surface in a 3.5:1 CO/O_2 mixture. Image S_2 corresponds to the highest observed reactivity. Images S, S_1 and S_2 are very similar. They all show the metallic surface with adatom islands. Finally, image S_3 shows a rougher surface, characteristic for the presence of a disordered surface oxide. $V_t=0.9V$ and $I_t=0.2$ nA.*

Steps are often considered as the special reaction sites in heterogeneous catalysis. One might wonder whether changes in step density could be responsible for the sudden increase in reaction rate. However, as the selected images in Fig. 6.14 already indicated, the variation in step density over the time interval in which the strong increase takes place in reactivity was as good as zero. This visual impression is confirmed by a quantitative analysis of the step density as counted in the STM images, which is shown in

94

Fig. 6.15, together with the CO_2 partial pressures. It is only near the end of the sequence, after the maximum in reactivity, under a high partial pressure of oxygen at which the STM images (c.f. image S_3 in Fig. 6.14) show that the surface oxidized, that the roughness suddenly increased.
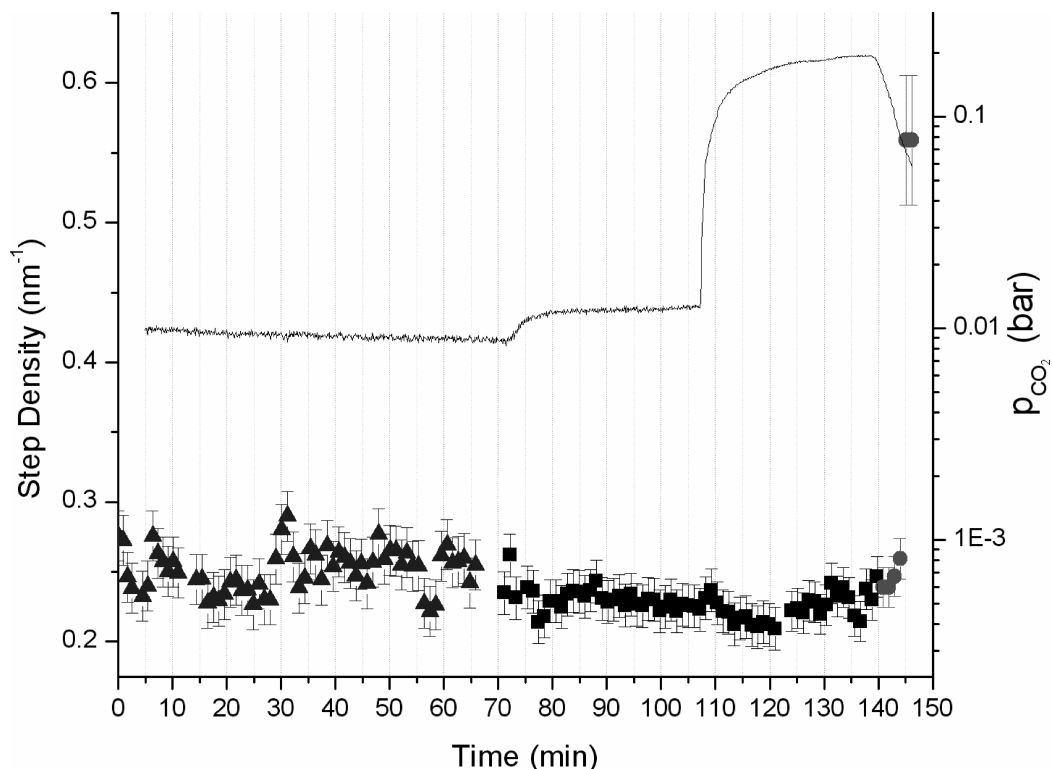

Figure 6.15: *Measured time dependence of the step density, illustrating the absence of a variation in this quantity while the CO_2 partial pressure goes through the stages shown before, including the sudden, strong increase in reactivity.*

We have repeated this experiment of stepping up from a CO-rich flow to the same O_2:CO pressure ratio of 0.7 ± 0.3 at a few different temperatures. In each case, we observed a high reactivity and except for the highest temperature, the high reactivity was reached by a spontaneous, upward step (factor 14 to 19) after a significant delay time. The temperature dependence of this delay time is shown in table 6.1. The temperature dependence of the delay can be interpreted as the signature of a thermally activated process (Arrhenius behaviour) with an activation energy of 1.2 ± 0.3 eV.

Starting from the maximum in the reactivity and slowly increasing the partial pressure of oxygen we noticed the frequent appearance and disappearances of small, adatom-island-like structures, as is illustrated in figure 6.17.As seen from Figure 6.18 these structures have heights in the order of 2.8 ± 0.2Å, which does not correspond to the step height of Pt(100).

Temperature (K)	Delay (s)	P_{CO_2} (low reactivity) (bar)	P_{CO_2} (high reactivity) (bar)
365	1052	0.025	0.445
368	2209	0.019	0.363
398	130	0.011	0.213
408	117	0.035	0.504
423	4		0.547

Table 6.1: Temperature dependence of the delay time between setting an O_2:CO partial pressure ratio of 0.7±0.3 and observing a spontaneous upward step in reactivity.

Image 1 has been acquired before the partial pressure of oxygen was increased. The two circles indicate regions where new structures, labelled I, II and III, will show up simultaneously with the increase in O_2 flow in images 2 and 3. First the structure I has appeared in image 2. In image 3, which has been recorded immediately after image 2, structure I has disappeared again, but the other two structures labelled II and III have been formed. In the next image (4) also structures II and III have disappeared. All these images have been acquired directly after each other. The time necessary to record an image was about 40 s. This implies that in the high reactivity state the surface was extremely mobile, new structures showing up and disappearing within the time of a single image. Actually these processes took place so fast that was difficult to follow them with our STM. Since the extra structures described here were not present before the increase in the O_2 partial pressure we conclude that their formation is due to the oxygen. Since as discussed before these structure appears only when we increase the O_2 pressure and have a step height higher than the step height of Pt(100) we may speculate that they are oxidic species.

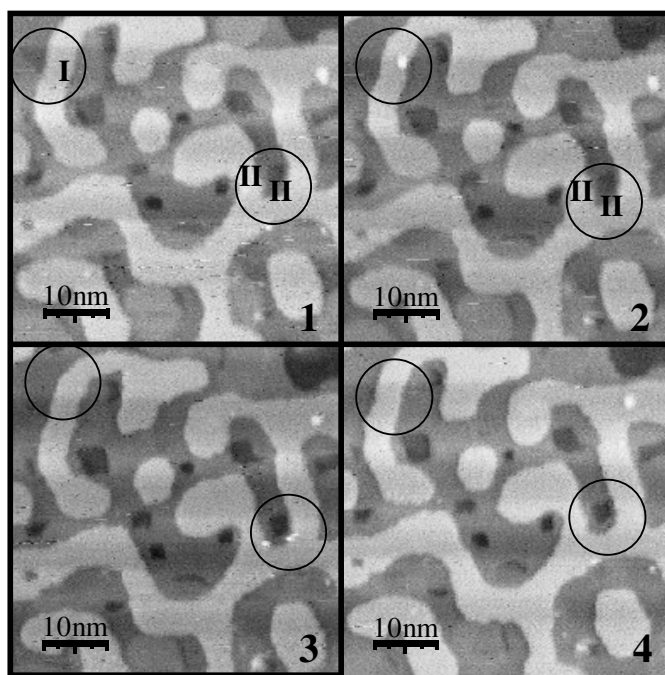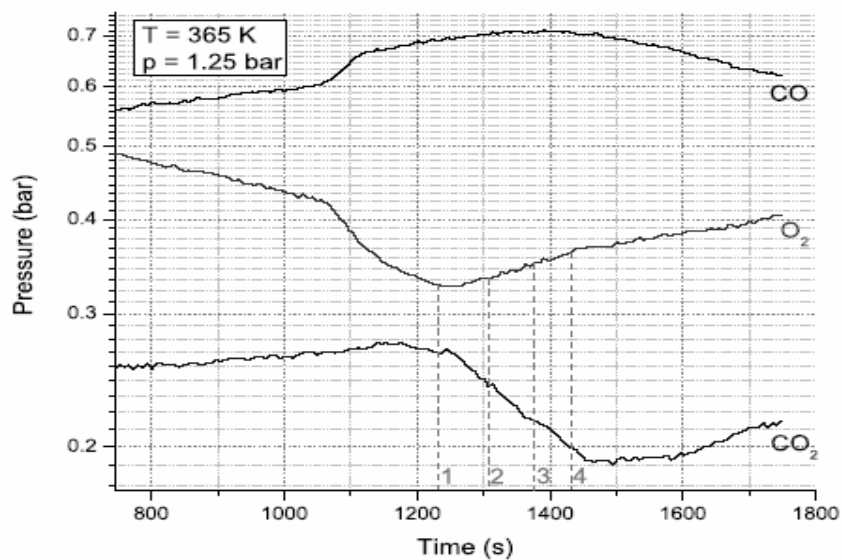***Figure 6.17:*** *STM images (50nm×50nm) recorded while the reaction rate was near its maximum and the oxygen partial pressure was increased. The circled regions illustrate the frequent formation and removal of adatom-island-like structures. The numbers in the top panel indicate the times and partial pressures of O_2, CO and CO_2 when the images were recorded, T=373 K. V_t=0.9V and I_t=0.2 nA.*
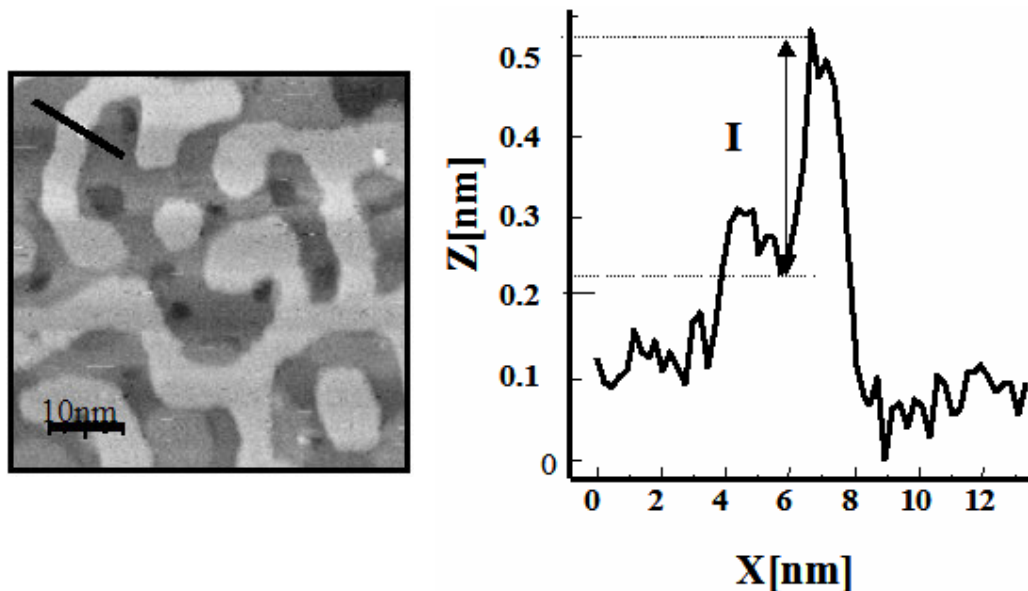
97

Figure 6.18: *Profile along the line in image 2. The height of the structure I does not correspond to the step height of Pt(100).*

6.3.4 Bistability and hysteresis

We have shown in previous chapters of this thesis for other model catalyst surfaces that if we plot the reaction rate (CO_2 pressure) as a function of CO pressure all experimental data for a particular surface fall on two branches: a low-reactivity branch, which is associated with a metallic surface and a high-reactivity branch, corresponding to some form of surface oxide. This behaviour has been observed for all three palladium surfaces investigated in Chapter 2 and for the Pt(111) surface, studied in Chapter 5, as well as for Pt(110) [21]. The case for Pt(100) is different in two respects. First, the range of CO pressures over which the surface oxide is more stable than the metal (at the relatively low temperatures of our experiment) is much smaller on Pt(100) than on the other platinum and palladium surfaces. In Fig. 6.19 we show three plots of CO_2 pressure versus CO pressure on Pt(100). Whereas in panels (a) and (b) a short oxide branch can be seen at low CO pressures, such a branch is no longer visible in panel (c). In fact, the only measurements in which the oxide branch was observed corresponded to the very first three oxidation-reduction cycles of the surface, after it had been prepared in our UHV system for the first time. As we already argued in Sect. 6.3.3, the maximum CO pressure at which the oxide was stable was probably reducing after repeated oxidation-reduction cycles, because of the influence of the steadily increasing density of steps. Interestingly, the STM images, discussed in Sect. 6.3.3, showed that at the lower CO partial pressures that we could reach in our experiment the surface still oxidized.

98

(a)

(b)

(c)
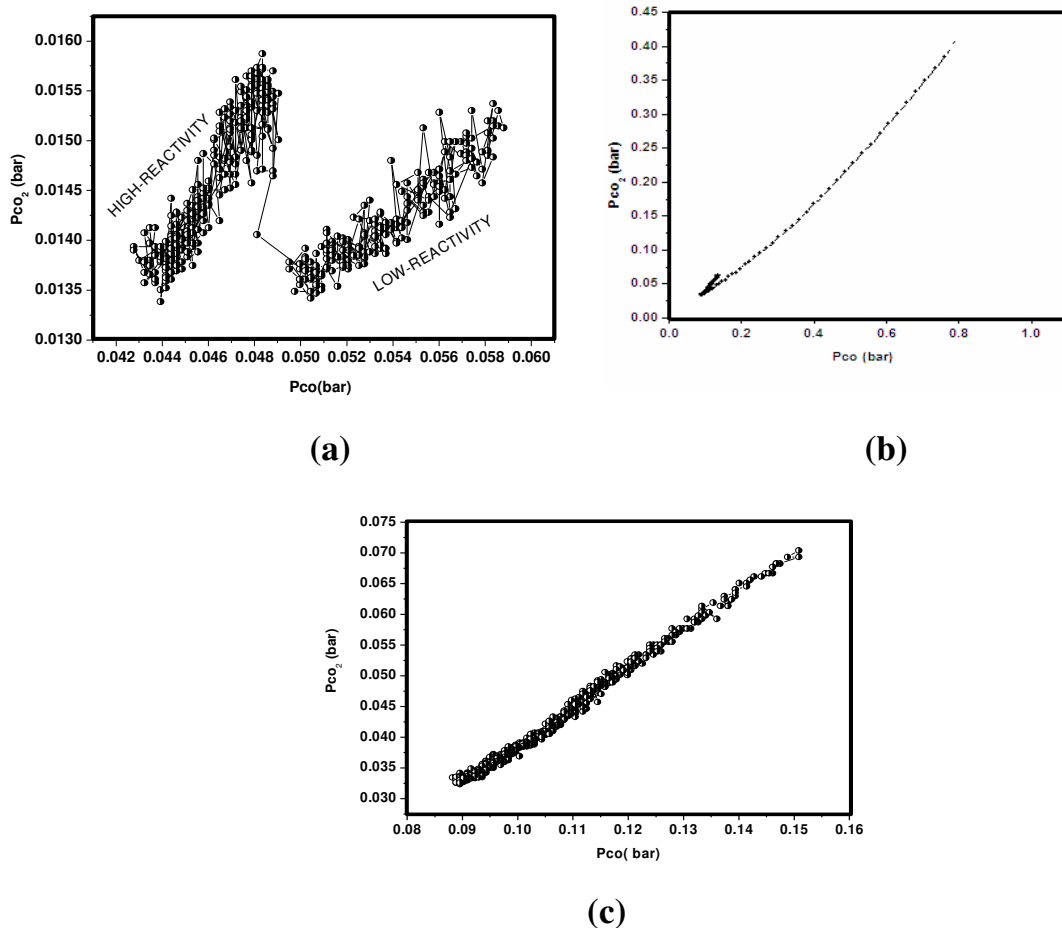
Figure 6.19: *CO$_2$ partial pressure (reaction rate) plotted as a function of CO pressure from three different sets of measurements on Pt(100). The reaction conditions were (a) P$_{total}$ = 1.25 bar, T = 423K; (b) P$_{total}$ = 1.75 bar, T = 430 K (c) and P$_{total}$ = 1.25 bar, T = 423 K. Graphs a and b illustrate the extremely limited range of CO partial pressures over which the oxide branch could be observed on Pt(100); in graph c no oxide branch can be distinguished anymore.*

However, as we can see from the 'oxide' branch in panels (a) and (b) of Fig.6.19, at these low CO pressures the Mars-van-Krevelen mechanism, responsible for the oxide branch, was so close to its intersection with the Langmuir-Hinshelwood branch, that no upward (downward) step could be measured in the CO$_2$ signal when the surface oxidized (reduced).

The second difference between the kinetics on Pt(100) and that on the other surfaces investigated in this thesis is that, as discussed in the previous section, there is a second rapid increase/decrease in reactivity, which occurred at much higher CO pressures. When again plotted in the form of P_{CO_2} versus P_{CO}, also this part of the behaviour indicates clear bistability (Fig.6.20).
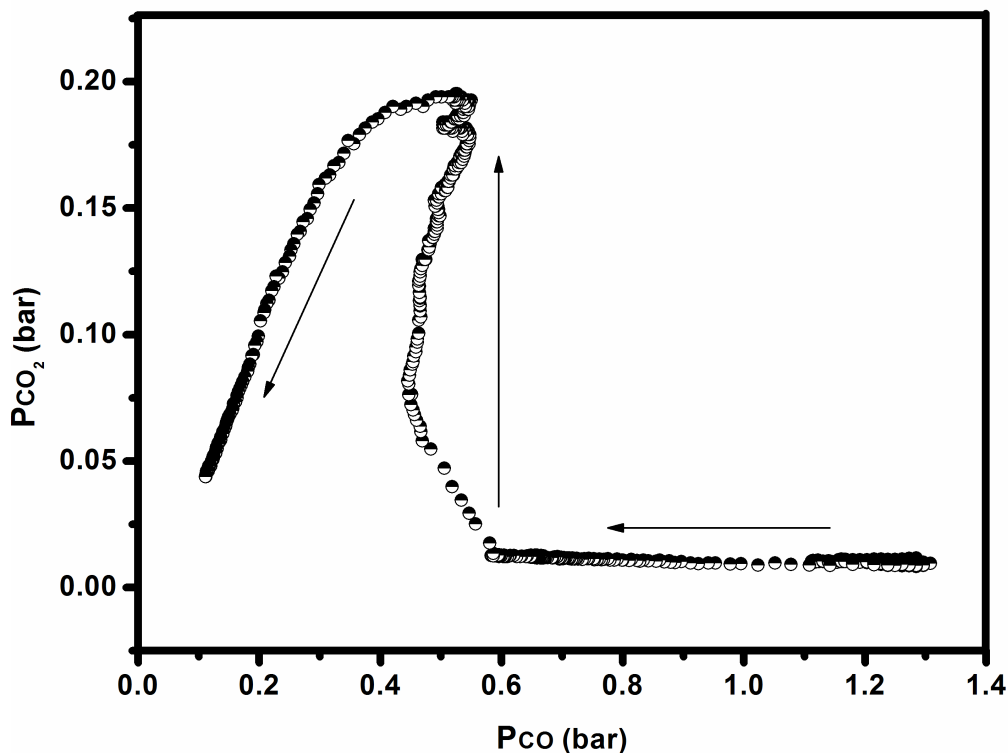
Figure 6.20: *CO₂ partial pressure (reaction rate) plotted as a function of CO pressure in the high P_{CO}-regime on Pt(100) at $P_{total} = 1.25$ bar and $T = 368$ K, illustrating the Langmuir-Hinshelwood bistability of this surface at atmospheric pressures.*

However, in this case, we have observed no changes in the STM images, indicating that this step was *not* induced by a phase transition of the metal substrate. In fact, this high-P_{CO} instability took place completely on the Langmuir-Hinshelwood branch. From this we infer that the observed transition is that from a mixed, two-dimensional overlayer of chemisorbed CO-molecules and O-atoms with a high CO-coverage to one with a low O-coverage. In other words, this instability is identified as the 'classic' fingerprint of the Langmuir-Hinshelwood bistability [23]. Several interesting questions remain. The complete absence of changes in the STM images indicates that we have been insensitive to the change in overlayer composition. Possibly, this means that the overlayer has been mixed on an atomic/molecular scale or, in case of segregated overlayer islands of adsorbed CO and adsorbed O, the dynamics of these islands has been so much faster than the imaging rate of the STM that the images have completely averaged over the islands. High-speed imaging or other forms of high-speed STM data acquisition may be used to push the time resolution on this by five or more orders of magnitude. However, at the high conversion

rates obtained in the present experiment, this may still not be enough to resolve the dynamics and/or structure of the adsorbate overlayer.

6.4 Conclusions

The study of CO oxidation by O_2 on Pt(100) at atmospheric pressures and elevated temperature has proved to be an interesting subject. Under these reaction conditions the Pt(100) surface behaves different compared to the other low-index surfaces of platinum, Pt(111) and Pt(110). We have observed that the hex-reconstruction of Pt(100) is lifted by exposure to CO, O_2 or mixtures of these gasses. Although the STM images clearly have indicated that at high O_2 pressures and low CO pressures, the surface is oxidized, the reaction kinetics have indicated that the corresponding Mars-van-Krevelen branch at low CO pressures is so close to the reactivity on the Langmuir-Hinshelwood reaction branch of the reduced surface that the two mechanisms could be distinguished from each other on the basis of the reaction kinetics measurements only in the first few oxidation-reduction cycles starting from a freshly polished surface. In later cycles the surface switched back to the LH branch at too low a CO pressure to observe a step in the reactivity. In addition to this combination of stepwise changes in STM images without changes in the reaction rate we have also observed stepwise changes in reaction rate accompanied by a complete absence of changes in the STM images. This new combination has been observed at higher CO pressures and we ascribe it to the traditional bistability on the LH branch. Although the rate constant for the CO_2 production is higher for the oxide than for the metal, the reaction can run at much higher CO pressures on the metal than on the oxide, so that the maximum production rate on the metal is much higher than the maximum rate on the oxide.

6.5 References

[1] X.C.Guo, A.Hopkinson, J.M.Bradley and D.A.King, *Surf.Sci.***278** (1992) 263.
[2] S.Hangstrom, H.B.Lyon and G.A.Somorjai, *Phys.Rev.Lett.***15** (1965) 171.
[3] D.G.Fedak and N.A.Gjostein, *Phys.Rev.Lett.***16** (1966) 171.
[4] D.G.Fedak and N.A.Gjostein, *Surf. Sci*. **8** (1967) 77.
[5] J.T.Grant, *Surf.Sci.***18** (1969) 228.
[6] C.Berg, H.J.Venvik, F.Strisland, A.Ramstad, A.Borg, *Surf.Sci.***409** (1998) 1.
[7] R.J.Behm, P.A.Thiel, P.R.Norton, G.Ertl, *J.Chem.Phys.***78** (1983) 7437.
[8] P.A.Thiel, R.J.Behm, P.R.Norton, G.Ertl, *J.Chem.Phys.***78** (1983) 7448.
[9] K.Griffiths, T.E.Jackmann, J.A.Davies, P.R.Norton, *Surf.Sci.138* (1984) 113.
[10] P.R.Norton, K.Griffiths, P.E.Binder, *Surf.Sci.***138** (1984) 125.
[11] W.Hosler, R.J.Behm, E.Ritter, *J.Rev.Dev.***30** (1986) 403.
[12] E.Ritter, R.J.Behm, G.Potschke, J.Wintterlin, *Surf.Sci.***181** (1987) 403.
[13] P.Gardner, M.Thushaus, R.Martin, A.M.Bradshaw, *Surf.Sci.***278** (1990) 112.
[14] K.Mase, Y.Murata, *Surf.Sci.***277** (1992) 97.
[15] A.Borg, A.M. Hilmen, E.Bergene, *Surf.Sci.***306** (1994) 10.
[16] C.Berg, H.V.Venvik, F.Strisland, A.Ramstad, A.Borg, *Surf.Sci.***409** (1998) .
[17] A.Sinsarp, Y. Yamada, M. Sasaki, S. Yamamoto, *Appl.Surf.Sci.***237** (2004) 587.
[18] V.Fiorentini, M.Methfessel and M.Scheffler, *Phys.Rev.Lett.***71** (1993) 1051.
[19] R.H.M. Smit, C. Untiedt, A.I. Yanson and J.M. van Ruitenbeek, *Phys. Rev. Lett.* **87** (2001) 266102.
[20] P.A.Thiel, R.J.Behm, P.R.Norton, and G.Ertl, *Surf.Sci.***121** (1982) L553.
[21] B. L. M. Hendriksen , PhD Thesis,Leiden University 2003.
[22] H.Hopster, H.Ibach and G.Comsa, *J.Catal.* **46**(1977) 37.
[23] H. Conrad, G. Ertl and J. Küppers, *Surf.Sci.***76** (1978) 323.

Appendix I

NO reduction by CO on Pt (100)

In this appendix we present preliminary results obtained with High-Pressure Scanning Tunneling Microscopy on the catalytic NO reduction by CO on Pt(100) at atmospheric pressure and various temperatures. We found that the formation of the products N_2 and CO_2 strongly depends upon the temperature and surface structure.

A.I.1 Introduction

The study of NO reduction by CO on Pt(100) constitutes an intriguing research subject. First of all the catalytic reduction of NO_x is of great importance for reducing air pollution [1]. Secondly, there is still a controversy in the literature concerning the mechanism of the NO+CO reaction. Also, it has been shown experimentally that this reaction exhibits interesting dynamical behaviour such as multiple steady states and kinetic oscillations [2-6]. As a consequence the NO/Pt(100) and NO+CO/Pt(100) systems have been investigated using various techniques over the years as scanning tunneling microscopy [7-8], low energy electron diffraction [9-10], vibrational spectroscopies [11-12] or X-ray photoemission spectroscopy [13-14].

As pointed out in Chapter 5 the clean Pt(100) surface adopts a quasi-hexagonal structure. Upon adsorption of various gases (ethylene, H_2, O_2, NO and CO) this reconstruction is lifted. King and collaborators summarized the similarities between the NO and CO adsorption as following: gases adsorb with high initial sticking probabilities; both lift the reconstruction of the clan hex surface; and in both cases the adsorption is almost entirely nondissociative. But are also remarkable differences in saturation coverages, in ordered structures and adsorption sites [15].

The basic reaction equation for the interaction of NO and CO is:

$$NO + CO \rightarrow \tfrac{1}{2}N_2 + CO_2$$
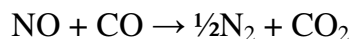
The key role in promoting the CO+NO reaction is played by the ability of the surface to dissociate NO [16]. Based on experimental observations by a variety of techniques it has been concluded that at room temperature NO adsorbs *molecularly* and that it lifts the hex reconstruction as we have already mentioned in the previous chapter. Upon heating above 390 K the molecularly adsorbed NO dissociates. The dissociation of chemisorbed NO, according to

$$NO_{ad} \rightarrow N_{ad} + O_{ad} \ ,$$
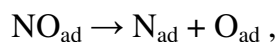
is immediately followed by the desorption of nitrogen,

$$2N_{ad} \rightarrow N_2 \ .$$
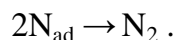
From the various models proposed to explain the reaction dynamics over Pt(100), we briefly describe only the two best known models in this section. One model is based on the fact that Pt(100) undergoes a surface reconstruction due to the adsorption of a few adsorbates, including NO and CO. King and co-workers have found that the hex $\rightarrow$ (1x1) surface phase transition depends non-linearly on surface coverage, and this nonliniarity is an essential ingredient in the dynamics of NO reduction on Pt(100) [17]. The other model is referred to as the so-called "vacancy model" and has been applied to the NO+CO reaction for the first time by Lesley and Schmidt [18]. The following reactions are used in this model in order to explain the autocatalytic behaviour of NO reduction (the square denotes an empty surface site):

$$CO + \square \leftrightarrow CO_{ads}$$
$$NO + \square \leftrightarrow NO_{ads}$$
$$NO_{ads} + \square \rightarrow N_{ads} + O_{ads}$$
$$N_{ads} + N_{ads} \rightarrow N_2 + 2 \square$$
$$CO_{ads} + O_{ads} \rightarrow CO_2 + 2 \square$$
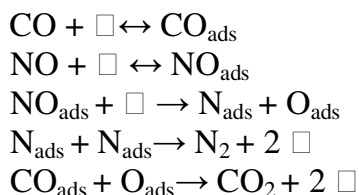
As can be seen the first two steps refer to the molecular adsorption of CO and NO on the surface. Both steps require an empty surface site. Due to the adsorption processes islands of adsorbates are formed and they grow until no more vacant surface sites are left. As a consequence the next step, dissociation of NO, is inhibited until one of the adsorbed species starts to desorb. When that is the case the dissociation can take place. This process is immediately followed by N_2 desorption and CO oxidation. The latter two reaction steps each produces two vacant sites, so that the process can continue until all CO and NO has reacted. This subprocess is autocatalytic in the sense that it produces more vacant surface sites than it requires [19].

Using our high-pressure STM, combined with mass spectrometry, we have performed a preliminary series of experiments on the NO+CO reaction on Pt(100), which we briefly present in the next section.

A.I.2 Results and discussions

The cleaning procedure for the Pt(100) sample has been described in Chapter 5. We have performed only three experiments, each at a different

temperature but all at the same total pressure of 1.25 bar. In this section we summarize our results, beginning with the lowest temperature.

T = 308 K

At this temperature we have not observed the formation of the two products, N_2 or CO_2. Image A from figure A.I.1 has been acquired after the sample had been heated to 308 K for 2h in an NO-rich gas flow. The quality of the original images was quite poor, so we differentially filtered them in order to enhance the contrast. As expected the exposure of clean hex-reconstructed Pt(100) to NO has led to the formation of square adatom islands corresponding to the unreconstructed Pt(100)-(1×1) surface. Image B has been recorded in a 1:1 mixture of NO and CO. These images clearly illustrate that when exposed to the gas mixture the surface has more adatom islands of different sizes and shapes.
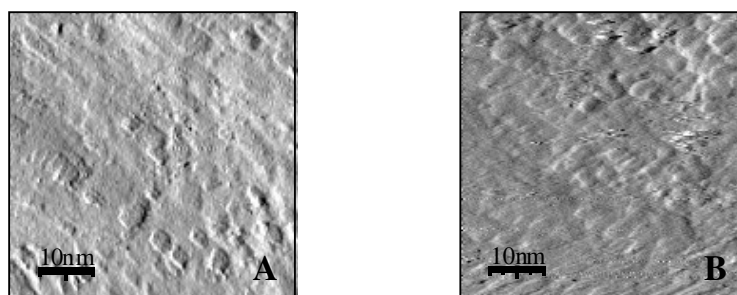

Figure A.I.1: Differentiated STM images (50 nm × 50 nm) of the Pt(100) surface at 308 K, illustrating (A) the formation of (1×1) adatom islands due to exposure to 1.25 bar of NO and (B) the formation of a high density of islands of various shapes due to exposure to 1.25 bar of a 1:1 NO/CO mixture. V_t=0.2 V and I_t=0.2 nA.

If a hex-reconstructed Pt(100) surface is exposed at room temperature to NO, the reconstruction is been lifted and c(2x4) structures are formed [7]. According to Miners et al. [20], if the NO-precovered surface is exposed to CO or a CO/NO mixture, two scenarios are possible. Either CO replaces NO and poisons the surface, or a mixture of CO and NO islands is formed. In both cases no reaction will take place at this low temperature of 308 K. Both scenarios could explain our experimental observations.

T = 383K

Figure A.I.2 displays the kinetics of NO+CO reaction as have been measured by the mass spectrometer at a constant total pressure of 1.25 bar and at 383 K. In order to differentiate between the CO and N_2 molecules that have the same molecular mass of 28 atomic mass units (amu), we have also followed the signals for ^{12}C, ^{16}O, ^{14}N, ^{15}N and $^{27}N_2$. We have further traced

in the spectrum mass 46, corresponding to the secondary reaction product NO_2. In order not to complicate our discussion we only show a selection of masses in Fig.A.I.2. The experiment of Figure A.I.2 started with a clean, hex-reconstructed Pt(100) surface that had been heated for 2 h in an Ar-rich flow. At a temperature of 383 K we have switched to an NO-rich flow at time $t = 0$. Accompanying the increase in NO signal we also noticed a significant increase in masses 28 (CO and/or N_2) and 44 (CO_2 and/or N_2O) and a small increase in the NO_2 signal. It is tempting to conclude from this that at this temperature, following the dissociation of adsorbed NO, the recombination of N_{ads} (which leads to the formation of N_2) and the reaction between $N_{ads}+O_{ads}$ (which leads to the formation of NO_2 and N_2O) took place.
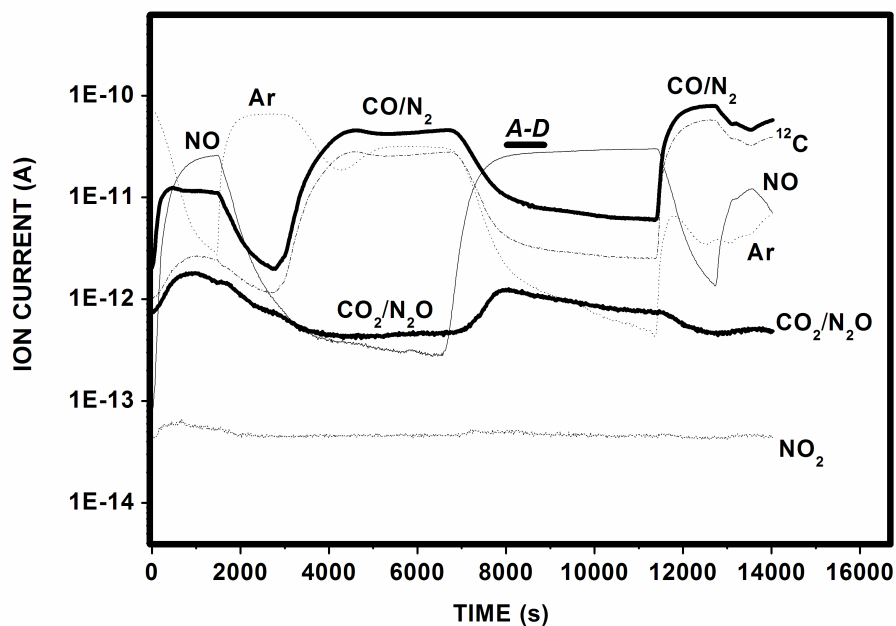
Figure A.I.2: *Kinetics of NO reduction by CO on Pt(100) at 383 K and 1.25 bar. First thick solid line in the figure corresponds to mass 38 amu, which can stand for one of the reactant gases-CO, but also for one of the desired reaction products N_2. The second ticker solid line corresponds to mass 44 amu that can correspond to the desired product CO_2, but also to a secondary product of this reaction N_2O.The thin solid line corresponds to the other reactant gas NO (mass 30 amu). The thin dotted line indicates the presence of Ar (mass 40 amu), while the dashed-dotted line corresponds to ^{12}C (mass 12 amu). The symbol A-B shows the time interval where the STM images presented in Fig.A.I.2 have been recorded.*

However, more experimental work is required to rule out the possibility that a dead volume in the NO gas line of residual oxygen from previous

experiments has reacted with the NO to form NO_2 and N_2O. At t = 1470 s we switched back to an Ar-rich flow. While the sample was in the pure Ar flow all other signals decreased. After this, at t = 32860 s, we slowly switched to a CO-rich flow. The CO-related mass signals (28 and 12) increased. In addition, only the signal of Ar, which shared its gas line with CO, increased. No other mass followed the increase in CO, which means that the adsorbed CO poisoned the surface. When we switched to an NO-rich flow at t = 6800 s, we found that after a short delay of a few hundred seconds the CO_2 signal increased. The fact that the signal that represents the masses of both CO and N_2 (28 amu) does not decrease as much as the ^{12}C signal (which corresponds to the CO molecules and not to N_2) constitutes a strong indication that N_2 is also formed. As we switched again to the CO rich flow at t = 11400 s, the CO_2 signal decreased. Also the N_2 signal ('difference' between the signals at masses 28 and 12) decreased. Assuming that prior to the increase in CO partial pressure the surface was NO-dominated, one might have expected the increase in CO pressure to be accompanied by a small increase in CO_2 and N_2 signals (at equal coverages of the reactants). However, it seems that CO reacted rapidly with the adsorbed NO and then poisoned the surface, as the reaction rate decreased really fast after switching to the CO-rich flow.

Figure A.I.3 shows a selection of STM images from a movie recorded simultaneously with the kinetics described above. As revealed by the images from figure A.I.3 the Pt(100) surface in an NO-rich flow shows the presence of vacancy islands, which disappear rapidly in time. Images B and C have been acquired consecutively after image A. The time interval required to record an image was approximately 1 minute. Image D shows a larger scale view of the surface and it has been recorded 6 minutes after image C. As can be seen there are still a few vacancy islands on the terraces. It seems that they prefer to appear on the wider terraces, but the wavy shapes of the steps indicate that vacancy islands close to steps (e.g. on narrow terraces) have coalesced with the steps. The shapes of the vacancy islands have a weak, hexagonal symmetry. We emphasize that we have not observed the formation of adatom islands, which we have observed when we exposed the hex-reconstructed surface to CO, as described in Chapter 6. One of the possible explanations for the presence of vacancy islands could be that NO did not lift the reconstruction but that it has led to an even higher-density structure of the first Pt layer than the original, hex-reconstructed surface.
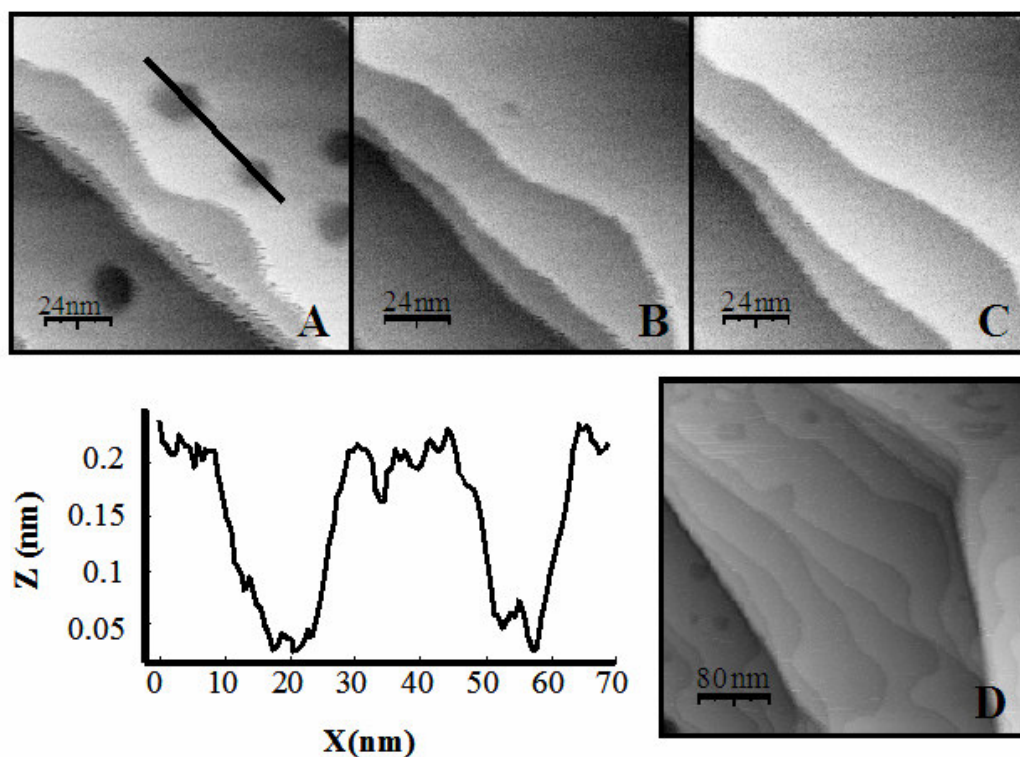
Figure A.I.3: STM images 100 nm × 100 nm (C-E) and 400 nm × 400 nm (F) showing the Pt(100) surface morphology in an NO-rich flow at a total pressure of 1.25 bar and at 383 K. The height profile along the line in image C indicates a depth of ~0.2 nm for the vacancy islands. V_t=0.8V and I_t=0.2 nA.

T=443 K

In the upper part of Figure A.I.4 the reaction kinetics at 1.25 bar and 443 K is depicted. Similar to the previous two experiments the sample has been heated for 2 h, but this time in a CO-rich flow. As indicated by arrow number 1 in figure A.I.4, at t = 3031 s we have switched to an NO-rich flow. The reaction rate for CO_2 production passed through a maximum, which we associate with the situation of equal coverages of the reactants on the surface ($\theta_{CO}=\theta_{NO}$). This behaviour is very reminiscent of Langmuir-Hinshelwood kinetics. Initially, the surface has been covered and poisoned by CO. At this temperature NO managed to adsorb on the surface and as the NO coverage increased beyond 50% there were less CO molecule to react with, so the reaction rate for CO_2 slowly decreased. At t = 8374 s (arrow number 2) we added again CO in the gas flow. This resulted in a modest, temporary increase in the CO_2 signal, which we again think corresponds to the situation of maximum reaction rate for equal coverages of NO and CO.
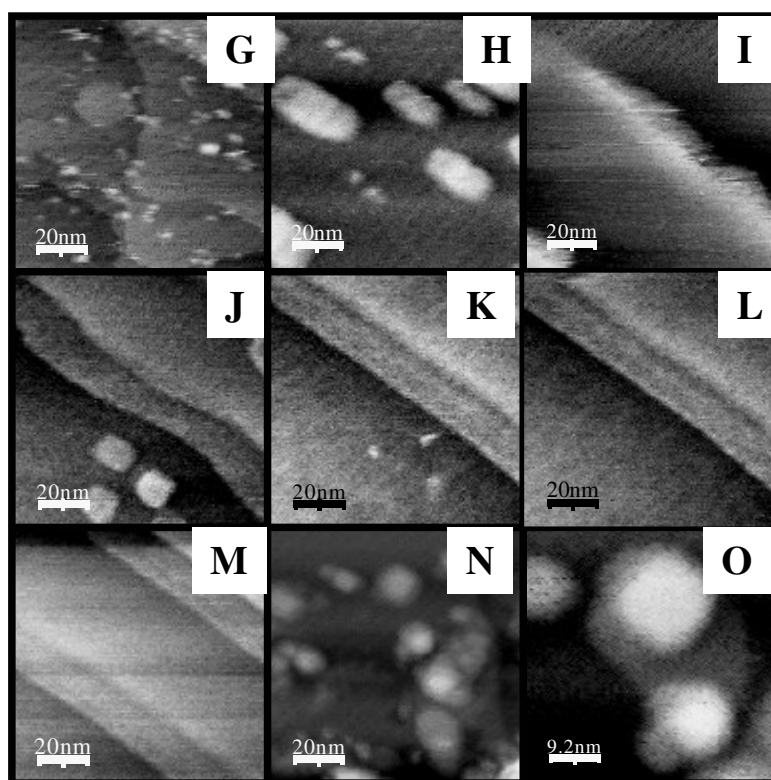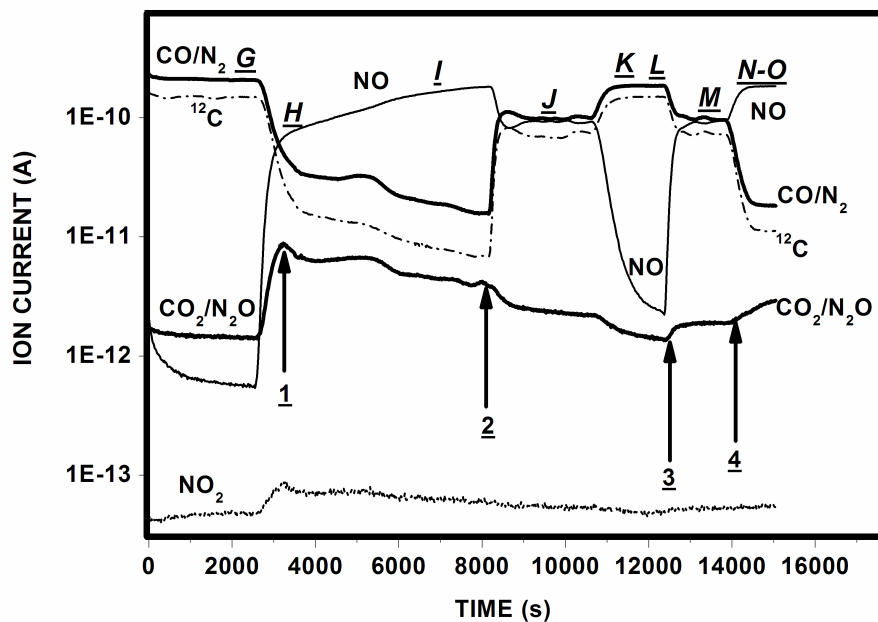
Figure A.I.4: *Reaction kinetics for the NO+CO reaction at 1.25 bar and 443 K (upper panel) and simultaneously recorded STM (lower panel) images reflecting the structural changes of the surface due to the exposure to NO, CO and NO/CO mixture (see text). The size of the images is 100 nm × 100 nm (J-N) and 46 nm × 46 nm (O). V_t=0.8V and I_t=0.2 nA.*

After this maximum, the CO_2 production rate decreased as the surface was exposed to a continuous flow of a 1:1 NO/CO mixture, which probably led to a slight over-population of the surface with CO. Adding more CO made the imbalance between adsorbed CO and NO more dramatic and decreased the rate of CO_2 production. At t = 12678 s (arrow 3) we added extra NO, so that the ratio NO:CO became again 1:1. This increased the CO_2 production rate again. The reaction rate increased further as we switched to a more NO-rich flow at t = 13889 s (arrow 4), thus approaching the maximum in the Langmuir-Hinshelwood mechanism again.

  The STM images acquired simultaneously with the kinetics described above are shown in Figure A.I.4 (b). Image G corresponds to the CO-covered surface. It shows the presence of highly mobile, small adatom island structures. Image H has been acquired immediately after switching to an NO-rich flow. Under these conditions, the surface contains square adatom islands, which proves that NO also lifts the reconstruction. Similar to the case of CO exposure, longer exposure to NO at high temperature was found to result in the smoothening of the surface, as illustrated in image I, which was recorded after the surface had been in the NO-rich flow for a time interval of 1h. Image J was acquired in the 1:1 NO/CO mixture. The image shows the re-appearance of adatom islands that we have seen before (image H) when the surface was exposed to an NO-rich flow. Image K was recorded in a CO-rich flow. During the long exposure to CO the adatom islands were decaying and the surface became smoother, as is seen in image L, which was recorded 30 minutes after image K. The flat surface from image L seems to remain unchanged when exposed to an equal mixture of CO and NO, as indicated by image M. When we exposed the smooth surface to an NO-rich flow, adatom islands with height between 0.6 and 1.0 nm were formed as shown in images N and O.

A.I.3 Conclusions

Our preliminary experimental results regarding NO reduction by CO over Pt(100) at ambient pressures (1.25 bar) and various temperatures (ranging from 308 K to 443 K) show Langmuir-Hinshelwood type behaviour. The reaction strongly depends on the temperature. Although NO and CO are both thought to lift the hex-reconstruction and 'restore' a (1×1) surface structure, the STM images obtained at the highest temperature provide strong evidence that the density of Pt atoms in the CO-covered surface is not the same as that in the NO-covered surface.

A.I.4 References

[1]   K. C. Taylor, *Automobile catalytic converters* (Springer, Berlin, 1984)

[2]   M. Slinko, T. Fink, T. Löher, H. H. Maden, S. J. Lombardo, R. Imbihil and G.Ertl, *Surf. Sci*. **264** (1992) 157

[3]   T. Fink, J. P. Dath, M. R. Basset, R. Imbihl and G. Ertl, *Surf. Sci.* **245** (1991) 96

[4]   M. F. H.van Tol, J. Siera, P.D. Cobden and B. E. Nieuwenhuys, *Surf. Sci.* **274** (1992) 63.

[5]   P.D. Cobden, J. Siera and B. E. Nieuwenhuys, *J. Vac. Sci.Technol.,A* **10** (1992) 2487.

[6]   C. A. de Wolf and B. E. Nieuwenhuys,*Catal.Today* **70** (2001) 287.

[7]   E. Ritter, R. J. Behm, G. Pötschke and J. Wintterlin, *Surf. Sci* **181** (1987) 403.

[8]   M. -B. Song, K. Momoi and M. Ito, *Jpn. J.Appl.Phys.***36** (1997).

[9]   H. P. Bonzel, G. Broden and G. Pirug, *J. Catal.* **53** (1978) 96.

[10] K. Masse and Y.Murata, *Surf.Sci.***242** (1991) 132.

[11] G. Pirug, H. P. Bonzel, H. Hopster and H. Ibach, *J. Chem. Phys.***71** (1979) 593.

[12] P. Gardner, M.Tüshaus, R. Martin and A. M. Bradshaw, *Surf. Sci.***282** (1990) 112.

[13] S. Sugai, K. Takeuchi, T. Ban, H. Miki, K.Kawasaki and T. Kioka, *Surf. Sci.***282** (1996) 67.

[14] E. D. L. Rienks, J. W. Bakker, A. Baraldi, S. A. Carabiniero, S. Lizzit, C. J. Weststrate and B. E. Nieuwenhuys, *Surf. Sci.***516** (2002) 109.

[15] Y. Y.Yeo, L.Vattuone and D. A. King, *J. Chem. Phys.***104** (1996) 3810.

[16] R. J. Gorte, L. D. Schmidt and J. L. Gland, *Surf. Sci.***109** (1981) 367

[17] A. Hopkinson, D. A. King, *Chemical Physics* **177** (1993) 433

[18] M. W. Lesley and L. D. Schmidt, *Surf. Sci.***155** (1985) 215

[19] A. Eichler and J. Hafner, *Journal of Cat*. **204** (2001) 118

[20] J. H. Miners et al., *Surf. Sci.***547** (2003) 355

Appendix II

Ethylene oxidation over Ag(111) and Pt(111)

In this appendix preliminary results are discussed for the partial and total oxidation of ethylene at atmospheric pressure and elevated temperature. Our results indicate that in the case of ethylene epoxidation the active catalyst is a thick, insulating oxide. For the total oxidation of ethylene on Pt(111) the reaction follows a Langmuir-Hinshelwood mechanism.

AII.1 General

Depending on the type of the catalyst and reaction parameter, the oxidation of ethylene can lead to the formation of ethylene oxide (epoxide) or to the formation of CO_2 and water, as seen in Figure A.II.1. The first reaction is also known as the selective or partial oxidation or the epoxidation of ethylene, while the second reaction is called the total oxidation or combustion [1].

$$C_2H_4 \xrightarrow[\;1/2O_2\;]{\Delta H = -104.6 KJ/mol} C_2H_4O \text{ (selective oxidation)}$$

$$\Delta H = -1423.5 KJ/mol \quad 3O_2$$

$$2CO_2 + 2H_2O$$
(total oxidation)

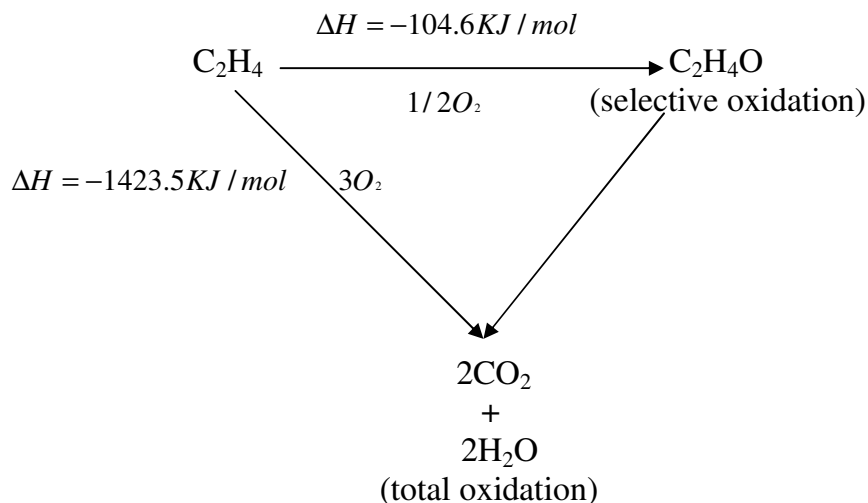**Figure A.II.1:** *Schematic representation of the possible reaction paths and products of the $C_2H_4+O_2$ reaction.*

In this appendix we show preliminary results obtained with our combination of high-pressure scanning tunneling microscopy and mass spectrometry on both reaction paths, namely partial oxidation of ethylene on Ag(111) and total combustion of ethylene on Pt(111).

AII.2 Partial oxidation of ethylene over Ag(111)

Introduction

Ethylene oxide is one of the most versatile chemical intermediates. With water it forms glycol and polyglicols, with ammonia and amines it forms ethanolamines, which are important solvents. Other important reactions are the polymerisation and the isomerization of ethylene oxide. Silver is the unique catalyst for the oxidation reaction of ethene to ethene oxide. All practical catalysts for the formation of this important compound are silver-based [1-3]. In spite of the existence of a large amount of literature, the data on the adsorption of ethylene, ethylene oxide, water and carbon dioxide on pure metallic silver are conflicting. Also the mechanism of the epoxidation reaction has not been elucidated. Before going into detail we first highlight some properties of silver and silver oxide [4-6]. Silver is the best electrical conducting material and the second best conductor of heat after diamond. The formation of silver oxide proceeds according to:

$$2Ag + 1/2O_2 \rightarrow Ag_2O \qquad \Delta H° = -28 kJ/mol$$
$$\Delta G° = -10 kJ/mol$$

Silver oxide decomposes above room temperature in air. According to Dushmann, silver oxide needs a partial pressure between 0.56 and 20.8 atm of oxygen pressure to remain stable at temperatures between 446 K and 575 K, where the oxidation reaction occurs [7].

Silver is a good catalyst for ethene epoxidation, because it forms weak bonds with ethene and oxygen. As mentioned above, the origin of the unique catalytic advantage of silver has not yet been clarified. In the last years, most of the existing surface spectroscopic techniques have been used to investigate the oxygen species adsorbed on a silver surface [8-15]. Combining the conclusions from all these investigations it seems that at least four oxygen species adsorbed on the Ag surface exist: molecularly adsorbed oxygen (O_2), superoxide (O^-_2) and peroxide (O_2^{2-}), atomically adsorbed species (O^- and/or O^{2-}) and, finally, subsurface oxygen [16]. Since ethylene does not adsorb on a clean silver surface, a reaction mechanism according to which the adsorbed oxygen on the silver surface reacts with ethylene from the gas phase seems plausible [17].

Van Santen and Kuipers proposed a mechanism for ethene epoxidation in which the selectivity of the reaction depends strongly on the oxygen coverage. At low coverages the oxygen is very strongly adsorbed, whereas at higher coverages the adsorption is much weaker. The reaction enthalpy for the formation of the epoxide from atomic oxygen, at low oxygen coverages is only 50-70 KJ/mol. In this case the total oxidation-a reaction

that is much more exothermic –is thermodynamically favoured, whereas epoxidation is hardly possible. At increasing oxygen coverages the charge on the oxygen atoms will decrease and, as a consequence the ethane oxide production increases [18-19].

An industrial catalyst for ethylene epoxidation contains the active element (silver) distributed on a support, usually α-alumina. The role of earth alkali metals is still controversial. It has been proved that in small concentrations potassium acts as a promoter. Also the addition of halogenated organic compounds increases the selectivity of the reaction [18-19].

Most of the fundamental, surface-science research on ethylene epoxidation is focused on the interaction of pure ethylene and oxygen with silver surfaces, usually of single crystals and usually at much lower pressures and temperatures than the conditions under which the industrial process runs. This may not be the best approach, since some of the most important aspects of the process, such as the active form of the catalyst (silver or silver oxide) under actual reaction conditions, cannot be addressed in this way. There is a large database about the various kinds of structures formed by oxygen on silver surfaces from UHV to ambient pressures [8-15].

Results and discussion

As has been explained in the previous chapters of this thesis, our experimental setup allows us to investigate catalytic systems "in situ" under semi-realistic conditions. In studying ethylene epoxidation on Ag (111) at ambient pressures and elevated temperatures, we have encountered several experimental difficulties, which we will point out together with he experimental observations. From the stoichiometric point of view we need a 2:1 C_2H_4:O_2 ratio to run the reaction. Figure AII.2 displays the reaction kinetics from an experiment performed at a constant total pressure of 1.25 bar. In the mass spectrum we follow C_2H_4O by not only recording mass 44 (which could also be CO_2), but also the most abundant fragments at masses 41 (C_2HO), 42 (C_2H_2O) and 43 (C_2H_3O).

As can be seen the temperature and the ratio between the partial pressures of the reactants play a crucial role in the ignition of the reaction. At t = 6023 s (indicated by arrow 1) even though the gas is already mixed in the proper, stoichiometric ratio of the reactants, the temperature it was still so low, T = 403 K, that the reaction rate was rather modest. Once we increased the temperature to 433 K, the reaction rate for the production of C_2H_4O increased (arrow 2). After a while, at t = 8830 s (arrow 3), we decreased the temperature back to 403 K and the mass signal for ethylene oxide decreased accordingly. It has been suggested in the literature that in order to ignite the reaction a silver catalyst needs to be preactivated. In our experiments we have followed the pre-treatment suggested by Tan and co-

authors. In order to activate the catalyst and ignite the reaction they annealed the crystal to 425 K in a 6:1 mixture of C_2H_4:O_2 for 2 h [20].
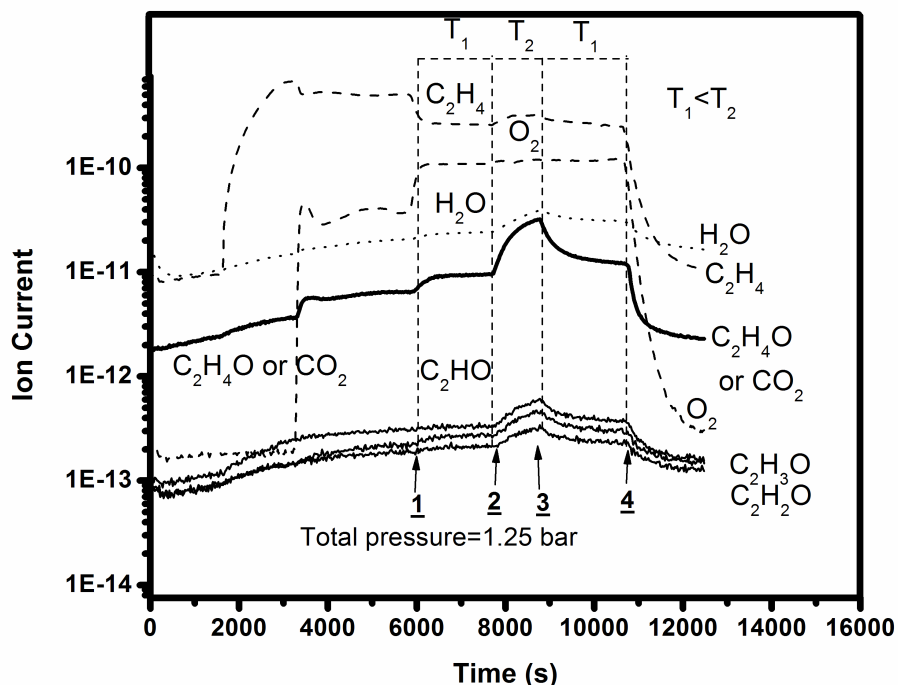

Figure A.II.2: *Kinetics during the epoxidation reaction on Ag (111) at a total pressure of 1.25 bar, recorded while we raised the temperature from 403 K to 273 K. Simultaneously with the increase in the temperature, an increase in the reaction rate is observed.*

The main purpose of this study was to image the surface with scanning tunneling microscopy under reaction conditions and investigate its morphology, in order to identify the active of the catalyst for this reaction. Unfortunately, we did not succeed in t his goal. As described above, the mass spectrometry signals clearly show that we did manage to run the reaction and the desired product, C_2H_4O, has been produced. However, the STM imaging under reaction conditions has been very difficult. Figure A.II.3 reveals that at room temperature both reactant gases (C_2H_4 and O_2) had no effect on the surface structure. Image A was acquired in low vacuum (10^{-2} mbar) at room temperature after the silver surface had been repeatedly cleaned by sputtering (3×10^{-5} mbar Ar^+) and annealing cycles (~1000 K). The surface in image A reflects the morphology of a single crystal with terraces and steps. Image B has been recorded in 1.25 bar of C_2H_4 at room temperature. The sputtering process has produced the vacancy islands with almost triangular shape. In spite of the presence of impurities, the metallic surface still can be easily recognized. Image C has been acquired in 1.25 bar of O_2 at room temperature. As one can see, the surface morphology is close to identical with the one from image B.
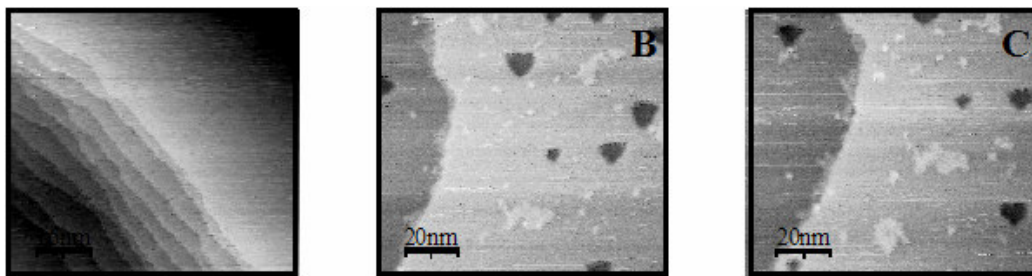
Figure A.II.3: STM images reflecting the structure of Ag(111) under different conditions at room temperature: (A) low vacuum (10⁻² bar); (B) 1.25 bar ethene; (C) 1.25 bar oxygen. The sizes of the images are 100 nm x 100 nm (B and C) and 80 nm x 80 nm (A). The tunneling parameters are V_t= 0.2 V and I_t=0.2 nm.

At high temperature we almost lost the resolution under high-pressure of a C_2H_2 rich-flow. In spite of the poor resolution, steps and terraces could still be recognized, as illustrated in figure A.II.4 (image D). Under an O_2-rich flow or in a mixture of O_2 and C_2H_4 the tip crashed repeatedly into the surface (upper part of image E). Under these conditions it has been impossible to acquire images. The reason for the tip crashes can only be the formation of a thick non-conducting layer on the surface, most probably a silver oxide. The growth of the non-conducting (silver oxide) layer was found to take place very rapidly, within a time interval of few seconds after the oxygen was admitted in the reactor. This process is very reproducible, it happened in all of the 12 experiments at elevated temperatures. The oxygen partial pressure has been varied between 1.25 bar and 200 mbar (close to the lowest pressure allowed by our present gas system).
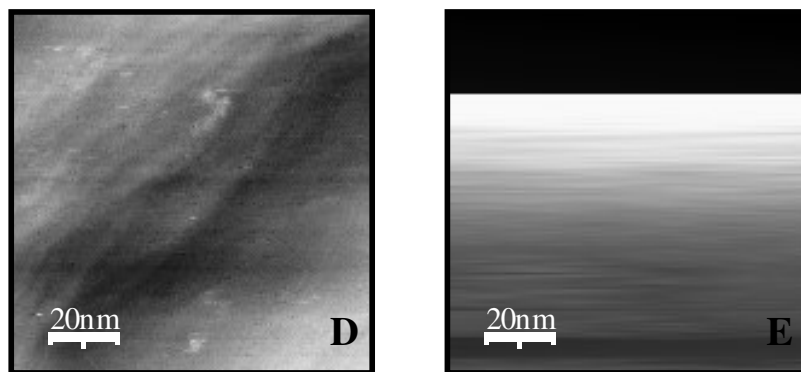

Figure A.II.4: STM images (100 nm x 100 nm) of Ag(111) exposed to 200 mbar of C_2H_4 at T~450K (image D) and to 200 mbar of O_2 at same temperature (image E). V_t=0.5 V, I_t=0.5 nA.

117

We should mention that we have not been able to perform experiments at a higher temperature (the maximum temperature has been 343 K), at which the silver oxide might be unstable and decompose. At present, our only evidence for the formation of the non-conducting silver oxide is the absence of tunneling current and, hence, the reproducible tip crash, but one cannot help wondering whether any of the structures for the silver oxide previously proposed on the basis of low-pressure, surface-science experiments is really relevant for the practical catalysis of ethylene epoxidation? Under industrial conditions, i.e. at high-pressure and high temperature and in the presence of both reactants gases, the current dispute in the literature whether the structure of the surface oxide is p(4x4) [21] or c(3x5√3) [22] might be completely irrelevant.

AII.3 Total oxidation of ethylene on Pt(111)

 Oxidation of hydrocarbons over platinum it is one of the key processes in car exhaust conversion and that forms the obvious motive for studying such a reactions. Ethylene it is a good choice for several reasons: it is a very simple hydrocarbon, it interacts with metal surfaces even at moderate temperatures and it gives only few possible oxidation products [23]. In spite of the large amount of experimental data under UHV conditions and near 1 bar, the $C_2H_4+O_2$ reaction over Pt surfaces is not fully understood. Both Langmuir-Hinshelwood and Eley-Rideal mechanisms have been suggested [24]. All previous studies have agreed on the fact that the main products in the case of the $C_2H_4+O_2$ reaction over a platinum catalyst are CO_2 and H_2O and very rarely the existence of partially oxidized species has been reported.
 The results discussed in this section are based on the measurements performed at a constant total pressure of 1.25 bar and a temperature of 403 K. Figure A.II.5 depicts the reaction kinetics. The following masses have been traced with the mass spectrometer: masses 28 for C_2H_4, 32 for O_2, 44 for CO_2 and 18 for H_2O. We have also followed the signals corresponding to he partially oxidized products. Since we did not notice any variation in their signals, they are not shown in the figure. At t = 6000 s the catalytic system was in an ethylene-rich flow. At t = 7027 s we switched to an O_2-rich flow. The increase in the oxygen signal was followed by a dramatic increase in the CO_2 signal and a more modest increase in the H_2O signal. At first glance the CO_2 production rate shows similar behavior to the CO oxidation over Pt(111). One readily distinguishes the two maxima in the CO_2 production rate marked by arrow number 1 (when we switch from a C_2H_4-rich flow to an O_2 rich flow) and by arrow number 7 (when we switch back from an O_2 rich flow to a C_2H_4 rich flow). These peaks could be attributed to the maxima in the Langmuir-Hinshelwood kinetics when the coverages of the reactant gases are equal. A more careful look at the first peak in the CO_2 production shows that the maximum value does not

correspond to equal coverages ($\theta_{C2H4}= \theta_{O2}=0.5$). The oxygen pressure is much higher than the ethylene pressure. In the case of the second peak marked by arrow number 7 the Langmuir-Hinshelwood theory applies. The maximum value in the CO_2 production rate corresponds to equal coverages of the reactant gases ($\theta_{C2H4}= \theta_{O2}=0.5$). Similar to the CO oxidation over Pt (111), while the catalytic system is in oxygen rich flow the CO_2 signal follows the minor reactant in this case C_2H_4. The arrow number 3 illustrates this conclusion when a small increase in the C_2H_4 signal is followed by a comparable increase in the CO_2 signal. After a while simultaneously with the decrease in ethylene pressure we notice a step down in the CO_2 signal (arrow number 4). The arrow number 6 indicates another increase in the CO_2 signal. This increase is small compared to the Langmuir-Hinshelwood peaks, but could be similar to the sharp peak recorded after the removal of the oxide, during the CO oxidation over Pt (111), mentioned in Chapter 3 of this thesis. If we focus now on the signal of the other product of the reaction H_2O, we again notice two maxima marked by the arrows numbers 2 and 5. Both peaks are acquired in a flow dominated by oxygen. The first maximum in the H_2O signal is recorded after 400 s from the detection of the first maximum in the CO_2 signal when we switch from a C_2H_4 rich flow to an oxygen rich flow. In contrast to this observation the second maximum in the H_2O signal (indicated by arrow number 5) is measured with approximately 286 s before the second peak in the CO_2 production rate indicated by arrow number 7 when we switch from an oxygen rich flow to an ethylene rich flow.
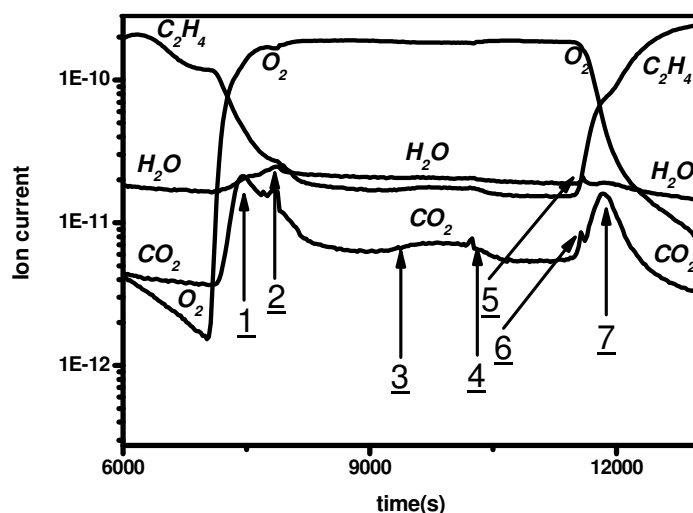

Figure A.II.5: *Reaction kinetics for the total oxidation of ethene on Pt (111) as recorded by the quadrupole mass spectrometer. $P_{total}=1.25$ bar , $T=413$ K.*

119

Simultaneously with the kinetics we also recorded STM images displayed in figure A.II.6. We should mention that before scanning the surface was exposed to a fluctuating mixture of C_2H_2/O_2 for approximately 2 hours at high pressure (1.25 bar) and elevated temperature. After this treatment we switched to C_2H_2 rich flow and then image F has been recorded. Image G has been recorded during the increase in the O_2 signal. Image H has been acquired in O_2 rich flow, while image I has been recorded at after we switch again to C_2H_2 rich flow. As can be seen the resolution of the images is very poor. All the images are showing a very rough surface consisting of "blobby" features. The multiple height profiles performed on these images showed step heights of 2.1-13 Å, witch do not correspond to the step height of Pt (111). At first glance image C (recorded in oxygen rich flow) shows brighter (higher) features compared to the other images, but this difference is not as obvious from the height profiles.
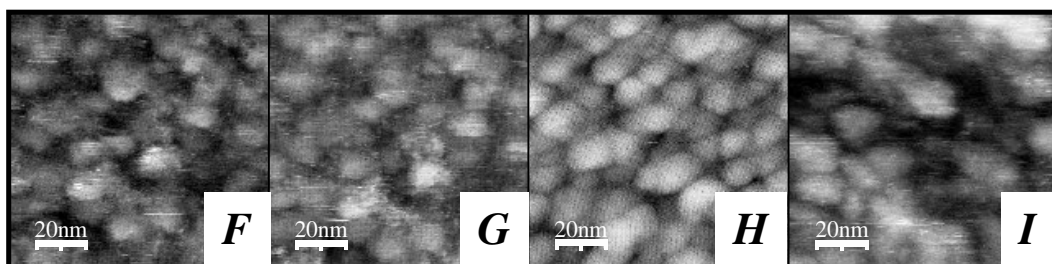

Figure A.II.6: *STM images (100nm×100nm) reflecting the morphology of the Pt (111) surface while exposed to 1.25 bar of C_2H_2 (images F and I) or/and 1.25 bar of O_2 (images G and H).V_t=0.1 V, I_t=0.2 nA.*

Summarizing all the information from the reaction kinetics seem to suggest that for the ethylene oxidation at atmospheric pressures and elevated temperatures over a platinum single crystal, follows a Langmuir-Hinshelwood type of mechanism . Before this experiment the Pt (111) sample has been repeatedly cleaned by sputtering and annealing cycles until a flat, free of impurities surface was obtained. Since the above series of STM images show a rough surface, we can take in consideration the possibility that under the reaction conditions the morphology of the sample has changed dramatically, maybe due to the surface intermediates (more likely carbonaceous species) formed during the reaction. We did not repeat this experiment so we cannot yet state that these data are reproducible.

A.II.4 Conclusions

In this appendix we have reported our results concerning the "in situ" investigation under semi-realistic conditions of two important reactions: ethene epoxidation and ethene combustion. Our experimental observations

reveal that in the case of the partial ethylene epoxidation on Ag(111), temperature plays a crucial role in the formation of the desired product (EtO) and, in contrast with the structures proposed for the sliver oxide catalyst based on more traditional surface-science experiments at low pressures, we find evidence for the formation of a thick, insulating oxide layer as the active form of the catalyst under practical conditions. The study of total ethene oxidation on Pt(111) indicates that the reactions follows the Langmuir-Hinshelwood mechanism similar to CO oxidation on Pt(111).

A.II.5 References

[1]   J. G. Serafin, A. C. Liu, S. R. Seyedmomir, *J. of Molec. Cat.* **A** 131(1998) 157.
[2]   C. N. Satterfield, *Heterogeneous Catalysis*, 2nd ed., McGraw-Hill, New York, 1991
[3]   *Ullmann's Encyclopedia of Industrial Chemistry*, 5th ed., Vol.**A11**, VCH, 1988
[4]   B. V. L'vov, *Thermochimica Acta* **333** (1999) 13.
[5]   A. Koller , J. Fiedlerova, *Thermochimica Acta* **92** (1985) 13.
[6]   R. Dallenbach, J. Painot, and P. Tissot, Polyhedron, Vol.1, No.2, (1982), 183
[7]   S. Dushmann ,*Scientific Foundation of Vacuum Technique,*2nd ed.,Wiley, New York (1962)
[8]   A. Sexton, R. J. Madix, *Chem. Phys. Lett.***76** (1980) 294
[9]   C. Backx, C. P. M. de Groot, P. Biloen, *Surf. Sci.***104** (1981) 300
[10]   M. A. Barteau, R. J. Madix, *Chem. Phys. Lett.* **97** (1983) 85
[11]   K. C. Prince, A.M. Bradshow, *Surf. Sci.* **126** (1983) 85
[12]   C. T. Cambell , *Surf. Sci.* **157** (1985) 43
[13]   A. Pushmann, J.Haase, *Surf. Sci.* **144** (1984) 559.
[14]   P .B. Clarkson, A. C. Cirrilo Jr., *J. Catal* **33** (1974), 392
[15]   K. Bange , T.E. Madey, J. K. Sass, *Chem. Phys. Lett.***113** (1985) 56
[16]   H. Nakatsuji, H. Nakai, K. Ikeda, Y. Yamamoto, *Surf. Sci.***384** (1997) 315
[17]   G. H. Twigg, *Proc. R. Soc. London Ser.* **A 188** (1946) 92
[18]   R. A. Van Santen and H. P. C. E. Kuipers, *Adv. Catal.* **35** (1987) 265.
[19   R. A. Van Santen and C. P. M. de Groot**,** *J Catal.***98** (1986) 530.
[20]   S. A. Tan, R. B. Grant and R. M. Lambert, *J. Catal.* **104** (1987)[19]
[21]   C. I. Carlisle et al., *Phys. Rev. Lett.* **84** (2003) 344
[22]   J. Schnadt et al., *Phys. Rev. Lett.* **96** (2006) 146101
[23]   U. Ackelid, L. Olsson, and L. G. Petersson, *J .of .Catal.* **161** (1996) 143
[24]   M. Sheintuch, and M. Avichai, *Ind. Eng. Chem. Res.* **27** (1988) 1152

Summary

The main theme of this thesis is the catalytic oxidation of CO, which we have investigated on several model catalyst surfaces at atmospheric pressures and elevated temperatures with the combination of Scanning Tunneling Microscopy and Mass Spectrometry. The general background of this work was discussed in Chapter 1. In addition, this chapter provided a brief description of the technique of Scanning Tunneling Microscopy and of the employed apparatus, namely a home-built High-Pressure Scanning Tunneling Microscope.

In Chapter 2 a short literature review on the CO oxidation on Pt group metals was presented. The bonding of CO molecules to these metals, the reaction mechanisms proposed for the CO-O_2 oxidation reaction and the non-linear behavior of this reaction were introduced.

CO oxidation on low-index and vicinal palladium surfaces was studied using scanning tunneling microscopy and mass spectrometry in Chapter 3. It was shown that, when exposed to ambient pressures of oxygen at elevated temperature, these surfaces oxidize irrespective of their orientation. In this pressure regime the oxides were shown to have a higher reactivity than the metallic surfaces. The reaction mechanism on the metallic palladium surfaces follows the classic Langmuir-Hinshelwood kinetics, while the reaction on palladium surface oxides exhibits Mars van Krevelen kinetics. As a consequence of the Mars van Krevelen mechanism, the oxide surfaces were found to roughen continually. In a certain window of partial pressure combinations of O_2 and CO reaction rate oscillations were observed on Pd(100) and on its vicinal surface Pd(1.1.17). We have shown that these oscillations correspond to the periodic switching of the surface between the metallic state with the Langmuir Hinshelwood reaction and the oxidic form with the Mars van Krevelen reaction.

A literature overview was given in the first part of Chapter 4 on various models describing the observed oscillatory behaviour of CO oxidation on Pt group metals. In the second part of Chapter 4 we introduced a completely new explanation for the oscillatory CO oxidation on palladium surfaces, which is based on two key features: (1) the observation that the oxide surface gradually roughens under reaction conditions and that the metal surface gradually smoothens and (2) the relation between the surface roughness and the CO partial pressure at which the surface switches between metal and oxide (and vice versa).

Chapter 5 presented our results for the CO-O_2 reaction at atmospheric pressure and elevated temperatures on Pt(111). CO adsorption was found to lead to the formation of a regular overlayer structure, identified as ($\sqrt{19}$x$\sqrt{19}$) R23.4°-13CO. The stability of this structure under different reaction conditions was discussed. These results were further used to illustrate the importance of temperature in a catalytic system. We showed

that at elevated temperatures Pt(111) oxidizes in an O_2-rich gas mixture and that the oxide has a higher reactivity than the metallic surface, similar to the palladium surfaces of Chapter 3. Also oscillations in the reaction rate were observed.

Chapter 6 was devoted to CO oxidation on Pt(100). In contrast with the other surfaces studied in this thesis, the clean Pt(100) surface exhibits a phenomenon called surface reconstruction. We found that exposure to either O_2 or CO lifts this reconstruction. In an O_2-rich flow and at elevated temperatures Pt(100) was observed to oxidize. Under these reaction conditions the oxide was only marginally more active than the metal surface and in most cases no difference could be observed at all between the reaction rates under conditions where both states of the surface were stable. However, since the metallic surface could be exposed to much higher CO partial pressures, spectacularly high conversion rates could be achieved on that surface. A second bistability was observed in this high-CO-pressure regime, which was identified as the traditional Langmuir-Hinshelwood bistability.

In addition to this investigation of the oxidation of CO by O_2 on various model catalyst surfaces we have briefly explored two related reaction systems, which were presented in the two appendices. In Appendix I we discussed preliminary results on the catalytic oxidation of CO by NO (or equivalently the catalytic reduction of NO by CO) on Pt(100), which show that the reaction rate depends strongly on the temperature and the catalyst structure.

The partial oxidation of ethylene on Ag(111) has been studied briefly in Appendix II. The results suggest that under reaction conditions the active catalyst might be a tick, insulating silver oxide. In addition, the complete oxidation of ethylene on Pt(111) at 1.25 bar and elevated temperature confirmed that the reaction follows a Langmuir-Hinshelwood type of mechanism.

Samenvatting

Het centrale thema van dit proefschrift is de katalytische oxidatie van CO, die we bestudeerd hebben op verschillende katalytisch actieve modeloppervlakken bij atmosferische drukken en hoge temperaturen met behulp van de combinatie van Scanning Tunneling Microscopie (STM) en Massaspectrometrie. Algemene overwegingen achter dit werk zijn aan de orde gekomen in Hoofdstuk 1. Tevens geeft dit hoofdstuk een korte beschrijving van de gebruikte techniek, STM, en van het gebruikte apparaat, een in Leiden en Amsterdam ontwikkelde hoge-druk scanning tunneling microscoop.

Hoofdstuk 2 beschrijft in het kort de literatuur met betrekking tot CO oxidatie aan de oppervlakken van metalen uit de platinagroep. Hierin zijn de binding van CO moleculen aan deze metalen, de verschillende reactiemechanismen die bestaan voor de CO-O_2 oxidatie reactie en het niet-lineaire gedrag van deze reactie geïntroduceerd.

CO oxidatie aan oppervlakken van palladium met lage Miller indices en vicinale oppervlakken (hoge Miller indices) wordt beschreven in Hoofdstuk 3 aan de hand van STM en massaspectrometrie. Hierin wordt aangetoond dat wanneer deze oppervlakken aan atmosferische drukken van zuurstof worden blootgesteld bij hoge temperaturen, zij alle oxideren, ongeacht hun oriëntatie. In dit drukgebied vinden we dat de oxides een hogere reactiviteit hebben dan de metallische oppervlakken. Het reactiemechanisme op het metallische palladiumoppervlak volgt de klassieke Langmuir-Hinshelwood kinetiek; de reactie aan de geoxideerde oppervlakken volgt het Mars-Van Krevelen mechanisme. Een consequentie van het Mars-Van Krevelen mechanisme bleek, dat de geoxideerde oppervlakken voortdurend ruwer worden. Binnen bepaalde combinaties van partiële CO en O_2 drukken zijn reactieoscillaties waargenomen op Pd(100) en Pd(1.1.17). We hebben laten zien dat deze oscillaties veroorzaakt worden door de periodieke omschakeling van het oppervlak tussen de metallische fase, waarbij de Langmuir-Hinshelwood reactie optreedt, en de geoxideerde fase, waarbij de reactie Mars-Van Krevelen kinetiek volgt.

Het eerste deel van Hoofdstuk 4 bestaat uit een literatuuroverzicht met betrekking tot de verschillende modellen die het geobserveerde oscillatiegedrag van CO oxidatie aan een oppervlak uit de platinagroep beschrijven. Vervolgens wordt in dit hoofdstuk een volledig nieuwe verklaring voor de reactieoscillaties in aanwezigheid van een palladiumoppervlak gegeven die gebaseerd is op twee belangrijke kenmerken: (1) de observatie dat het oxide geleidelijk aan ruwer wordt onder reactiecondities en dat het metallische oppervlak geleidelijk aan gladder wordt en (2) de relatie tussen de ruwheid van het oppervlak en de partiële CO druk waarbij het oppervlak omschakelt tussen metallisch en geoxideerd en vice versa.

Hoofdstuk 5 beschrijft de resultaten voor de CO-O_2 reactie aan het Pt(111) oppervlak bij atmosferische drukken en hoge temperaturen. Het blijkt dat CO adsorptie leidt tot de vorming van een regelmatige overlaagstructuur, die geïdentificeerd is als ($\sqrt{19}$x$\sqrt{19}$) R23.4°-13CO. De stabiliteit van deze structuur onder verschillende reactie-omstandigheden is besproken; de resultaten die hieruit volgden zijn verder gebruikt om het belang van hoge temperaturen in een katalytisch systeem te illustreren. We hebben aangetoond dat bij hoge temperaturen het Pt(111) oppervlak oxideert in een zuurstofrijke omgeving en dat het geoxideerde oppervlak een hogere reactiviteit vertoont dan het metallische oppervlak, net als in het geval van de palladiumoppervlakken beschreven in Hoofdstuk 3. Tevens zijn reactieoscillaties waargenomen.

Hoofdstuk 6 is gewijd aan CO oxidatie aan een Pt(100) oppervlak. In tegenstelling tot de andere in dit proefschrift bestudeerde oppervlakken, ondergaat het schone Pt(100) oppervlak een verschijnsel dat oppervlakreconstructie wordt genoemd. We hebben gezien dat bij blootstelling zowel aan O_2 als aan CO deze reconstructie verdwijnt. In een zuurstofrijke omgeving, bij hoge temperaturen, nemen we waar dat het oppervlak oxideert; onder deze reactieomstandigheden was het geoxideerde oppervlak echter nauwelijks reactiever dan het metallische oppervlak, en in de meeste gevallen kon zelfs geen verschil in activiteit tussen beide oppervlakken worden waargenomen onder condities waarin zowel het geoxideerde als het metallische oppervlak stabiel was. Omdat het metallische oppervlak echter aan veel hogere partieeldrukken van CO blootgesteld kon worden dan het oxide, konden in dit geval spectaculaire omzettingssnelheden van CO in CO_2 bereikt worden. Een tweede bistabiliteit is waargenomen in dit regime van hoge CO partieeldrukken, die we geïdentificeerd hebben als de traditionele Langmuir-Hinshelwood bistabiliteit.

Naast het onderzoek aan de oxidatie van CO met behulp van O_2 aan verschillende katalytisch actieve modeloppervlakken hebben we kort twee gerelateerde reactiesystemen bestudeerd, hetgeen in twee appendices wordt gepresenteerd. In appendix I zijn de voorlopige resultaten van CO oxidatie met behulp van NO (ofwel de reductie van NO door middel van CO) besproken, die laten zien dat de reactie sterk afhangt van de temperatuur en de structuur van het katalytisch actieve oppervlak.

De partiële oxidatie van ethyleen aan het oppervlak van Ag(111) is kort bediscussieerd in appendix II. De resultaten duiden erop dat onder reactieomstandigheden een dik, isolerend zilveroxide de actieve katalysator is. Daarnaast wijst de complete oxidatie van ethyleen aan Pt(111) bij 1.25 bar en hoge temperatuur erop dat deze reactie een soort Langmuir-Hinshelwood mechanisme volgt.

List of publications

This thesis is partly based on the following articles:

1. *Looking at heterogeneous catalysis at atmospheric pressure using tunnel vision*
   B.L.M. Hendriksen, **S.C. Bobaru**, J.W.M. Frenken, *Topics in Catalysis* 36 (2005) 43

2. *Bistability and oscillations in CO oxidation studied with Scanning Tunnelling Microscopy inside a reactor*
   B.L.M. Hendriksen, **S.C. Bobaru**, J.W.M. Frenken, *Catalysis Today* 105 (2005) 234

3. *Oscillatory CO oxidation on Pd(100) studied with in situ Scanning Tunnelling Microscopy*
   B.L.M. Hendriksen, **S.C. Bobaru**, J.W.M. Frenken, *Surface Science* 552 (2004) 229

4. *Structure and reactivity of Surface Oxides on Pt(110) during catalytic CO Oxidation*
   M. D. Ackermann, T. M. Pedersen, B. L. M. Hendriksen, O. Robach, **S. C. Bobaru**, I. Popa, C. Quiros, H. Kim, B. Hammer, S. Ferrer, and J. W. M. Frenken , *Phys. Rev. Lett*. **95** (2005) 255505

5. *New role for steps in catalysis*
   B. L. M. Hendriksen, M. D. Ackermann, **S. C. Bobaru,** I. Popa, S. Ferrer and J.W.M. Frenken, submitted to *Nature*

6. *CO oxidation on Pt(111) at atmospheric pressure*
   S. C. Bobaru, B. L. M. Hendriksen and J. W. M. Frenken,in preparation for submission to *Surface Science*

7. *CO oxidation on vicinal palladium surfaces at atmospheric pressure*
   S. C. Bobaru, B. L. M. Hendriksen J. Gustafson, E. Lundgren and J. W. M. Frenken, in preparation for submission to *Journal of Catalysis*

8. *Atmospheric CO oxidation on Pt(100)*
   S. C. Bobaru, C.T. Herschleb and J. W. M. Frenken, in preparation for submission to *Chemical Physical Letters*

Curriculum Vitae

S. C. Bobaru was born in Drăgoeşti, Vâlcea (România) on 2 July 1975. After receiving her Bachelor's degree in Physics-Chemistry from West University, Timişoara, România in 1998, she pursued her studies at the same university and obtained her Master's degree in Physics in 2000, specializing in physics of crystalline materials. The research for her master thesis entitled "*Evaluation of Image Quality of Electronic Portal Imagining for Megavoltage Photon Beams"* was done at Ørsted Laboratory, University of Copenhagen, Denmark during a six months scholarship. As a PhD student she first joined the group of Prof. Dr. Simion Simon at Department of Condensed Matter, Faculty of Physics, "Babeş-Bolyai"University, Cluj-Napoca, Romania on 2001, on a project entitled "*The use of spectroscopic techniques in medicine".* From May 2002 to October 2006, she has worked as a PhD student in the Interface Physics Group of Prof. J.W.M. Frenken, at the Kamerlingh Onnes Laboratory, Leiden University, The Netherlands. Her research in this period on the relationship between the structure and the reactivity of a catalyst has formed the basis for the present thesis on "*High-pressure STM studies of oxidation catalysis".*